WAVE ATTENUATION FUNCTION OF MANGROVES ALONG SINGAPORE'S NORTHERN COAST

LEE WEI KIT

(B. Sci. (Hons.), NUS)

A THESIS SUBMITTED FOR THE DEGREE OF MASTER OF SOCIAL SCIENCES

DEPARTMENT OF GEOGRAPHY

NATIONAL UNIVERSITY OF SINGAPORE

2016

DECLARATION

I hereby declare that this thesis is my original work and it has been written by me in its entirety. I have duly acknowledged all the sources of information which have been used in the thesis.

This thesis has also not been submitted for any degree in any university previously.

LEE WEI KIT

18TH AUGUST 2016

Acknowledgements

I would like to express my sincere gratitude to my supervisor, Dr. Daniel Friess who has provided guidance and support throughout the course of this study. I appreciate the time he has taken and patience in providing valuable advice especially in the aspect of research method, critical thinking and thesis writing.

I would like to thank S.K. Ooi and Serene Tay for providing waves simulation and bathymetry data; Tan Xiao Yi for Singapore's mangrove GIS data; Pim Willemsen for Mandai mangrove flow velocity data; Dr. Edward Webb for lending field equipment; National Parks Board staff Samantha Lai, How Choon Beng, Benjamin Lee, Noel Thomas, Robert Teo and Mohamad Yusoff for assistance in granting field research permit (NP/RP936-5), study site access and logistic during fieldwork.

I am grateful to friends who have helped in the fieldwork and desktop study: Pierre, Benjamin Thompson, Rachel, Valerie, Rayna, Leon, Zhangxin, Wei Bin, Pim Willemsen, Daniel Richards, Siqi, Siaw Fun, Joanna Yeo, Siew Kin, Kunlun, Sarah Seo and Sam Gandhi. Additional thanks to Wei Bin, Zhangxin, Rachel, Valerie, Jared, Martin, and Gladys who have helped to proofread my thesis. I would also like to thank Elva and Nisha for their assistance and guidance in laboratory work; and Ms. Pauline Lee and Mr. Tow from Department of Geography for administrative assistance.

I am truly thankful to Dr. Vladan Babovic for allowing me to spend time on my thesis; and my colleagues Aurelie, Abhishek, Fabien and Martin for lending support and help to cover my groundwater project duty when possible.

Finally, I would like give a heartfelt thanks to my family and friends for every support and encouragement given over the past years.

Table of Contents

Abstract

Urbanization and increasing populations in the coastal zone have increased the exposure of people to coastal hazards. The coastal vulnerability associated with the rapidly urbanizing coastal zone is likely to be exacerbated by climate change in the coming decades. Despite population and development pressures, mangroves in an urban landscape can provide multiple ecosystem services, including coastal protection. One aspect of coastal protection, the wave attenuation ability of mangroves, was found to be an important mechanism in protecting the coastal zone from flooding, storm surge and erosion. Although evidences have demonstrated the wave attenuation ability of mangroves, no wave attenuation study has been conducted in disturbed mangroves, which often have different ecological and physical characteristics compared to natural mangroves. This study has investigated the wave attenuation extent and the wave attenuation factors of disturbed mangroves through studying the mangrove fragments along Singapore's northern coastline.

Using site-specific vegetation, physical and hydrodynamic parameters, wave attenuation extent in mangroves were quantified by the nearshore wave evolution model from the Integrated Valuation of Ecosystem Services and Tradeoffs (InVEST) modelling suite. Average and extreme hydrodynamic conditions were simulated to illustrate the wave attenuation extent under these conditions. The results showed the potential of Singapore's mangroves for wave attenuation, especially during extreme hydrodynamic conditions. Mean wave height reduction was 7.71% and 62.47% under average and extreme hydrodynamic conditions respectively. Wave breaking was the main cause of the increased reduction in wave height during extreme events. Variations across sites were observed with a large wave height reduction range between -0.46 to 50.71% and 2.79 to 92.21% for average and extreme hydrodynamic conditions respectively. The large range was caused by a combination of physical, vegetation, and

hydrodynamic factors, and the effects varied with average and extreme conditions. Mangrove forest density and width were found to positively correlate with the extent of wave attenuation by mangroves during extreme hydrodynamic condition. Among the vegetation structures, mangrove roots were found to be the main wave attenuation contributor in both average and extreme conditions.

The degree of wave attenuation found in this study are comparable to some natural mangroves, showing the wave attenuation potential of disturbed mangroves of Singapore. The analysis of wave attenuation factors also shed light on the factors influencing the wave attenuation extent. In a broader context, this study has demonstrated the potential of wave attenuation by urban disturbed mangroves. This wave attenuation ability is increasingly recognized as an important ecosystem services in the face of increasing coastal vulnerability. In the rapidly urbanizing coastal zone, anthropogenic pressures coupled with natural stressors, such as sea level rise, can lead to mangrove degradation. Such phenomena is likely to become more common in the coming decades. The understanding of wave attenuation ability and the wave attenuation factors will help to incorporate urban mangrove ecosystems into coastal management plan and provide essential coastal protection to the coastal community.

List of Tables

List of Figures

1 Introduction

1.1 Coastal vulnerability

The coastal zone, often defined as the area within 100 km of the coast or 50 m above mean sea level, encompasses more than one third of the world's population (Barbier et al., 2008; Gedan et al., 2011). This number continues to rise as urban coastal populations expand, and could reach 6 billion by 2025 (Creel, 2003; Curran et al., 2002; Small & Nicholls, 2003). Urban expansion in the coastal zone has increased the exposure of populations and properties to natural hazards such as erosion, coastal floods, storm surges and even tsunamis (Arkema et al., 2013; Nicholls et al., 1999). Coastal vulnerability is also likely be amplified by the effects of climate change, such as sea level rise and the increase of unpredicted extreme events (IPCC, 2014; Klein & Maciver, 1999; Nicholls et al., 1999, 2008; Shepard et al., 2012). The increasing coastal vulnerability was expected to continue throughout 21st century and could incur high economic costs (IPCC, 2014). A study has estimated, by the 2080s, more than 500 million people living within the coastal zone will be exposed to the threats of coastal flooding as the sea level rises, an increase from 200 million in the 1990s (Nicholls et al., 1999).

1.2 Mangroves in an urban landscape

Rapid urbanization within the coastal zone has also damaged the coastal ecosystems. Coastal ecosystems fringing an urbanized coastline often face multiple threats including coastal development, expansion for agriculture and aquaculture, river damming, land reclamation and pollution (Barbier & Cox, 2003; Barbier et al., 2011; Lai et al., 2015; Richards & Friess, 2016; Small & Nicholls, 2003). Mangroves within an urbanized coastal zone, in particular, were often found to experience thinning, degradation, and destruction (Everard et al., 2014; Lee et al., 2014; Mohamed et al., 2009; Phan et al., 2014). In Vietnam, the loss of more than half of the mangroves in the

years between 2000 and 2012 was attributed to urbanization (Richards & Friess, 2016). Higher mangrove loss was also found near rapidly urbanizing regions such as Bangkok region and southern Malaysia (Richards & Friess, 2016).

Despite human population and development pressures, mangroves within an urbanized coastal area can provide multiple ecosystem services to the coastal urban community. These ecosystem services include carbon storage, fishery production, coastal protection, and cultural values (Barbier et al., 2011; Brander et al., 2012; Friess et al., 2016; Thiagarajah et al., 2015). Friess et al. (2016) and Phang et al. (2015) studied the carbon storage in both biomass and soil within the mangroves in Singapore and found substantial storage of carbon in Singapore's disturbed, urban mangroves. Thiagarajah et al. (2015) and Richards & Friess (2015) shed light on the important role of urban mangroves in providing a myriad of tangible and abstract cultural ecosystem services to local population. A valuation study estimated the value of a threatened mangroves near the urbanizing city of Mumbai, India to be US$ 7.73 – 8.28 million (Everard et al., 2014). Among the ecosystem services provided by mangroves, coastal protection was found to be an important service as a densely populated urban coastal zone faces natural hazards, such as coastal flooding, erosion and storm events (Huxham et al., 2015). A number of studies have valued the coastal protection function of mangroves at US$ 1,879 – 12,163 ha^{-1} (Barbier, 2007; Sathirathai & Barbier, 2001). The estimation was conducted based on mangroves in rural areas; the coastal protection benefits in a densely populated urban coastal zone could potentially be higher. The increasing coastal vulnerability in the urbanized coastal areas in the face of climate change will only amplify the need for coastal protection function of mangroves (IPCC, 2014; Klein & Maciver, 1999; Shepard et al., 2012).

1.3 Coastal protection by mangroves

The ability of mangroves in providing coastal protection has been observed in the aftermath of extreme events (Alongi, 2008; Badola & Hussain, 2005; Barbier, 2007; Chang et al., 2006; Danielsen et al., 2005; Gedan et al., 2011; Kathiresan & Rajendran, 2005; Lee et al., 2014; McIvor et al., 2012; Spalding et al., 2014). In the wake of cyclone Odisha in 1999, studies conducted in Orissa, India suggested that less property damage and deaths were observed in villages protected by mangroves compared to those that were not protected (Badola & Hussain, 2005; Das & Vincent, 2009).

Mangroves were also suggested to be able to protect coastal communities in some instances from larger scale events such as tsunamis. Several studies were conducted to investigate the coastal protection provided by mangroves in the aftermath of Indian Ocean tsunami in December 2004 (Alongi, 2008; Chang et al., 2006; Danielsen et al., 2005; Kathiresan & Rajendran, 2005). One example of these studies showing a comparison across different villages in Tamil Nadu found less damage and fewer loss of human lives in some villages, an effect partly attributed to the presence of mangroves (Kathiresan & Rajendran, 2005). However, some scientists argued otherwise. Kerr and Baird (2007) in particular argued that the scientific evidence and observations regarding the mangrove protection function during tsunamis were statistically unconvincing and anecdotal. It was even suggested that the mangroves could cause more damage in instances when the tsunami magnitude exceeds the protective capacity of mangroves (Forbes & Broadhead, 2007). While the role of mangroves in tsunami mitigation remains controversial, their ability to protect coastal zone against storm events is generally accepted (Alongi, 2008; Badola & Hussain, 2005; Barbier, 2016; Das & Vincent, 2009; Forbes & Broadhead, 2007; Gedan et al., 2011; Kerr et al., 2006).

1.4 Wave attenuation by mangroves

Mangroves provide protection to the coastal community against storms and coastal floods mainly through their wave attenuation ability (Barbier, 2011; Barbier et al., 2008; Gedan et al., 2011; McIvor et al., 2012; Spalding et al., 2014). The wave attenuation ability of mangroves has been investigated by researchers through field, laboratory, and modelling studies (Barbier et al., 2011; McIvor et al., 2012; Spalding et al., 2014). Mangroves were found to be able to attenuate waves within a short distance. In some studies, a reduction of more than 50% of wave height was observed within 100 m into the mangroves (Magi et al., 1996; Mazda et al., 1997a; Vo-Luong & Massel, 2006). As waves propagate through a mangrove forest, the vegetation acts as an obstacle to the water flow, creating a drag force thereby changing the hydrodynamics. A few studies have shown that the wave attenuation extent is related to the structure of mangroves, in particular, the mangrove's roots (Horstman et al., 2014; Massel et al., 1999; Mazda, et al., 1997b). On the other hand, the wave attenuation extent is also related to the roughness of the bottom sediment, which slows the water flow as it interacts with the bottom boundary layer, creating an opposing frictional force (Mazda et al., 2007). In a natural setting, both biophysical factors combined to induce wave energy dissipation and wave height reduction within a mangrove forest (Lee et al., 2014; Mazda et al., 1997b; Mazda et al., 2007; McIvor et al., 2012).

1.5 Research need

The wave attenuation function of urban disturbed mangroves

Both natural and anthropogenic factors can cause mangrove disturbances (Allen et al., 2001; Mohamed et al., 2009). A disturbed mangrove could experience fragmentation, a change in forest composition or 'cryptic ecological degradation' *sensu* Dahdouh-Guebas et al. (2005), and thinning (Everard et al., 2014; Lee et al., 2014; Mohamed et

al., 2009; Phan et al., 2014). The different ecological and physical characteristics of disturbed mangroves, compared to a natural mangroves, could affect their ecosystem function such as coastal protection (Lee et al., 2014). Most of the previous studies on the wave attenuation function of mangroves have been conducted in natural mangroves or mangroves of bigger sizes. The wave attenuation function of a disturbed mangrove is not understood. Moreover, in the face of increasing coastal vulnerability, the disturbed mangroves could provide essential coastal protection to the urban coastal areas through attenuating waves and, thus reduce the coastal flooding and erosion. The extent of wave attenuation function provided by urban disturbed mangroves should, therefore, be studied. Investigating the extent of wave attenuation in the disturbed mangroves of Singapore could shed light on the wave attenuation function of such mangroves, which we expect to become more common in the future; and their potential in coastal vulnerability reduction.

Coastal management planning in coastal cities

Coastal management in an urbanized coastal cities usually involves the building of hard structures such as sea walls in order to protect shoreline from erosion or storm surges (Bacchiocchi & Airoldi, 2003; Benoit & Roberts, 2007). The replacement of natural habitats with artificial structures has resulted in the direct loss of coastal habitats, along with their ecosystem services (Chapman & Underwood, 2011; Goodsell et al., 2007). In recent years, natural habitats such as mangroves and seagrasses have been integrated into the coastal protection measures, in combination with hard structures such as sea walls to protect the shoreline and minimize the negative impacts associated with the hard coastal protection approach (Bouma et al., 2009; Chua, 2010; Lai et al., 2015; Morris, 2007). The use of natural habitats such as mangroves for shoreline protection demands the understanding of context-specific physical and ecological characteristics in order to provide effective solutions (Chapman & Underwood, 2011). The investigation of mangroves' wave attenuation capacity, and the subsequent coastal

management implications illustrated in this study, could inform coastal management planning in coastal cities.

Ecosystem function of mangroves in Singapore

The study of mangrove's wave attenuation function in Singapore could provide a more complete picture of the role of mangroves in the urban context of Singapore. The ecosystem service provision of a mangrove is dependent on the needs of the local people. For example, in rural areas, mangroves could be used for fuelwood and for provision of food and building material. In an urbanized coastal zone, the use of ecosystems such as mangroves for education, recreation and other non-material purposes could outweigh the use of mangroves for provision of food or natural resources (Bolund & Hunhammar, 1999; Thiagarajah et al., 2015). There is an increasing number of studies on the ecosystem services provided by mangroves in Singapore, especially in the last five years (Friess et al., 2016; Phang et al., 2015; Richards & Friess, 2015; Thiagarajah et al., 2015). While not previously considered, coastal protection function, such as wave attenuation by mangroves, could play a role in Singapore. Studies have suggested the possibility of tropical cyclones in this region, and while the likelihood of occurrence is very low, this poses a risk to the low-lying coastlines of Singapore (Chang, 2003). In addition, ship wake generated in Singapore's waters could pose a threat to the shoreline stability. As such, the need for the wave attenuation function of mangroves is present in Singapore. The coastal protection service of mangroves in Singapore, in particular through wave attenuation, is currently unknown.

1.6 Objectives and approach

The aim of this study was to understand the wave attenuation function and the main wave attenuating factors of the disturbed mangroves in Singapore. This study was

conducted at mangroves along the northern coastline of Singapore's main island. In order to achieve this aim, two objectives were identified:

- *To quantify the extent of wave attenuation of the mangroves along Singapore's northern coastline under average and extreme hydrodynamic conditions*

  The average and extreme hydrodynamic conditions present different environment for the waves to propagate into the mangroves. This hydrodynamic difference could affect the extent of wave attenuation by the mangroves. Understanding the different hydrodynamic conditions is important to highlight the benefits of mangroves not only during normal days but also the potentially more valuable wave attenuation function during extreme events.

- *To investigate the factors affecting the wave attenuation within the mangrove area along Singapore's northern coastline*

  The wave attenuation within a mangrove forest is influenced by various physical, hydrodynamic, and vegetation factors. The capacity of each factor to influence wave attenuation differs from one another and is site-specific. Acquiring the knowledge on the influence of various factors affecting the wave attenuation will provide insights into the underlying biophysical processes that took place during the wave attenuation.

A process-based modelling approach, supported by extensive field data collection, was used to study the wave attenuation function of mangroves. Field and desktop studies were carried out to understand and collect relevant data on the physical, hydrodynamic and vegetation characteristics at study sites. A nearshore wave evolution model in the GIS-based Integrated Valuation of Ecosystem Services and Tradeoffs (InVEST) modelling software was used to simulate wave attenuation extent using site-specific

data as model setup. The wave attenuation and the main wave attenuation factors were analyzed in terms of wave energy dissipation and wave height reduction.

2 Literature review

The wave attenuation function of mangroves has been investigated and described by researchers through various laboratory, field, and modelling studies. The knowledge of the underlying physical processes of wave attenuation as the waves move through the vegetation is important in understanding both the extent of the wave attenuation and the factors affecting the wave attenuation. In this chapter, the mechanism of wave attenuation is first described, followed by laboratory, field, and modelling studies that have elucidated various physical and ecological contributors to wave attenuation.

2.1 Mechanism of wave attenuation

During the process of wave propagation, wave energy is transmitted through space with water as the medium. The wave form is usually assumed to follow Linear Wave Theory (LWT) (Figure 2.1) (Airy, 1845). In reality, however, the sea surface is made up of waves of various heights and periods which are constantly interacting with one another. Nevertheless, the linearized wave form has been shown to be able to provide reasonably good representation of waves for many ocean and coastal engineering purposes.

As waves propagate towards the shallow water, the frictional force generated from bottom sediment acts against the propagating waves, resulting in the dissipation of wave energy. The slower bottom flow layer caused by slope and bottom friction could also induce wave breaking. The wave breaking process dissipates wave energy by converting it into turbulent kinetic energy. When waves propagate into areas with coastal vegetation such as mangroves, saltmarshes, and seagrass, the physical obstruction created by the vegetation structure dissipates the wave energy by exerting a drag force (Leonard & Luther, 1995; McIvor et al., 2012; Möller, 2006; Spalding et al., 2014). The wave attenuation caused by bottom friction is relatively small compared to other wave dissipation mechanisms such as wave breaking and vegetation drag force

(Mazda et al., 1997a; Vo-Luong & Massel, 2008). In some instances, the non-breaking waves induce wave shoaling, resulting in an increase of wave height (Van Rijn, 2008).

Figure 2.1 Illustration of idealized wave form based on LWT and its characteristics.

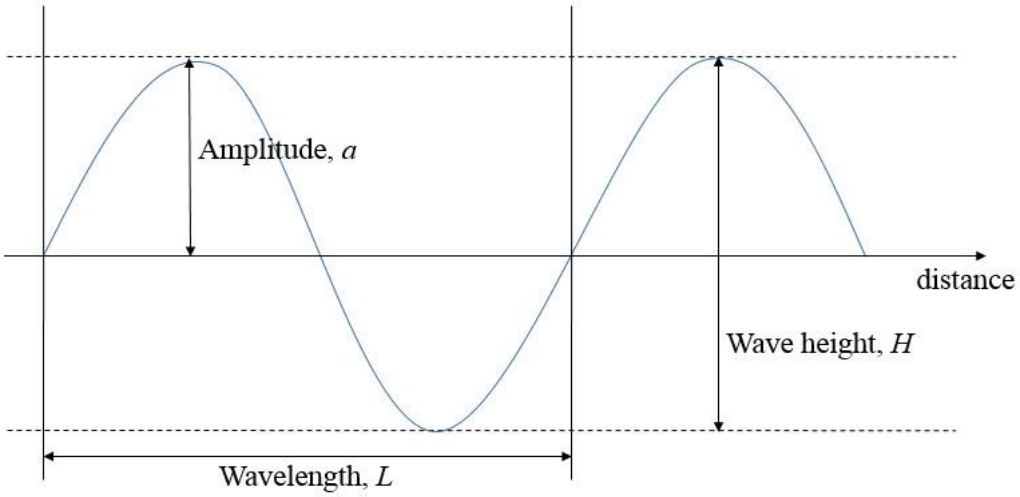

2.2 Wave attenuation by mangroves

2.2.1 Laboratory studies of wave attenuation

The laboratory provides a controlled environment for studying the hydrodynamic changes caused by vegetation or physical factors. In laboratory studies, researchers have used simplified mangrove tree models in designated arrangements to imitate the mangrove forest structure. Both Struve et al. (2013) and Zhang et al. (2015b) observed a reduction in flow velocity across the vegetation field. A drag coefficient within the mangroves of 0.8 – 4.4 was estimated by Struve et al. (2013) while a smaller range (1.2 – 1.8) was calculated by Zhang et al. (2015b), which matches the value of a bottom made of coarse materials. Furthermore, Zhang et al. (2015b) also highlighted a more complicated flow pattern within the vegetation field through an observed increase of flow velocity and turbulence between individual tree models. In both studies, vertical flow resistance was not uniform in the water column. As demonstrated by Zhang et al. (2015b), flow velocity increases vertically along the water column until the top of prop

roots. Above prop roots, the velocity becomes constant. Such effect was also observed in some field studies (Brinkman, 2006; Brinkman et al., 1997).

The role of mangrove in attenuating tsunami waves has also been investigated. A study found that approximately 40% of tsunami wave height was reduced in the presence of mangrove vegetation, albeit comparatively lower than an artificial breakwater (Harada et al., 2002). The difference was due to the higher porosity in the model setup, which allows less obstruction to water flow. This result highlighted the effects of structures, natural or artificial, in wave attenuation and that such effects are dependent on the porosity/density. In another study, the vegetation structure effects were taken into account by Husrin et al. (2012) and Strusińska-Correia et al. (2013) through parameterization of mangrove vegetation. The studies highlighted the effects of mangrove width and water level on wave attenuation ability of mangroves. For example, within the same experiment, a tsunami wave height has been observed to decrease after passing through mangrove forest models, with a recorded wave height of 0.07 m at the back of 0.75 m and 1.5 m wide mangrove forest models, and a recorded wave height of 0.03 m at the back of a 3.0 m mangrove forest model. An increase in forest width increases the distance for which waves were exposed to opposing frictional force, and therefore translate to more energy dissipation by mangrove vegetation. More importantly, experiments have also shown the influence of the physical environment (the foreshore) on wave attenuation during large scale events such as the tsunami. Wave breaking occurs when a high wave passes through a shallow foreshore prior to reaching the mangrove forest. This wave breaking process, together with the turbulence generated, causes an increase in wave energy dissipation. The effect of turbulence could continue to influence the wave as it propagates across the forest.

Shortcomings of laboratory studies

The laboratory experiments were set up using only a single species structure in a rather homogenous model structure arrangement. Such setup does not reflect the heterogeneous mangrove stands in reality. In addition, the applicability of experimental findings to other mangrove species with different root geometries such as *Avicennia* with pencil-like pneumatophores, is limited. The differences in the root geometry directly influence the submerged vegetation structure and volume, thereby increases vegetation density, especially near the bottom of a tree.

2.2.2 Field studies of wave attenuation

Field wave attenuation studies conducted in a natural setting could complement laboratory studies by overcoming some of the shortcomings. The wave attenuation measurement reflects the combined effects of physical and vegetation characteristics in a natural setting. Using manual measurements, Bao (2011) observed a wave height reduction of 0.1 – 0.5 m across 100 m in mangroves in Vietnam. In another study employing a similar method, up to 85% of incoming wave height reduction was observed within 90 m into the forest, compared to 64% on the open mudflat (Nguyen, 2013). Using statistical analysis, both studies highlighted a linear relationship between the wave height and the incident wave height and an exponential relationship between wave height and vegetation structure. The main limitation in both studies, however, was the lack of measurements for high waves. The statistical relationship was established based on measurements in waves that were lower than 70 cm in height. Such limitation was probably imposed by the measurement method which only suitable for a low wave energy environment, and not for storms or cyclones due to safety concerns (Davidson-Arnott, 2009).

The use of pressure and wave sensors is a popular method for continuous water level and wave data collection (Brinkman, 2006; Horstman et al., 2014; Magi et al., 1996;

Mazda et al., 2006; Mazda et al., 1997a; Quartel et al., 2007; Vo-Luong & Massel, 2006). Compared to manual measurement, these sensors can capture more parameters, such as water surface fluctuations and pressures, simultaneously. In addition to the ability to capture more data for an extended period of time, these sensors also provide a better measurement accuracy than manual measurement. A number of wave attenuation studies in Thailand, Vietnam, and Japan have been conducted using pressure sensors. In these studies, vegetated areas were found to have a higher wave height reduction (0.002 – 0.012 m^{-1}) compared to non-vegetated area (0.0012 – 0.002 m^{-1}) (Horstman et al., 2014; Quartel et al., 2007). The difference in the wave attenuation rate was mainly due to the additional drag force caused by the vegetation, as opposed to non-vegetated areas where only the bottom friction force contributed to the wave energy dissipation. Similar vegetation effects could also explain the wave attenuation rate difference between the *Rhizophora stylosa*-dominated forest (45 – 85% over 25 m) and the non-vegetated area (2 – 7% over 25 m) observed at Shiira, River, Japan (Magi et al., 1996).

Mangroves have been shown to exhibit high wave attenuation rate over a short distance, albeit with variations between sites. Approximately 30 – 70% of wave attenuation was found over a short distance of less than 30 m or a rate of 0.01 – 0.035 m^{-1} (Bao, 2011; Magi et al., 1996; Vo-Luong & Massel, 2006). Such a high rate, however, was not observed in other mangroves (0.002 – 0.012 m^{-1}) (Horstman et al., 2014; Mazda et al., 1997a; Quartel et al., 2007). The difference in the wave reduction rate at different mangroves could be the result of topography, incident wave height, and vegetation characteristics. For example, the relatively lower wave attenuation rate (0.002 m^{-1}) observed within the vegetated areas in Tong Kin delta, Vietnam was mainly due to the absence of prop roots or pneumatophores for *Kandelia candel*. The absence of a dense root structure reduces obstruction of water flow and lowers the wave energy dissipation.

Shortcomings of previous wave attenuation studies

- A lack of studies in disturbed mangroves

A majority of the studies were carried out in Vietnam, Thailand, Japan, and Australia (Bao, 2011; Horstman et al., 2014; Magi et al., 1996; Mazda et al., 2006; Mazda et al., 1997a; Nguyen, 2013; Quartel et al., 2007). Most of these mangroves are natural or replanted mangroves. No studies were conducted in the disturbed mangroves, which are usually narrower in width, less dense, and different in terms of forest structure (Allen et al., 2001; Phan et al., 2014).

- Paucity of vegetation parameter data

Vegetation is one of the main wave attenuation factors. Understanding the influence of the vegetation parameters on wave attenuation is instructive in uncovering the underlying physical processes. However, most of the field studies have only qualitatively described the vegetation parameters (Magi et al., 1996; Nguyen, 2013; Quartel et al., 2007; Vo-Luong & Massel, 2006). There are a few exceptions nevertheless, Mazda et al. (1997b) and Horstman et al. (2014) have measured the vegetation counts and vegetation roots, stems, and branches, and converted these data into cross-sections of vegetation cover. The cross-sections of vegetation cover were then used to investigate the relationship between vegetation structure and density with wave attenuation extent observed. Nevertheless, some parameters, such as the spatial distribution of mangrove trees, were still lacking or were not included in these studies.

- Spatial distribution of vegetation

The spatial distribution of vegetation creates a density variation within the vegetation field, affecting the wave energy dissipation by frictional force,

reflection, turbulence, refraction within the mangrove forest. In the field studies, the wave height/energy measurement collected along transects has reflected the combined effects of spatial density variation and other physical processes generated from wave-vegetation interactions. However, due to the lack of spatial vegetation data as well as the complexity in quantifying effects of each energy dissipation process, not all physical processes were quantified in these studies. The spatial distribution of vegetation field could be more important in a disturbed mangrove forest, especially in the presence of natural and artificial geomorphological features that could further complicate wave transformation in the horizontal direction.

- Range of meteorological events studied

Most of the field studies described above were conducted during non-storm periods. This is mainly due to the fact that occurrence of storms is hard to predict, although it is not entirely impossible (Zhang et al., 2012). The risk of compromising on fieldwork safety during storms and the loss of equipment are also a concern (Granek & Ruttenberg, 2007). The wave attenuation ability and the physical processes involved could vary in different storm events. As shown by Horstman et al. (2014), higher wave attenuation during storms was partly the result of higher incident wave heights and the occurrence of wave breaking processes. However, only two field studies have actually measured the wave attenuation during storms (Horstman et al., 2014; Mazda et al., 2006). Even in these two studies, the measurements were carried out in a small-scale storm events. The maximum wave height recorded in these studies remained low, approximately 16 cm and 30 cm respectively.

Table 2.1 Overview of laboratory, field and modelling studies on mangrove wave attenuation and hydrodynamic changes.

Study sites	Methods/ approaches	Vegetation types	Hydrodynamic effect/ wave attenuation rate	Influencing factors	References
Laboratory studies					
-	Electromagnetic flowmeter and 3D acoustic doppler velocimeter (ADV)/ scenarios of flow rates and water depths	*Rhizophora* (root and trunk)	≈50% flow velocity reduction when roots were submerged; ≈ 75% flow velocity reduction when ¾ or a whole tree was submerged	Water level, vegetation density, mangrove structure	Zhang et al., 2015b
-	Pressure transducers and wave gauges/ scenarios of tsunami flow conditions (solitary wave and tsunami bore) and breaking/non-breaking waves	Parameterized *Rhizophora* (root and trunk)	Solitary wave transmission (Kt): 0.53 – 0.992 in non-breaking waves and 0.34 – 0.94 in breaking waves; Kt in tsunami bore: 0.24 – 0.5 for 1.5 m forest width and 0.1 – 0.25 for 3 m forest width	Foreshore, forest width, incident wave height, water depth	Husrin et al., 2012; Strusińska-Correia et al., 2013
-	Velocity measuring device/ scenarios of mangrove forest with different vegetation density and stem diameter	*Rhizophora* (root)	Velocity in the creek 51 – 191% increases with 220 m^{-2} density and 21 – 106% with 110 m^{-2}; decreases in water depth of 15 -25% in high flow condition and 2 – 10% in low flow	Vegetation density, stem diameter, flow velocity	Struve et al., 2003
-	Elevation, current and pressure sensors/ scenarios of high and low wave heights across	Generic vegetation model with root, trunk and canopy	≈ 25 – 60% of wave height reduction by vegetation (porosity 0.964 – 0.973);	Porosity/density	Harada et al., 2002

	vegetation and artificial permeable structures		≈ 70 – 75% wave height reduction by artificial structures (porosity 0.36 – 0.75)		
Field studies					
Palian, Thailand	High and low frequency pressure sensors buried at locations along transects	*Avicennia* at fringe mangrove and *Rhizophora* at the back mangrove	0.0032 – 0.012 m^{-1}	Vegetation density, vegetation type, mangrove structure, incident wave height	Horstman et al., 2014
Kantang, Thailand	High and low frequency pressure sensors buried at locations along transects	*Avicennia* at fringe mangrove and *Rhizophora* at the back mangrove	0.0024 – 0.0061 m^{-1}; 0.0058 m^{-1} during storm	Vegetation density, vegetation type, mangrove structure, incident wave height	Horstman et al., 2014
Kien Giang coast, Vietnam	Manual/visual measurement using fixed poles along transects	Three dominant species: *Avicennia alba*, *Sonneratia alba* and *Rhizophora apiculata*	≈ 90% of wave height reduction in transects with mangroves and breakwaters; ≈ 60% of wave height reduction in open areas	Vegetation density, incident wave height, mangrove structure, canopy closure	Nguyen, 2013
Red River delta, Vietnam	Manual measurement of wave height by people standing along transects	Six dominant species: *Rhizophora mucronata, Sonneratia caseolaris, Sonneratia griffithii, Aegiceras corniculatum, Avicennia marina* and *Kandelia candel*	0.0055 – 0.01 m^{-1}	Vegetation density, incident wave height, mangrove structure, canopy closure	Bao, 2011
Can Gio, Vietnam	Manual measurement of wave height by people standing along transects	Six dominant species: *R. mucronata, S. caseolaris, S. griffithii, A. corniculatum, A. marina* and *K. candel*	0.017 m^{-1}	Vegetation density, incident wave height, mangrove structure, canopy closure	Bao, 2011

Red river delta, Vietnam	Pressure sensors and electromagnetic flow devices attached to tripod and installed along transects	Dominated by *K. candel* with some *Bruguiera* spp. and *A. marina*	0.004 – 0.012 m^{-1} within mangrove; 0.0005 – 0.002 m^{-1} outside of mangroves	Water depth, cross section vegetation cover, mangrove type	Quartel et al., 2007
Can Gio, Vietnam	Pressure sensors installed above 1 cm sea bed along transects	*Avicennia* sp. and *Rhizophora* sp. in the first 100m; mainly *Rhizophora* sp. at back mangroves	Wave energy reduction of 50 – 70% within 20 m	Water depth and vegetation structure	Vo-Luong & Massel, 2006
Vinh Quang, Vietnam	RMD-type wave Recorders	Predominantly *Sonneratia* sp.	0.001 – 0.006 m^{-1} within mangroves; 0.001 – 0.002 m^{-1} at non-vegetated area	Water depth, incident wave height, vegetation structure and condition	Mazda et al., 2006
Cocoa Creek, Australia	Wave gauges and pressure sensors along transects	Dominated by *R. stylosa*, *Aegiceras* sp. and *Ceriops* sp.	Energy transmission factor = 0.45 – 0.80 over 160 m	Water depth, distance of wave propagation in the mangrove	Brinkman et al., 1997; Brinkman, 2006
Nadara river, Japan	Wave gauges and pressure sensors along transects	Dominated by *Bruguiera gymnorrhiza*	Energy transmission factor = 0.9 – 1.0 over 40 m	Water depth, distance of wave propagation in the mangrove	Brinkman et al., 1997; Brinkman, 2006
Oonoonba, Australia	Wave gauges and pressure sensors along transects	Dominated by *Sonneratia* sp. and *Rhizophora* sp.	Energy transmission factor = 0.15 – 0.75 over 40 m	Water depth, distance of wave propagation in the mangrove	Brinkman, 2006

Tong King delta, Vietnam	Water level gauges and electromagnetic current meters installed 2 cm above sea bed along transects	Replanted *K. candel*	0.01 – 0.22 per 100 m	Vegetation density, mangrove structure, mangrove age	Mazda et al., 1997a
Shiira river, Japan	RMD-type wave Recorders	Dominated by *R. stylosa*	0.45 – 0.85 per 25 m within mangroves; 0.05 – 0.06 per 25 m at non-vegetated area	Vegetation density, type, age and width; incident wave height and water depth	Magi et al., 1996
Modelling studies					
Ben Tre province, Vietnam	SWAN-VEG (Stimulating Waves Nearshore + vegetation structural parameters)	Replanted forest dominated by *Rhizophora* sp. and naturally regenerated area dominated by *Avicennia* sp.	60% wave height reduction in replanted forest; 40% in naturally regenerated forest; wave height reduction decreases from 60% to -4% when vegetation cover reduces from 70% to 0%; wave height reduction decreases from 46% to 21 – 29% when forest width decreases from 1.5 km to 0.5 km	Mangrove width, mangrove density, mangrove type	Cuc et al., 2015
Merritt Island National Wildlife Refuge (MINWR), Florida, USA	Integrated Valuation of Ecosystem Services and Tradeoffs (InVEST) model for Coastal Protection	*R. mangle*, *A. germinans* and *Laguncularia racemosa*	48.5 ± 1.4 m and 114.4 ± 2.9 m of mangrove cross-shore extent required to reduce 75% and 90% incident wave height respectively	Mangrove width, incident wave height, mangrove structure	Doughty, 2015

Kien Giang, Vietnam	Regression model developed based on field measurement by Bao (2011)	Three dominant species: *A. alba*, *S. alba* and *R. apiculata*	≈ 75% less mangrove width required for coastal protection when density increases from 3500 stems ha^{-1} to 7000 stems ha^{-1}	Vegetation density, mangrove structure, mangrove width, incident wave height	Nguyen, 2013
Cat Ba/ Can Gio/ Hoang Tan/ Thai Binh/ Tien Long, Vietnam	Regression model developed based on field studies at Red River delta and Can Gio, Vietnam	Dominant species at Cat Ba: *A. corniculatum*; Can Gio: *A. marina*, *R. mucronata*, *S. caseolaris*; Hoang Tan: *S. caseolaris; A. marina*, *A. corniculatum*; Thai Binh: *K. candel*, *A. corniculatum*; Tien Lang: *S. caseolaris*	Other than Can Gio, existing mangrove forests have less than required mangrove width (> 120 m); Can Gio forest offers moderate to strong protection	Vegetation density, mangrove structure, mangrove width, incident wave height	Bao, 2011
Kanika Sands, Sri Lanka	SWAN-VEG	*R. mucronata*	≈ 90% wave height reduction within 1000 m ; 90% less vegetation density decreases the reduction from > 90% to 70% in 300 m	Vegetation density, vegetation structure	Narayan, 2009
Pakarang Cape, Thailand	Combination of linear shallow-water wave theory and nonlinear shallow water wave theory with parameterized bottom friction	*Rhizophora* sp. and *Bruguiera* sp.	≈ 30% of tsunami height reduction; mangrove forest effective at 3 m inundation; 50% and 100% vegetation destroyed at 4.5 m and 6 m inundation respectively	Water level, tree size	Yanagisawa et al., 2009

2.2.3 Modelling studies of wave attenuation

Laboratory and field studies are limited by their ability to study multiple scenarios of different physical, vegetation and hydrodynamic settings. This shortcoming can be overcome using modelling studies. Two common modelling approaches have been utilized to study wave attenuation of mangroves. The bottom friction or bed roughness approach simulates the physical processes within a mangrove forest using calibrated bottom friction parameters (Van Rijn, 1989). The calibration of the bottom friction parameters requires reliable site-specific data in order to obtain accurate mangrove and bottom sediment representation at each study site (Broekema, 2013; Burger, 2005). Another popular approach uses parameterized vegetation structure, often assumes the shape of cylinders, to calculate the dissipation of wave energy within mangrove forests (Dalrymple et al., 1984; Kobayashi et al., 1993; Mendez & Losada, 2004; Vo-Luong & Massel, 2008). Other wave energy dissipation mechanisms such as wave breaking and friction force were incorporated to calculate the wave attenuation extent. This approach has been employed in some models such as SWAN and nearshore wave evolution model within the InVEST modelling suite (Guannel et al., 2015; Suzuki et al., 2012).

Using vertical schematization to account for vegetation structure, a number of modelling studies have quantified wave attenuation against mangrove extent (Cuc et al., 2015; Doughty, 2015; Narayan, 2009; Yanagisawa et al., 2009). Studies on wave attenuation in Sri Lanka and Florida, USA mangroves during storm events found that a 90% reduction in wave height was achieved in a distance of 1 – 1.3 km (Doughty, 2015; Narayan, 2009). Other studies showed lower wave attenuation rates (Cuc et al., 2015; Yanagisawa et al., 2009). In Vietnam, 40 – 60% reduction of wave height were found over 1.5 km of mangrove forest (Cuc et al., 2015). When tested in 3-m tsunami

waves, relatively lower wave height reductions of 26% and 45% were found 400 m and 1000 m into mangrove forests, respectively (Yanagisawa et al., 2009). The attenuation rates in these studies were not linear. Higher wave attenuation was usually observed at the front of the mangroves and decreases as the waves propagate further into the mangrove forest. For example, approximately 50 – 80% of wave height reduction was found within 400 m of mangrove forest with medium to very high density. The wave height reduction becomes almost flat after 800 m into the mangroves (Figure 2.2) (Narayan, 2009). In Florida, USA, 75% of the wave height was reduced in the first 48.5 m while an additional 15% was reduced within the next 80 m (Doughty, 2015). The non-linearity in wave attenuation pattern in coastal vegetation was highlighted by Koch et al. (2009). Such non-linearity was suggested to be the result of the proportion of vegetation structure submerged and the spatial distribution of coastal vegetation (Barbier et al., 2008; Koch et al., 2009).

Figure 2.2 Transmitted wave height across mangrove forest of different densities. Hs = significant wave height. (Source: Narayan, 2009)

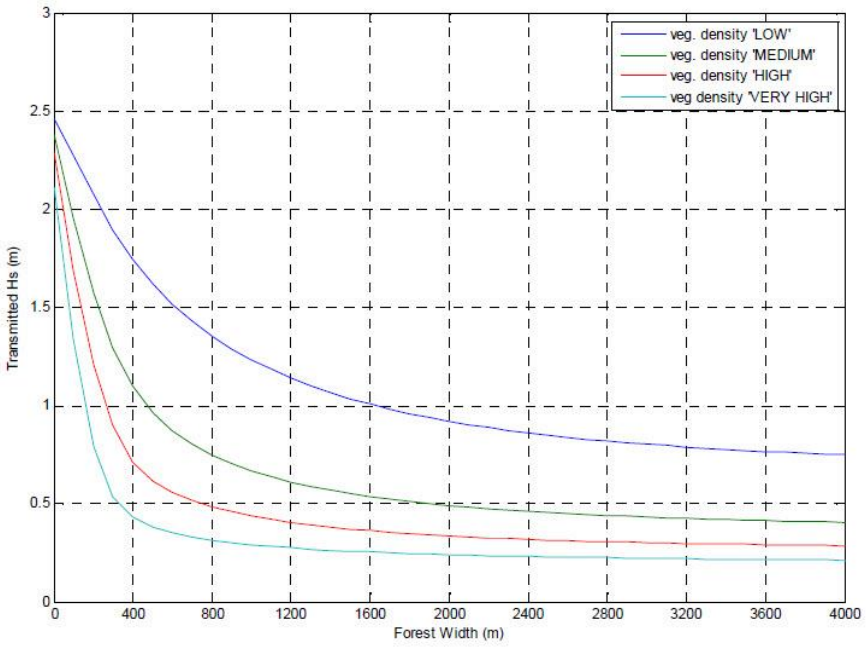

Modelling studies could be a useful coastal management planning tool in studying the effects of different coastal management options (Bao, 2011; Narayan, 2009; Nguyen, 2013). For example, the statistical model developed by Bao (2011), which was later utilized by Nguyen (2013), identified the relationships between wave height reduction and various factors including incident wave height, average tree height, tree density, and canopy closure for mangrove forests in Vietnam. Using this statistical model, a management recommendation for coastal protection (critical mangrove width) was inferred based on the existing mangrove condition and local storm history. In Sri Lanka, Narayan (2009) investigated the effects of hypothetical mangrove extension and thinning. The study found that a mangrove belt of only 300 m, instead of the existing 1.5 km, was sufficient to protect the Dhamra Port from cyclones. Additional coastal engineering options were simulated to test their effectiveness in coastal protection improvement (Narayan, 2009).

Shortcoming of modelling studies

- Simplification of complex processes

  Modelling studies usually involve certain simplifications (Cuc et al., 2015; Suzuki et al., 2012). For example, Narayan (2010) assumed the presence and distribution of mangrove species at Kanika Sands based on a desktop study of local topography and general elevation distribution of mangrove species. Yanagisawa et al. (2009), on the other hand, simply used bottom friction coefficients to represent the effects of a higher *Rhizophora* root density. A number of studies also used bulk drag coefficients to represent the physical processes associated to the spatial arrangement of vegetation such as vortex pattern generated as the water flows through a vegetation field (Cuc et al., 2015; Guannel et al., 2015; Narayan, 2009; Suzuki et al., 2012).

- Exclusion of processes in model setup

Due to the model limitations, some of the effects observed in the laboratory and field studies such as turbulence and inertia force could not be represented (Cuc et al., 2015; Mendez & Losada, 2004; Suzuki et al., 2012). As shown in laboratory studies, turbulence could cause the dissipation of energy in the water column, directly or indirectly (Strusińska-Correia et al., 2013; Zhang et al., 2015b). The inertia force could momentarily increase the wave force especially during extreme events such as tsunamis (Harada, 2003). In addition, most existing numerical models did not include the swaying motion of vegetation. Such effect could potentially be important when mangrove canopies are inundated (Mazda et al., 2006). The exclusion of some physical processes was justified as their contribution to wave attenuation were deemed insignificant in most cases (Mendez & Losada, 2004).

2.3 Factors affecting wave attenuation within mangrove area

Most studies not only quantified the rate or magnitude of wave attenuation, but they also attempted to identify the physical processes and factors affecting wave attenuation function of mangroves. Although only a few studies have quantified vegetation parameters in detail, the findings in these studies have generated insights into the factors influencing the wave attenuation function of mangroves. The main factors include mangrove width, vegetation density, structures, and incident wave height (Mazda et al., 2006; McIvor et al., 2012; Spalding et al., 2014).

2.3.1 Mangrove width

Mangrove width, given their role in influencing wave attenuation, is important in the provisioning of coastal protection. According to a study on the protection function of

mangroves, statistical analyses showed that mangrove width was the main factor in reducing the damage incurred to the coastal villages hit by cyclone Odisha (Das & Vincent, 2009). The influence of mangrove width on wave attenuation was also highlighted in a tsunami laboratory experiment (Strusińska-Correia et al., 2013). The result showed 20 – 33% of the wave force was reduced in a forest model 0.75 m wide, and 66 – 86% for a forest width of 3 m (Strusińska-Correia et al., 2013). While the experiment has illustrated that an increase in mangrove width is associated to a higher wave energy reduction, the experiment has tested only for small magnitude of tsunami force over a laboratory-scale vegetation field. The translation of the findings to large-scale tsunami events should be further investigated in order to provide a more realistic the relationship between mangrove width and wave attenuation. Using a statistical model and local mangrove structural data, Nguyen (2013) found that a critical mangrove width of 80 – 177 m were required to offer sufficient coastal protection against wave height up to 3 m storms, highlighting the importance of mangrove width in coastal protection. The critical mangrove widths required vary across mangroves, and are dependent on various vegetation, coastal physical and hydrodynamic characteristics. Although site-specific vegetation data were used to devise the statistical relationship, the hydrodynamic data used were collected during low wave period. The critical mangrove widths recommended by Nguyen (2013) for large storms should be further studied.

Non-linearity in wave attenuation patterns should be considered when analyzing the effects of mangrove width on wave attenuation (Barbier et al., 2008; Koch et al., 2009). Such non-linearity in wave attenuation were observed in a number of field and modelling studies (Bao, 2011; Narayan, 2009). The non-linear pattern of wave attenuation suggests that the distance travelled by waves within a mangrove forest

might be a better indication of wave attenuation ability of mangroves, compared to mangrove width.

2.3.2 Mangrove density

Mangrove density is related to the amount of physical obstruction in the water column. A denser mangrove forest creates more drag through increased obstruction to the water flow. In a number of field studies, mangrove density was represented as the proportion occupancy proportion of physical tree structure at a certain height or a projected cross section perpendicular to the ground (Horstman et al., 2014; Mazda et al., 1997b; Vo-Luong & Massel, 2008). In a field study in Trang, Thailand, the vegetation occupied a proportion of 0.03 – 0.1 at 1 m above ground was found in a denser *Rhizophora*-dominated forest; while a sparser forest (dominated by *Sonneratia* and *Avicennia*) had only approximately 0.03 vegetation cover at corresponding height. Such difference in density resulted in 2 – 4 times higher wave attenuation rates in the denser forest (Horstman et al., 2014). In numerical studies, the effects of density on wave height reduction were tested using different mangrove thinning scenarios (Cuc et al., 2015; Narayan, 2009). For example, in a replanted mangrove forest dominated by *Rhizophora apiculata*, a reduction in vegetation cover rate from 70% to 50% and 35% yields a reduction in wave attenuation from 60% to 51% and 42% respectively (Cuc et al., 2015). The importance in understanding the mangrove density effect was highlighted in a study conducted at Kien Giang coast, Vietnam (Nguyen, 2013). The study suggested that the critical mangrove width required for coastal protection against historical storm events had to be more than doubled when the mangrove density was halved.

2.3.3 Mangrove structure

Biotic structures of different mangrove types can affect their wave attenuation ability (Hashim et al., 2013; McIvor et al., 2012; Spalding et al., 2014). The difference in the effects of mangrove structure is the most obvious when examining the wave attenuation effects of mangrove roots. In a study conducted within a *Sonneratia*-dominated mangrove forest, the wave height reduction rate was higher (0.006 m^{-1}) when pneumatophores were barely submerged, compared to (0.002 m^{-1}) when pneumatophores only occupied less than a quarter of water depth (Mazda et al., 2006). The root effects were more apparent when compared to observations in a *K. candel*-dominated forest (Mazda et al., 1997a). As *K. candel* does not has pneumatophores or prop roots, wave attenuation rate within the replanted *K. candel* mangrove forest was only 0.002 m^{-1}, three times lower than the *Sonneratia*-dominated mangrove forest (Mazda et al., 2006; Mazda et al., 1997a).

The effects of root structure was noticeably different for *Rhizophora* as the geometry of their prop roots is distinctly different compared to roots of other mangrove types (Figure 2.3). The geometry of the prop roots also leads to higher density, which in turn, results in higher wave attenuation (section 2.3.2). In a flume study, a denser *Rhizophora* root structure near the bottom was found to reduce approximately 50 – 75% of flow velocity compared to less dense upper section of the prop roots (Zhang et al., 2015b). The investigation of root effect was not as straightforward in a natural setting. By comparing the measurements from Cocoa Creek and Oonoonba, Australia and Nadara River, Japan, the mangroves dominated by *Rhizophora stylosa* showed a relatively low wave height reduction (0.0019 m^{-1}); while the mangroves at Oonoonba, Australia, with mixed *Rhizophora* and *Sonneratia*, showed the highest wave height reduction among the three sites (approximately 0.024 m^{-1}) (Brinkman, 2006; Brinkman et al., 1997). The

difference in wave attenuation was also affected by the higher wave height at Oonoonba, Australia. Higher wave height increased the submerged portion of roots, hence, increasing the wave attenuation rate (Brinkman, 2006; Brinkman et al., 1997). Other complex physical processes, such as wave reflection between dense roots and wave shoaling, were also suggested as contributors to the wave attenuation observed.

Figure 2.3 Example of structural difference between *Rhizophora* prop root (left) and *Bruguiera* knee roots (right).

In general, the effects of trunks on wave attenuation are considered less pronounced compared to roots. The wave attenuation study conducted in a *K. candel*-dominated mangrove forest in Red River delta, Vietnam could be used to infer the effects of trunks on wave energy dissipation (Quartel et al., 2007). In the study, the water flow resistance increases as the water depth increases. This is the result of an increased projected cross-sectional area obstructing the water flow. The physical process indicated in this finding is consistent with previous studies on water flow obstruction by projected obstruction area of mangrove structure (Massel et al., 1999; Mazda et al., 1997b; Quartel et al., 2007; Vo-Luong & Massel, 2006).

The canopy, on the other hand, has a high potential for wave attenuation (Mazda et al., 2006; McIvor et al., 2012). The dense foliage increases flow obstruction and friction, resulting in wave energy dissipation (McIvor et al., 2012; Spalding et al., 2014). Mazda et al. (2006) found that when water level reaches the mangrove canopy, the wave height reduction was approximately 50% within 100 m, or a reduction rate of approximately 0.006 m^{-1}. The effects of canopy were also suggested by Quartel et al. (2007) to have caused the exponential increase in flow resistance. However, the canopy flow resistance was not quantified.

2.3.4 Incident waves

Incident wave height could also influence the wave attenuation rate. In a study conducted in Vinh Quang, Vietnam, a linear relationship between rate of wave height reduction and incident wave height was found in a mangrove dominated by *Sonneratia* spp. (Mazda et al., 2006). This relationship was based on two conditions: i) the water depth is sufficiently high so the bottom friction does not affect the wave height; and ii) the water level is sufficiently high to reach the branches and leaves. The same relationship was not observed in non-vegetated areas and when the water level does not reach the canopy (Mazda et al., 2006). In another study in Thailand, the wave attenuation rate during a storm period (higher waves) was approximately three times the rate of non-storm period within the same mangrove zone (Horstman et al., 2014). The higher wave attenuation was the result of wave breaking processes, as the higher waves propagated through shallow water (Horstman et al., 2014). The effects of wave breaking were also highlighted as the main mechanism in wave attenuation through a tsunami experiment (Strusińska-Correia et al., 2013).

2.4 Limitations of current studies

The laboratory, field, and modelling studies have provided evidence on the wave attenuation ability of mangroves. As shown in the studies, significant wave attenuation could be achieved over short distances (Bao, 2011; Magi et al., 1996; Vo-Luong & Massel, 2006). However, these studies were mainly conducted in natural or larger mangroves. The variability of mangrove wave attenuation rates found in field and modelling studies also suggested the site-specific nature of mangrove wave attenuation ability. Moreover, the lack of detailed vegetation parameters and other wave energy dissipation factors have limited the analyses. Understanding the site-specific wave attenuation extent and the influencing factors could improve the coastal management planning process (Bao, 2011; Narayan, 2009; Nguyen, 2013). The study of urban disturbed mangroves could help to understand the wave attenuation function in such setting and the implications on coastal management planning.

3 Study site description

3.1 Singapore's climate

Singapore is an island state with a total land area of approximately 719.1 km^2, comprising the main Singapore Island, Pulau Ubin and Pulau Tekong in the northeast, and other islands in the south (Department of Statistics Singapore, 2016). The climate in Singapore is characterized by two monsoon seasons, the Northeast Monsoon and the Southwest Monsoon. The Northeast Monsoon (December to early March) usually brings substantial rainfall and strong winds (up to 30 – 40 km hr^{-1}) in the northeasterly direction. The Southwest Monsoon (June to September) is usually accompanied by southwesterly winds. Sumatra squalls are common during the Southwest Monsoon season, often accompanied by strong winds (up to 26 m/s maximum gusts was recorded) and heavy rain (National Environment Agency, 2016).

No categorized cyclones or tropical storms have made landfall in Singapore because of its proximity to the equator. The closest tropical storm that formed near Singapore was tropical storm Vamei, which made landfall along the southeastern coast of Peninsular Malaysia, just 60 km north of Singapore, in December 2001. Tropical storm Vamei was a rare event as it was the first tropical storm that formed at such close proximity to the equator. It brought heavy precipitation and caused severe landslides and loss of life in Malaysia and disruption to Singapore's Changi Airport. In the aftermath of Vamei, a study on its formation estimated the probability of occurrence of such an event to be once in 100 – 400 years (Chang, 2003).

3.2 Hydrodynamic conditions in Singapore waters

Singapore waters exhibit a semi-diurnal tidal pattern. The tidal pattern is influenced by tidal signals from both the Indian Ocean and the Pacific Ocean (Chen et al., 2005). The presence of various small islands, complex coastal geometries and varying bathymetry complicate the tidal dynamics in Singapore waters, as well as spatial variations in tidal magnitudes (Chan et al., 2006). The neighbouring landmasses of Malaysia and Indonesia limit the fetch distance and prevent the generation of high waves in the local waters. The longest fetch distance in the northeasterly direction from Taiwan to the South China Sea rarely generates sufficient waves as the strongest winds and the longest fetch direction seldom coincide (Chia et al., 1988). During the Southwest Monsoon, strong gusts from Sumatra squalls sometimes generate waves as high as one meter. However, the waves generated are usually dissipated by the shallow reefs and islands around Singapore.

Strong winds accompanying the monsoon season could generate another phenomenon called the sea level anomaly (SLA) (Tkalich et al., 2013). SLA is the variation of sea level generated from large scale meteorological and oceanographic factors such as wind, atmospheric pressure, sea surface temperature, and fresh water run-off (Tkalich et al., 2009). In this region, SLA is strongly correlated with monsoon winds during both Northeast and Southwest Monsoon seasons (Tkalich et al., 2009). An approximately 20 – 30 cm seasonal mean sea level deviation could be observed during the Northeast Monsoon when the wind blows along the long northeasterly fetch. An extreme historical SLA of more than 80 cm above mean sea level has been recorded (Tkalich et al., 2009)

3.3 Mangroves in Singapore

Being home to 56 of the estimated 70 known mangrove species worldwide, Southeast Asia has the highest mangrove species richness globally (Polidoro et al., 2010). In Singapore, 35 mangrove species have been recorded (Yang et al., 2011).

Singapore has a long history of mangrove clearance due to human activities. Some mangrove loss was experienced during Singapore's colonial period (1819 – 1965) for charcoal and firewood production and land reclamation (Hilton & Manning, 1995; Wee & Corlett, 1986). The mangrove loss accelerated after independence (1965), with more than 50% of mangrove cover lost due to coastal development and land reclamation (Hilton & Manning, 1995; Lai et al., 2015; Yee et al., 2010). River damming for coastal freshwater reservoirs (Ziegler et al., 2014) was another contributor to mangrove loss (Friess et al., 2012b). Currently, mangrove forests only cover less than 1% of Singapore's total land area (Yang et al., 2011). The remaining mangrove forests in Singapore are projected to lose a further 33% by 2030 based on published government development plan (Lai et al., 2015). Most of the current surviving mangroves are in fragments or as fringe mangroves, with more than half located on offshore islands. The mangrove patches offshore of Singapore are found on Pulau Ubin (149 ha), Pulau Tekong (144 ha), Pulau Pawai (42 ha), Pulau Semakau (39 ha), Pulau Senang (26 ha) and Pulau Seletar (11 ha). On mainland Singapore, the largest mangrove patch is situated in Sungei Buloh Wetland Reserve (SBWR) with 202 ha in size, after the inclusion of Kranji nature trail in 2015. It was followed by Western catchment (92 ha), Sungei Khatib Bongsu (26 ha) and Mandai mangroves (20 ha) (Lai et al., 2015; Yang et al., 2011).

Four mangroves sites, namely Mandai mangroves (MAN), Sungei Buloh Wetland Reserve (BUL), Pulau Ubin (UBI) and Pulau Tekong (TEK) along the northern coast of Singapore were studied (Figure 3.1). The sites were chosen based on their sizes and locations (two on each side of the Johor Straits, separated by Singapore-Johor causeway). The mangroves on the eastern side of Johor Straits (UBI and TEK) are bigger in size compared to MAN and BUL. All of the sites have a history of disturbance from various human activities. Parts of the Sungei Buloh Wetland Reserve and Pulau Ubin were deforested for aquacultural use. Although it has since been abandoned, the shape of the ponds, sluice gates and dikes are still visible. Mangroves have started to recolonize some of these abandoned aquaculture ponds, within which sparse mangrove vegetation was observed. Mandai mangrove is located approximately 3 km to the east of Sungei Buloh Wetland Reserve. It used to be connected to Sungei Buloh Wetland Reserve before shrimp farming activities, development of Kranji industrial estate and construction of Kranji reservoir destructed the fringing mangroves connecting the two mangrove patches. Mandai mangrove has a history of human inhabitation. It used to support three villages, namely Kampong Mandai Besar, Kampong Mandai Kechil and Kampong Loring Fatimah until the government relocated the villagers into public housing in the 1980s (Friess et al., 2012b). Pulau Tekong has been used for military training purposes. The relatively less human presence has promoted an increase of mangrove extent, from 73 ha to 162 ha between 1993 and 2002 (Lai et al., 2015). Nevertheless, the mangroves on Pulau Tekong were still affected by coastal erosion and land reclamation around the island.

Field data collection was conducted at all sites except TEK due to the military activities on the island, so access is heavily restricted. In addition to the study sites, vegetation characteristics from Pasir Ris Park (RIS) and Sungei Khatib Bongsu (KHA) were also

collected to provide additional data for better representation of mangrove vegetation along the northern coast. RIS and KHA were not included in the scope of this study as they are geographically sheltered and not exposed directly to the waves in the Johor Straits.

Figure 3.1 The spatial distribution of mangroves on Singapore's coast (Tan & Friess, *unpublished data*). Red box indicates the study site; blue box indicates the additional sites for vegetation characteristics data collection; the number in the bracket denotes the size of the mangroves patches studied.

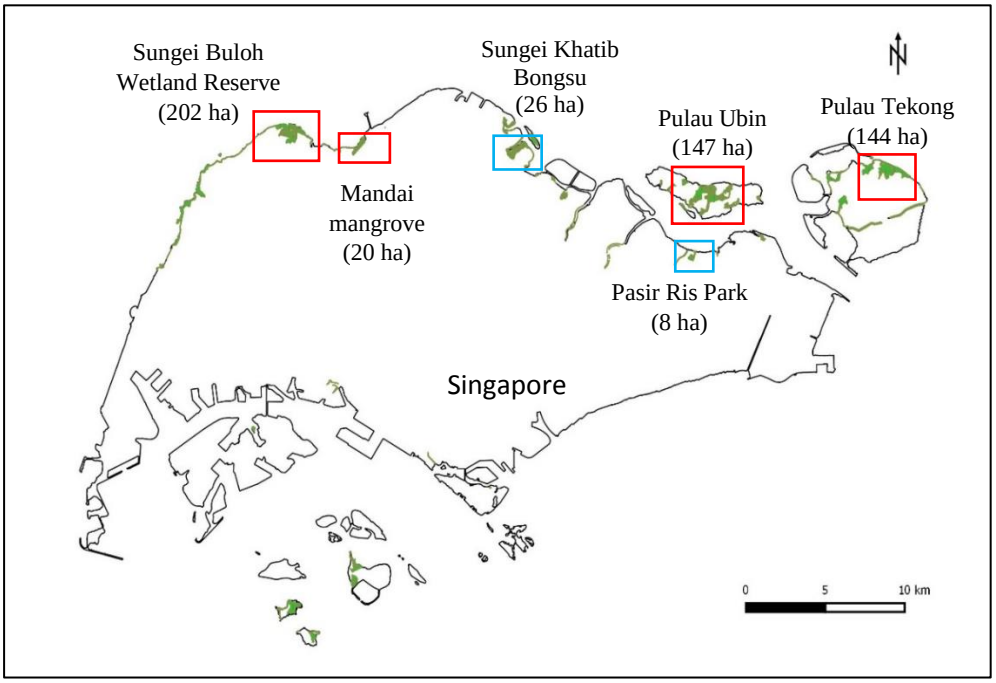

4 Materials and methods

4.1 Overview

A modelling approach was employed to simulate the nearshore wave evolution as the waves propagate towards the shore and into the mangroves. Field, desktop, and laboratory studies were conducted to collect vegetation, coastal physical and hydrodynamic data. The data types and formats to be used as model inputs are listed in Table 4.1. Hydrodynamic conditions were used as model settings for the simulation of wave attenuation extent. Wave attenuation and its influencing factors were then analysed using simulation outcomes together with vegetation, coastal physical, and hydrodynamic data. Figure 4.1 describes the work flow in this study.

Figure 4.1 Schematic diagram of the work flow in this study.

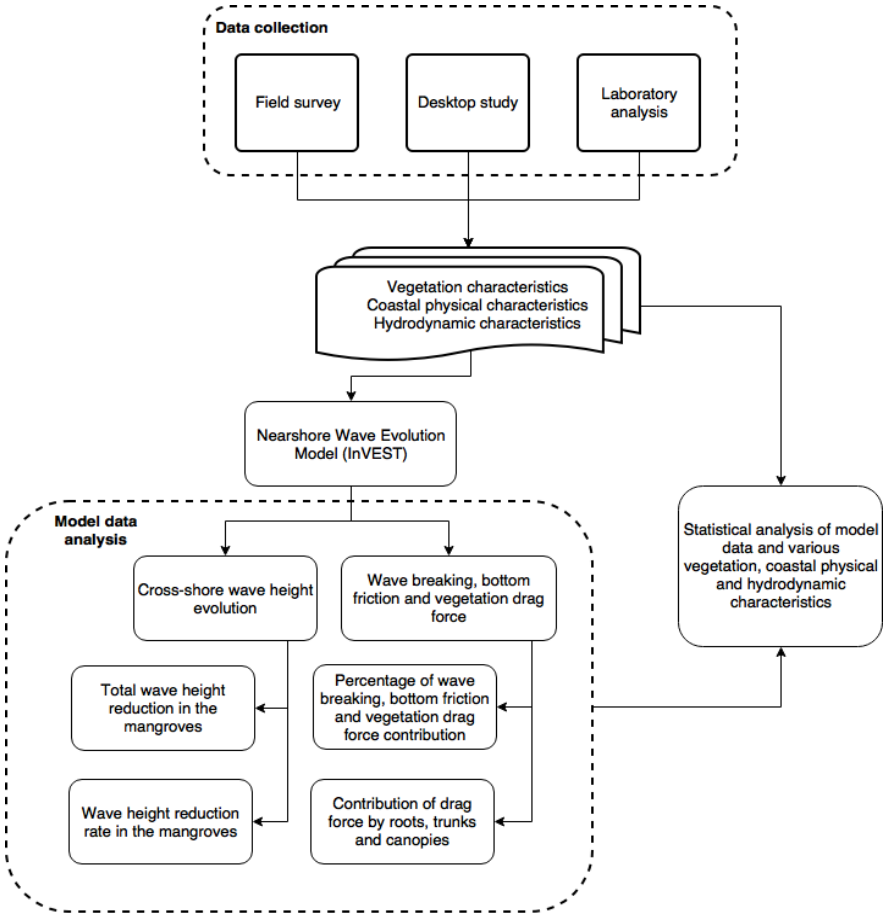

Table 4.1 Data input, format and source used for the nearshore wave evolution model.

Input parameters	Data input	Unit	Data source	Section
Vegetation characteristics				
Vegetation structure	Average height and diameter of mangrove tree roots, trunk and canopy at each model transect	M	Field study	4.2.1.1
Mangrove density	Average density of mangrove tree and roots at each model transect	m^{-2}	Field study	4.2.1.2
Mangrove extent	Mangrove width at each model transect	M	Field study	4.2.1.3
Coastal physical characteristics				
Cross-shore profile	Bathymetry	m	Singaporean Nautical Charts	4.2.2.1
	Mangrove zone elevation changes	m	Field study	4.2.2.1
Sediment size	Average sediment size within each model transect	mm	Field study and laboratory analysis	4.2.2.2
Bulk density	Average bulk density within each model transect	kg m^{-3}	Field study and laboratory analysis	4.2.2.2
Erosion coefficient	-	-	Default value	-
Hydrodynamic characteristics				
Water level	Mean Sea Level (MSL) and Mean High Water (MHW)	m	MPA tidal chart	4.2.3.1
Wave height	Wave height under average and extreme hydrodynamic condition	m	Singapore Regional Model (SRM) wave simulations	4.2.3.2
Wave period	Wave height under average and extreme hydrodynamic condition	s	Singapore Regional Model (SRM) wave simulations	4.2.3.2

Surge elevation	High tides, storm surge and SLA with reference to MSL	m	MPA tidal chart, Singapore Regional Model (SRM) wave simulations	4.2.3.1; 4.2.3.2
Storm duration	Duration of the natural forcing to be applied	hour	Default value	-
Model spatial resolution	Spatial resolution of the model	m	Default value	-

4.2 Data collection

4.2.1 Vegetation characteristics

4.2.1.1 Vegetation diversity and tree structure

Field surveys were conducted from December 2014 to March 2015. Transects perpendicular to the coastline were set up at each study site. Depending on the mangrove cross-shore distance, several 7-meter radius plots located at regular intervals were surveyed. Vegetation characteristics were measured within each plot. A total of 1300 trees were recorded in 59 plots along 17 transects across four sites. Figure 4.2 shows an overview of the parameters measured.

Figure 4.2 Overview of vegetation parameters, soil parameters and cross-shore elevation profile collected in the field study.

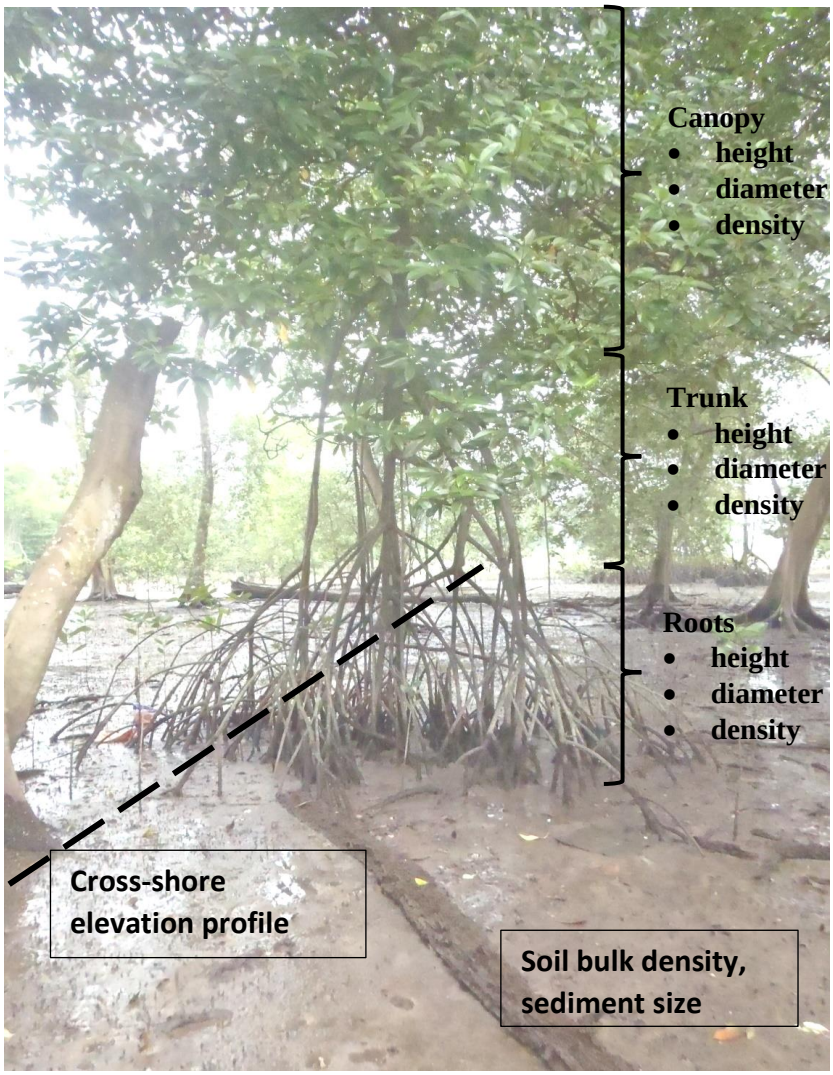

Transect length was dependent on the cross-shore length of mangrove forest. Each transect starts at the land edge and ends at the seaward edge of the mangrove. At some transects, the land edge of the mangroves was not accessible due to high density of shrubs and *Taliparitti tiliaceum*. Along each transect, several 7-meter radius plots were established at regular intervals for the measurement of vegetation and soil characteristics (Table 4.2; Figure 4.3). The number of transects per site and the number of plots per transect were dependent on the length of the coastline, length of transects and homogeneity of vegetation and geomorphology. At UBI where the size of mangrove forest is bigger but vegetation relatively homogenous, the number of transects were lower and the plots were further apart from one another. At BUL and MAN, on the other hand, the more heterogeneous mangrove vegetation and sediment characteristics were better represented with more plots of shorter plot intervals. In addition, two 0.5 m x 0.5 m subplots were randomly placed on both halves of each 7-meter radius plot for root measurement and soil sample collection.

Table 4.2 Field sites, total number and intervals of transects; and number and plot intervals at each site.

Sites	Number of transects	Transect intervals	Number of plots	Plot intervals
BUL	5	100 – 150m	15	30 – 60m
MAN	5	≈100m	16	30 – 60m
UBI	4	100 – 500m	18	≈200m
RIS*	3	30 – 60m	10	50 – 100m

*Additional site for vegetation data collection

Figure 4.3 Plan view of the layout of 7-meter radius plots for vegetation survey and 0.5 m x 0.5 m subplots for pneumatophores and soil samples collection.

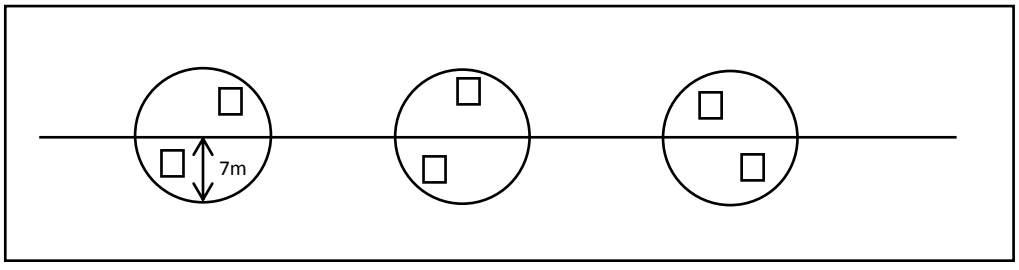

Within each 7-meter plot, the diameter-at-breast-height (DBH) for all trees with a DBH larger than 5 cm were measured, similar to Kauffman and Donato (2012). Each tree was identified to genus level (species-level information was not required) and its DBH measured using a calibrated DBH tape. For trees located at the edge of a plot, only those with more than 50% basal area located within the plot were surveyed. Fallen trees were surveyed when the roots of the tree were traceable to inside the plot. Dead trees, where their base was traceable to within the plot, were also included in the survey. The dead trees were included to account for their physical obstruction to the water flow and contribution to the wave attenuation. The diameter of a tree canopy was measured using a transect tape. The radius of tree canopy in two opposite directions was measured using the tree trunk as center of the canopy. The diameter of a tree is the sum of the radii measured.

Table 4.3 Total number of trees surveyed in all plots and number of trees with height measured.

Sites	**Number of plots**	**Number of trees measured**			**Number of trees with height measured**
		Alive	**Dead**	**Total**	
BUL	15	152	3	155	50
MAN	16	240	18	258	36
KHA	-	9	0	9	9
RIS	10	242	19	261	47
UBI	18	586	31	617	19
Total	59	1229	71	1300	161

Counts and types of pneumatophores within the 0.5 m x 0.5 m subplot were recorded (Figure 4.3). Roots of *Avicennia*, *Bruguiera* and *Sonneratia* were measured. For *Avicennia* and *Sonneratia*, the root diameter was measured at the middle section of the root using a caliper. For *Bruguiera*, given the slightly irregular root shape, the diameters of *Bruguiera*'s knee roots were determined by measuring at the middle

section of the roots at two directions and averaged. The root height of pneumatophores and knee roots was measured from the base to the tip using a ruler.

The height of tree trunk and tree canopy were measured using a Nikon Forestry Pro Laser Rangefinder 8381. For height measurements, the horizontal distance and the angle of difference between the observer and tree structure of interest were measured. Trigonometry was then used to calculate the height (Figure 4.4; Equation 1). Tree canopy height was measured from the lowest branch to the top of canopy for all genera. Trunk height measurement is slightly different between genera. For *Avicennia*, *Bruguiera* and *Sonneratia*, the height of tree trunk was measured from base to the lowest branch; whereas, for *Rhizophora*, the base of the trunk was measured at the highest prop roots. As height measurements are time consuming, not all trees surveyed were measured. The selection of trees for height measurement were based on i) a clear line of sight between the observer and the tree to be measured; and ii) the tree structure being measured could be visually identified confidently. Additional individuals were measured around the plots using the same selection criteria. Selective height measurement could introduce sampling bias. In order to minimize the bias associated to site-specific environmental conditions, such as forest composition, impact of nutrition, size of mangrove forest, forest density, etc., the tree heights were collected from all study sites. In addition, the tree heights were collected from trees of different ages (inferred from the DBH of trees) to minimize the height measurement bias associated with trees' maturity. Despite the measures taken, some bias might persist since the trees living in a very dense canopy, which could not be reliably measured, were not represented. In total, the height of 161 individuals were measured.

Figure 4.4 Example of measurement in the field survey for tree height calculation using trigonometry. Horizontal distance between observer and tree measured was determined. The angle between observer's eye level and the top as well as base of tree were recorded.

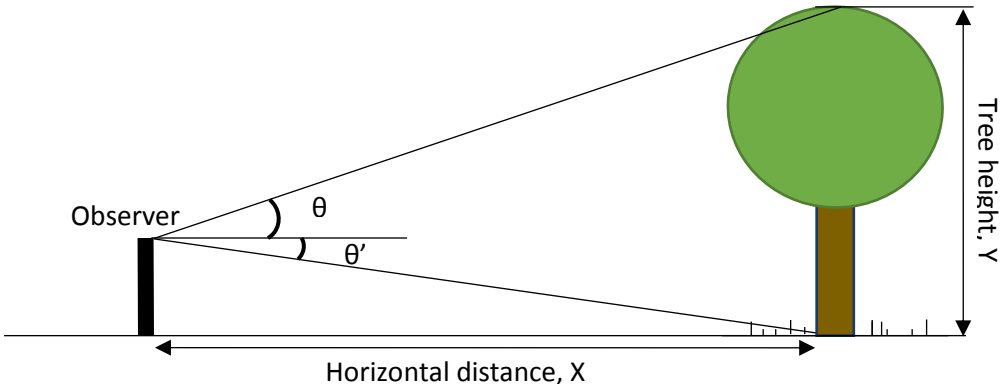

Equation 1 Elevation change, Y calculation using horizontal distance, X and angle θ

$$Y = X\ tan\ \theta + X\ tan\ \theta'$$

Figure 4.5 (a) Measuring the height of pneumatophores within each 0.5 m x 0.5 m subplot using a ruler and; (b) measuring the diameter of pneumatophores using a caliper.

The vegetation data collected were post-processed to the data format required as model inputs (Table 4.1). Only one set of vegetation parameters was required as inputs for each transect model. As such, vegetation parameters of the dominant genus within each transect was used. The dominant genus was defined as the genus with the highest percentage of individual recorded within each transect. For TEK, where field survey data was not available, the dominant genus was identified by pooling all trees measured in all sites.

Vegetation structure parameters for each of the four main genera, namely *Avicennia*, *Bruguiera*, *Rhizophora* and *Sonneratia* were calculated. For the root characteristics of *Avicennia*, *Bruguiera* and *Sonneratia*, average root height, diameter, and density were obtained from field surveys. The root characteristics of *Rhizophora* were adapted from Zhang et al. (2015b). For trunk diameter, average DBH was calculated for each genus. For the height of trunk, the height of canopy, and the diameter of canopy, simple linear regression was used to estimate tree canopy structure of each genus.

4.2.1.2 Mangrove density

The density for trunk and canopy were obtained by calculating the number of individual tree per meter square (Equation 2). The root counts and the dominant root types were recorded within each 0.5 m x 0.5 m subplot (Figure 4.3). The root density for each genus was calculated by averaging the root density of each subplot with the dominant root type (Equation 3).

Equation 2 Transect trunk and canopy density calculation

$$Density\ of\ trunk\ or\ canopy\ of\ a\ transect\ (m^{-2}) = \frac{Number\ of\ tree\ \ within\ a\ transect}{Total\ plot\ area\ within\ a\ transect\ (m^2)}$$

Equation 3 Root density calculation for each root type

$$Root\ density\ (m^{-2}) = \frac{\Sigma(\frac{Number\ of\ root\ within\ a\ subplot}{0.25\ m^2})}{Number\ of\ subplot}$$

4.2.1.3 Mangrove extent

Mangrove extent was analysed using existing remote sensing data, specifically Pleiades multispectral satellite imagery (dated from 2013) at a spatial resolution of 2 m. Feature classification was conducted using a Maximum Likelihood supervised classification algorithm (Tan & Friess, *unpublished data*). This was supplemented with 2013 – 14 imagery from Google Earth, where Pleiades was unavailable due to cloud cover or data restrictions. Mangrove extent for each transect was cross-checked by superimposing GPS coordinates of plots and mangrove extent coordinates recorded in the field on Google Earth image.

The mangrove extent at each transect were transformed into a 1D cross-shore profile. The position of the land edge and sea edge of the mangrove forest was referenced to the position where MSL intersected with the shoreline (cross-shore distance, X = 0). The positive cross-shore distance (X > 0) value indicates seaward distance; while negative cross-shore distance value (X < 0) indicates shoreward distance.

4.2.2 Coastal physical characteristics

4.2.2.1 Cross-shore profile

The cross-shore profile of each transect comprises elevation changes within the mangrove zone and the offshore bathymetry profile. Elevation changes within the mangrove zone were collected in the field survey and were merged with bathymetry profiles obtained from Nautical Charts.

Within mangrove zone

A total of 17 profiles were measured, covering 5600 meters of cross-shore distance. Cross-shore profiles within the mangrove zone were measured using a Nikon Forestry Pro Laser Rangefinder 8381. The laser rangefinder has an accuracy of approximately 0.2 m for horizontal distance below 100 m and the accuracy for angle measurement is 0.1^{o} for angle below 10^{o}. The cross-shore profile is made up of a series of segments (Figure 4.6). In order to calculate the elevation change of the segment between point A and point B, the horizontal distance, X and the angle, θ were measured and recorded. The elevation change, Y was then calculated using trigonometry. Equation 4 shows the elevation change calculation for each segment.

Equation 4 Elevation change, Y calculation using horizontal distance, X and angle θ

$$Y = X \tan \theta$$

Figure 4.6 Example of elevation change measurement between point A and point B. Horizontal distance and angle of difference, θ between point A and point B were measured.

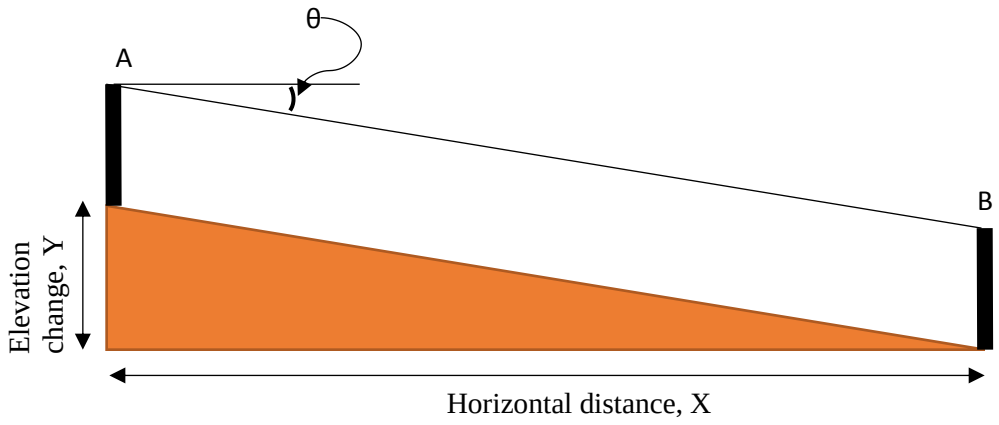

The length of each segment was determined by the condition of the forest as the laser rangefinder requires a clear line of sight for distance measurement. Any obstruction in the line of sight could deflect the laser beam and produce inaccurate reading. The segments were 5 – 40 m in length, depending on the vegetation density. Cross-shore profiles were measured from the landward edge of the mangrove. However, at MAN,

due to the dense back mangrove vegetation at some transects, the cross-shore distance measurement started approximately 5 – 10 m into mangroves. For TEK, since no field survey was conducted, the slope within the mangrove area was represented using an average slope profile from all transects measured.

Bathymetry profile

Bathymetry profiles were extracted from Nautical Charts published in Edition 10/2014 by Marine and Port Authority of Singapore (MPA). The coordinates were referenced to the World Geodetic System 84 Datum (WGS 84) and the depth referenced to Chart Datum (CD). The bathymetry contour lines were available at 0 m, 2 m, 5 m, 10 m, 15 m, 20 m, 30 m, 50 m and 100 m intervals. Water depth along the Johor Straits is relatively shallow (10 – 15 m), reaching up to 20 m in some areas.

Bathymetry profiles along each transect were extracted from the Nautical Charts using measuring tools in ArcGIS. Transects within each study site were extended towards offshore by creating a polyline towards the opposite coast. Starting from 0 m depth with reference to CD, distance intervals between contour lines were measured and recorded. Bathymetry profiles along transects were then generated by interpolation between the interval points recorded.

Merging cross-shore profile

Bathymetry profiles and elevation changes within the mangrove zone were processed and merged using R program (RStudio Team, 2015). The sea edges of mangroves at each transect were assumed to be at MSL with reference to CD. The cross-shore elevation profiles within the mangrove zone were then referenced to the MSL. The elevation change between MSL and CD was linearly interpolated based on the distance between sea edge of mangroves and the start of bathymetry profile.

The merged cross-shore profiles with reference to MSL were truncated at the deepest part of the bathymetry, which is the position for boundary condition application. Any reflection or interaction with the seabed and nearby landmasses were taken into account in the preparation of the boundary condition through Delft3D wave simulation module. At some transects, bathymetry profiles showed some artificial sharp drops, due to the contour line intervals in the Nautical Charts. However, these sharp drops showed negligible effect on the wave height evolution, as observed in the initial model runs. Therefore, in order to preserve localized elevation changes within the mangrove area, no profile smoothing factor was applied to the cross-shore profiles.

4.2.2.2 Sediment characteristics

Sediment sample collection was carried out in conjunction with the vegetation survey in the same transect and plot set up (Figure 4.3) Soil samples for bulk density and sediment size analysis were collected from each plot. A total of 118 soil samples were collected from the 59 plots surveyed.

Bulk density

At the center of each plot, 125 cm^3 (surface area of 5 cm^2 and 5 cm deep) of soil was collected, kept in a Ziploc bag and brought back to the laboratory for further analysis. The soil sample was collected as close to the centre of the plot as possible to ensure consistency across plots.

Bulk density, defined as mass of a unit volume of dry soil, is a measurement of degree of soil compactness. In general, soil with a higher percentage of fine particles has a lower bulk density. The procedure employed in the bulk density laboratory analysis follows Sarkar and Haldar (2005). In the laboratory, the wet soil samples were put into previously cleaned and weighed crucibles. The total weight of wet soil samples and crucibles were weighted and recorded. The wet soil samples were then dried in the oven

at 105 °C until constant weight has reached. After drying, the weight of the soil sample and crucible were recorded. Bulk density of the soil sample was calculated using the following formulas:

Equation 5 Equation for bulk density calculation

$$\begin{aligned} Weight\ of\ crucible\ (g) &= A \\ Weight\ of\ crucibles + dry\ soil\ sample(g) &= B \\ Weight\ of\ dry\ soil\ (g) &= B - A = C \\ Volume\ of\ soil\ (cm^3) &= D \\ Bulk\ density\ (g\ cm^{-3}) &= \frac{C}{D} \end{aligned}$$

Sediment size

For each plot, approximately 100 g of homogenized soil sample was collected. The soil samples within each plot were collected down to 5 cm depth from three spots within the 0.5 m x 0.5 m subplot (Figure 4.3). Roots and rubbish in the soil samples were removed. The soil samples collected were chilled and transferred to laboratory for further analysis.

In the laboratory, sediment size analysis was carried out using the Malvern Mastersizer 2000. Prior to sediment size measurements, pre-processing of soil samples were required to i) remove particles of more than 2 mm; ii) remove cementing agent such as organic matter and carbonate; and iii) disperse soil particles. Particles of more than 2 mm were removed due to the measurement limit of Malvern Mastersizer 2000. The removal of cementing agents such as organic matter and carbonate is an essential step, especially with mangrove soil which usually contains high amount of organic matter. Under the influence of natural biological, physical, and chemical processes, fine particles, such as silt and clay, could aggregate into flocs with organic matter and carbonate acting as cementing agent (Vaasma, 2008). Organic matter could be eliminated by wet oxidation using potassium dichromate or hydrogen peroxide (Allen

& Thornley, 2004; Schumacher, 2002). Thermal combustion and hydrochloric acid were used to remove carbonates (Murray, 2002; Schumacher, 2002). Dispersion of sediment particles was carried out by adding dispersing agent such as sodium hexametaphosphate. The pre-processing steps as illustrated in Figure 4.7 follow the method in Sarkar and Haldar (2005).

Figure 4.7 Flow diagram illustrating the procedure for particle size characterization.

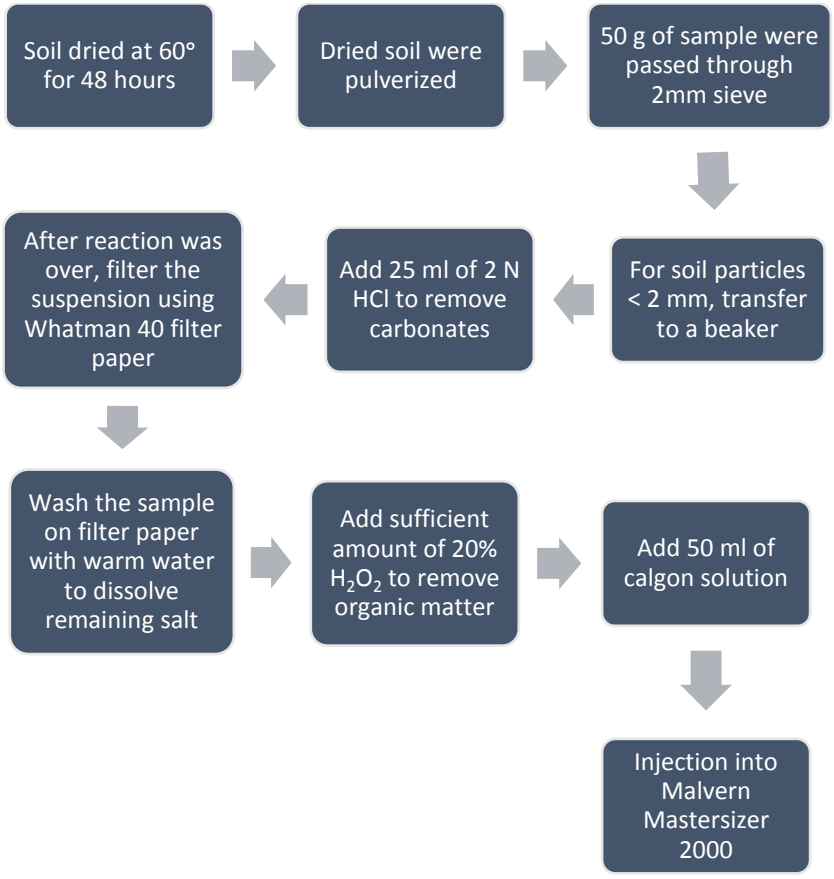

After pre-processing, particle sizes were measured using Malvern Mastersizer 2000. Malvern Mastersizer 2000 utilises laser diffraction particle sizing technology to quantify the particles size down to 0.02 µm. Focused laser beam were passed through the sediment particles in a flow cell and were scattered. The magnitude of scattering is inversely proportional to the size of the particles. The angular intensity of the scattered laser light was measured by photosensitive detectors. Particle sizes was then calculated

based on scattering intensity and angle information in Mie scattering model (assumed volume equivalent sphere diameter).

Soil samples in dispersing solution were injected into the particle analyzer using a pipette. The samples were stirred to prevent deposition of larger particles and sampling bias. Ultrasonic dispersion and mechanical dispersion were also used in dispersing soil particles. Oversaturation of injected samples might cause the overlapping of particles and deviation of laser diffraction. In order to prevent oversaturation of samples, saturation level of the injected samples was kept at 10 – 12% as recommended by the manufacturer. After each measurement, the analyzer was flushed at least three times using tap water to ensure the machine is clean before injection of next sample. The measurement steps were repeated three times for each sample to reduce potential human error arising from sample injection.

The average particle size distribution for each soil sample was then calculated at the 10, 25, 50, 75, and 90 percentiles. D50, the median sediment size, was used to describe soil characteristics within each plot. Minimum, median, and maximum particle sizes were used for model input for each transect. The bulk density measurement for the corresponding plot was used in association with the sediment size. For TEK, where field measurements were not available, sediment size were calculated by averaging sediment size measurement from all plots surveyed.

4.2.3 Hydrodynamic characteristics

4.2.3.1 Water and tidal level

The tidal datum in Singapore is categorized into five main tidal levels, with reference to Chart Datum (CD) (Table 4.4). The tidal levels are recorded by tidal stations network, maintained by MPA. The vertical datum of each tidal station was verified

annually. The water level sensor on board of each tidal station was also checked once a year.

Due to the slight tidal variation across Singapore, the tidal levels used for each study site were obtained from tidal stations that are located closest to respective study sites (Figure 4.8), as published by MPA. For MAN and BUL, the tidal levels from Tuas tidal station, located at approximately 20 km to the south, was used. Although Sembawang tidal station is located closer to BUL and MAN, the tidal condition is different due to the division of the Johor Straits by the causeway connecting Singapore to Peninsular Malaysia. For UBI and TEK, Tanjong Changi tidal station, located approximately 10 km to the south, was used.

Table 4.4 Definition of five main tidal levels in Singapore tidal stations and tidal range.

Tidal level	**Abbreviation**	**Definition**	**Tidal range (ref. CD)**
Mean High Water Spring	MHWS	Average height of the high waters of spring tides above Chart Datum	2.5 – 3.1
Mean High Water Neap	MHWN	Average height of the high waters of neap tides above Chart Datum	2.1 – 2.5
Mean Level	ML	Average height of the surface of the sea at a tide station for all stages of the tide over a 19 year period	1.6 – 2.0
Mean Low Water Neap	MLWN	Average height of the low waters of neap tides above Chart Datum	1.2 – 1.4
Mean Low Water Spring	MLWS	Average height of the low waters of spring tides above Chart Datum	0.5 – 1.0

The tidal datum used in the InVEST model is based on tidal datum standards established by the National Oceanic and Atmospheric Administration (NOAA). The tidal levels required are MSL and Mean High Water (MHW) with reference to MSL.

Since MHW is not officially published by MPA, the MHW level was calculated by averaging MHWS and MHWN.

Equation 6 Calculation of MHW for model input from Singapore tidal levels

$$MHW = \left(\frac{MHWS + MHWN}{2}\right) - MSL$$

Figure 4.8 Spatial relation between MPA tidal stations (red) and study sites (green). BUL = Sungei Buloh Wetland Reserve; MAN = Mandai mangroves; UBI = Pulau Ubin; TEK = Pulau Tekong.

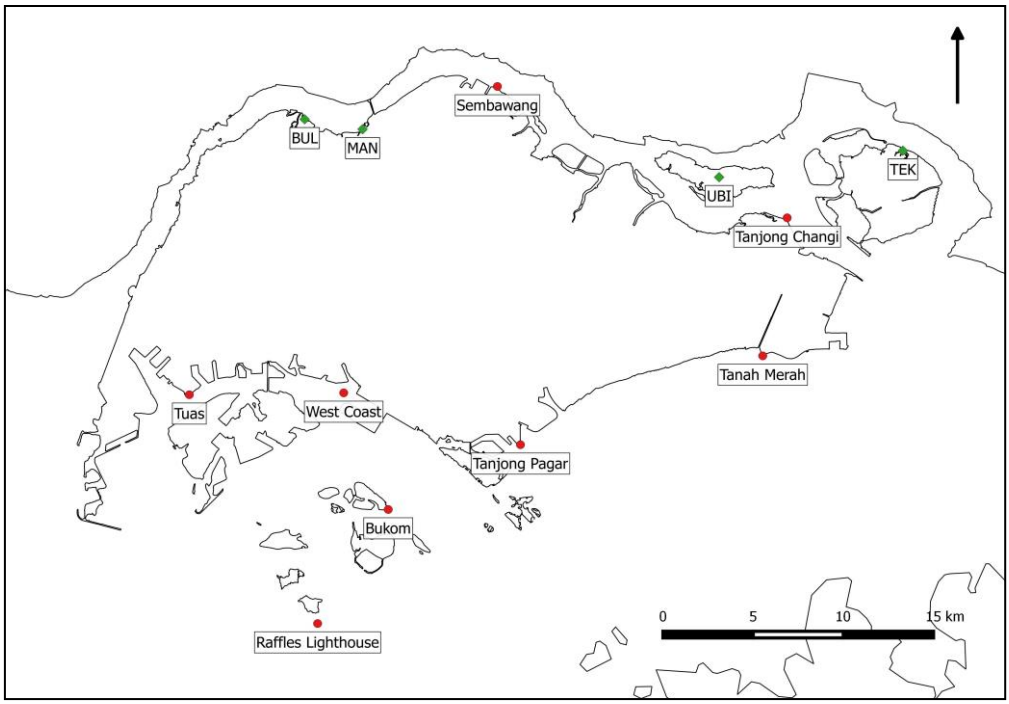

4.2.3.2 Significant wave height and wave period

Offshore wave heights and wave periods were generated in Delft3D using Singapore Regional Model (SRM). Delft3D is an open source modelling suite for studying hydrodynamics, sediment transports and water quality. The boundary of SRM covers part of South China Sea (SCS), Andaman Sea, and Java Sea (Figure 4.9). The use of such a large domain for modelling Singapore waters reduces the influence of stronger tidal signal at the model boundary. The SRM comprises approximately 36,500 grid cells made up of varying sizes from 20 x 40 km^2 to 150 x 200 m^2 in the interior of

Singapore. A spherical, curvilinear grid was applied in this model. The SRM has been well calibrated and validated for large-scale tide interaction and wind-driven waves simulation (Kurniawan et al., 2011).

Figure 4.9 SRM boundary and grid (left) and bathymetry of SRM (right). The legend shows depth in meters with reference to MSL.

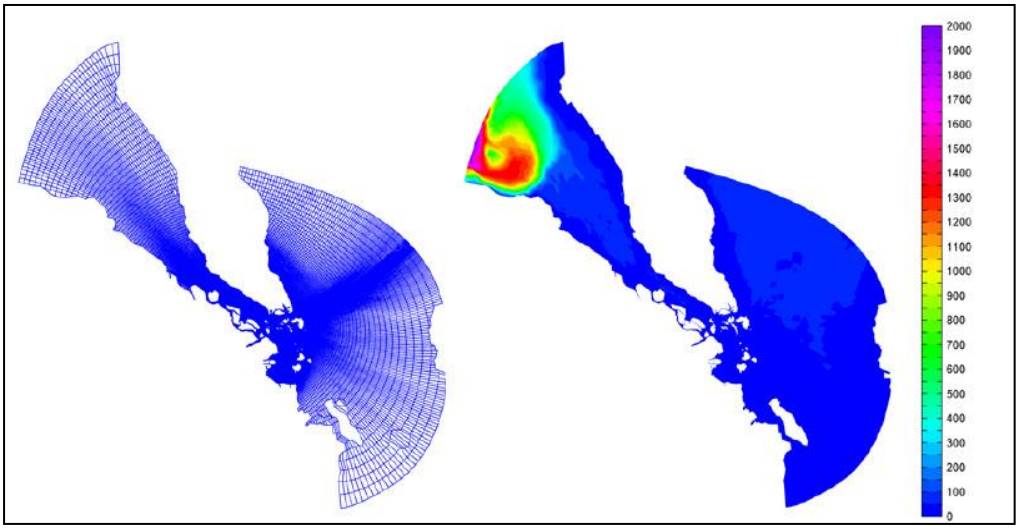

Average hydrodynamic conditions

Significant wave height and wave period of year 2012 were simulated in Delft3D using SRM. Wind forcing was obtained from the European Centre for Medium-Range Weather Forecasts (ECMWF). Hourly wave heights and wave periods were generated for 90 tidal stations within the SRM domain. Figure 4.10 shows the selected tidal stations surrounding Singapore.

Similar to the selection approach used in determining tidal levels for each study site (section 4.2.3.1), wave height and wave period data used were selected based on geographical proximity. For MAN and BUL, wave height and wave period data from Lim Chu Kang were used. Lim Chu Kang tidal station is located 6 km and 3 km to MAN and BUL respectively. The hydrodynamic conditions at TEK and UBI were obtained from tidal station P3 and Tanjong Changi respectively.

Figure 4.10 Selected tidal stations around Singapore (blue) and study sites (green). BUL = Sungei Buloh Wetland Reserve; MAN = Mandai mangroves; UBI = Pulau Ubin; TEK = Pulau Tekong

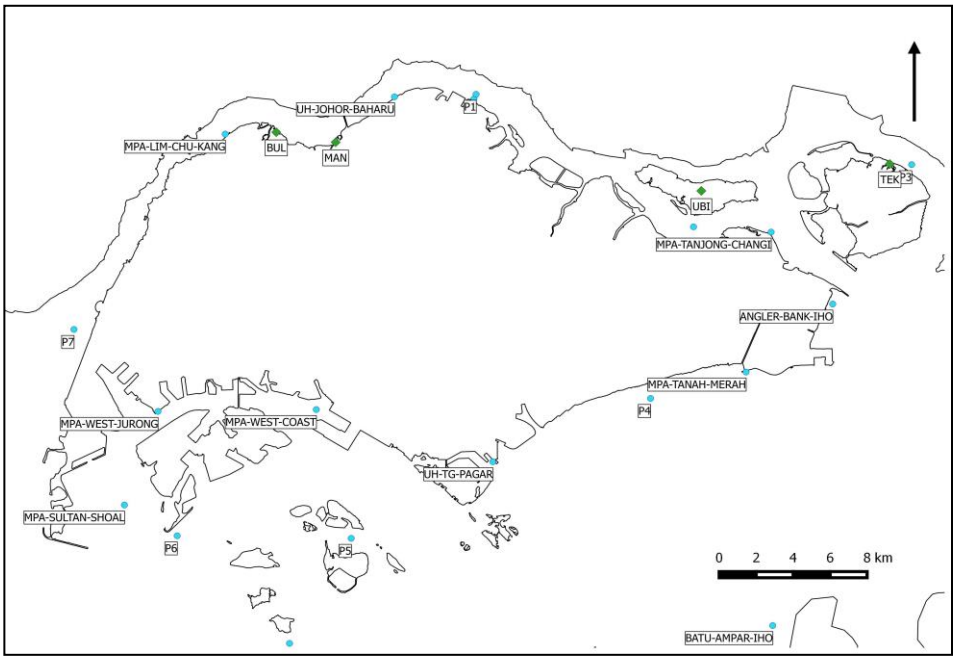

The average hydrodynamic conditions of each site were calculated by averaging the significant wave heights and wave periods for the whole year of 2012. An example of the simulated significant wave height and peak wave period was illustrated in Figure 4.11 and Figure 4.12.

Figure 4.11 Hourly significant wave height of Raffles Lighthouse tidal station for year 2012 generated in simulation using SRM in Delft3D environment.

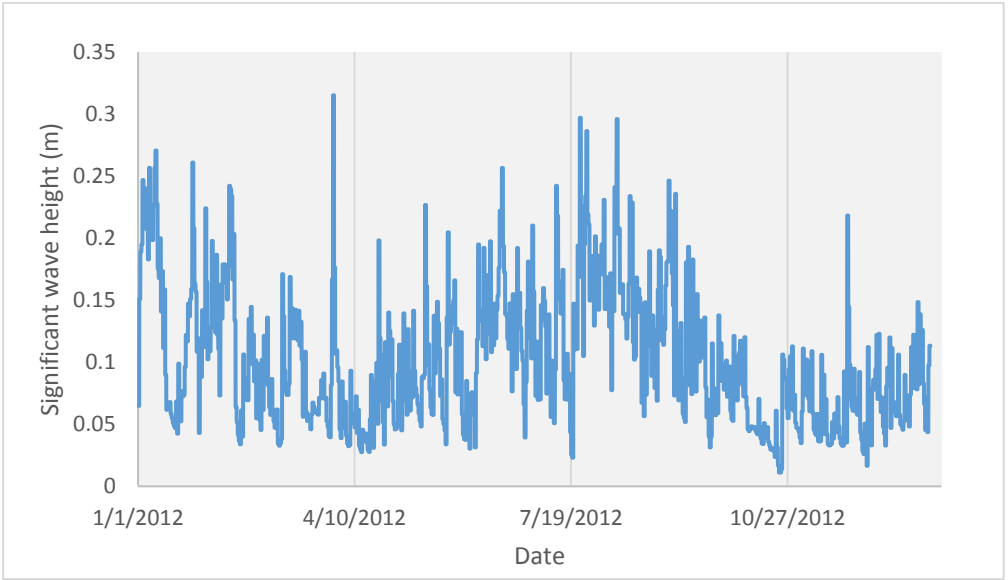

Figure 4.12 Hourly peak wave period of Raffles Lighthouse tidal station for year 2012 generated in simulation using SRM in Delft3D environment.

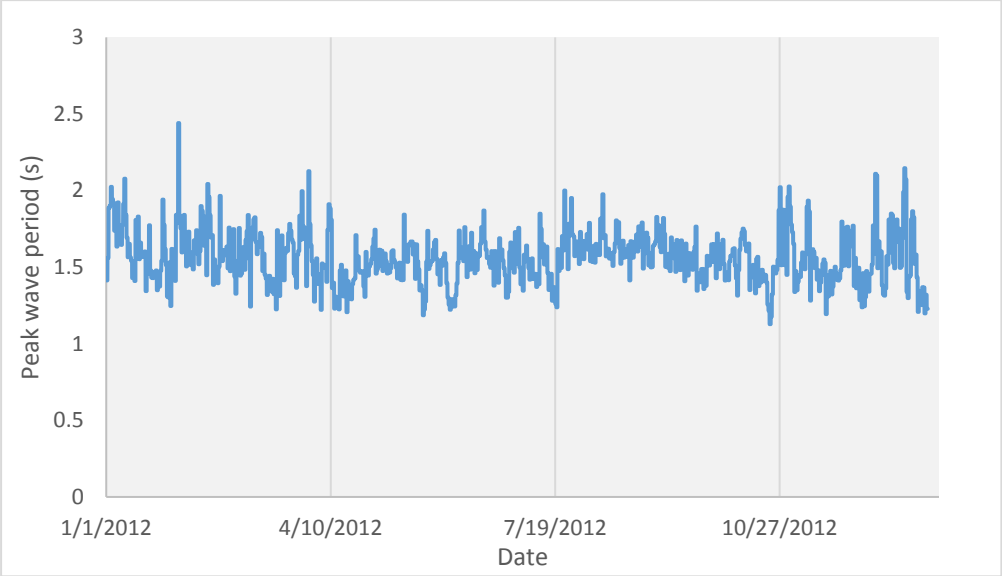

Extreme hydrodynamic condition

Extreme hydrodynamic conditions were simulated using significant wave heights and peak wave periods from the modelled 'worst case scenario' of tropical storm Vamei, based on an analysis by Tay (2010). Typhoon track and intensity were obtained from Joint Typhoon Warning Centre (JTWC) and Japan Meteorological Agency (JMA). Maximum sustained wind of up to 65 knots was recorded (Joint Typhoon Warning Center, 2001). A hindcast of hydrodynamic conditions during tropical storm Vamei was conducted in Delft3D. After calibration of hydrodynamic and wind models based on the hindcast data, sensitivity analyses using different tracks, speeds, and sizes were conducted. The simulated 'worst case scenario' of typhoon was defined as the typhoon track that induced the highest surge level based on tidal stations in Singapore's waters. Figure 4.13 shows the simulated worst track of typhoon (track 2) that moved from east to west into Singapore Straits and made landfall at Pulau Bintan, Indonesia. As the typhoon moves from the east to the west, water from surrounding water bodies is forced into Singapore Straits, generating high surge level (Tay, 2010).

Figure 4.13 Position of typhoon eye in track 1 and 2 (left) and other tracks simulated to determine the track for 'worst case scenario'(right) (Source: Tay, 2010).

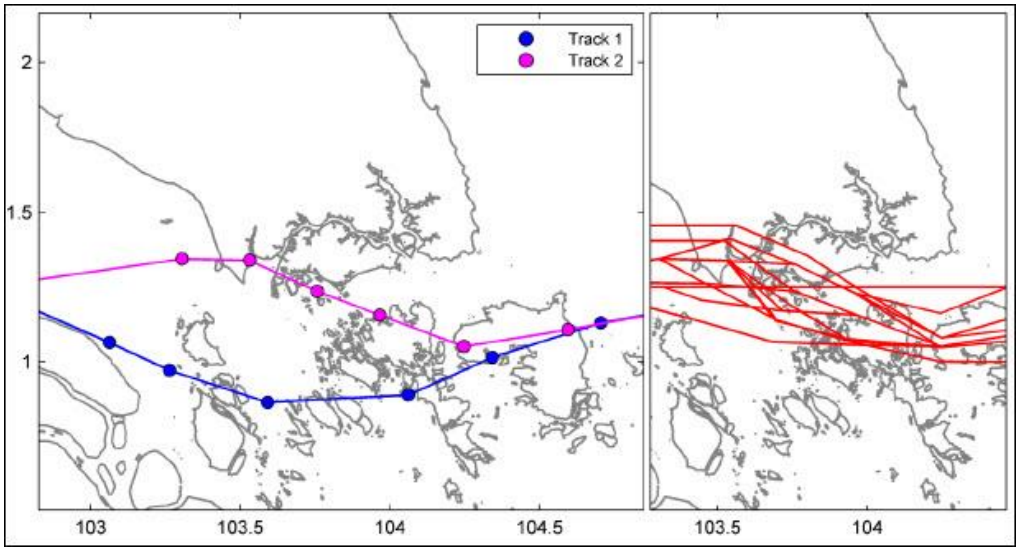

Based on the ‘worst case scenario’, the surge level and SLA were generated at 13 tidal stations around Singapore. The highest surge level in this ‘worst case scenario’ reaches 1.6 m above MSL. In combination with SLA and high tides, the total water level could rise to 2 – 2.8 m above MSL, depending on location. Wave height and wave period of each study site were obtained from the closest tidal stations. MAN and BUL uses the hydrodynamic parameters simulated at Lim Chu Kang tidal stations; while UBI and TEK uses the hydrodynamic data from tidal station at Pasir Ris and Tekong respectively.

4.3 Nearshore Waves Evolution Model

4.3.1 Model

The nearshore wave evolution model used in this study is part of the InVEST 3.2.0 software. InVEST is a suite of open source software models used for the quantification and valuation of ecosystem services. It was developed and maintained by Natural Capital Project, a partnership between Stanford University, University of Minnesota, The Nature Conservancy, World Wildlife Fund, and other collaborators. Applications include strategic environmental assessments, marine spatial planning, establishing

payment for watershed services, etc. (Natural Capital Project, 2016). The software requires the input of site-specific data to produce an accurate model for local application. Coastal Protection model, to which the nearshore wave evolution is a part of, runs in the ArcGIS ArcToolBox environment. The model employs vertical layer schematization approach to account for vegetation root, trunk and canopy structure (Guannel et al., 2015; Mendez & Losada, 2004). The nearshore wave evolution model calculates the transformation of offshore wave height as the waves propagate towards the shore (Appendix A).

The choice of model used is dependent on the size and structure of mangroves as well as the study objectives. In this study, in order to provide a representative result of the wave attenuation extent by Singapore's mangroves, which have a site-specific history of anthropogenic influence, a few mangrove sites have been studied. The one-dimensional nearshore wave evolution model used in this study provides a time-efficient computing framework for spatial coverage with sufficient site customization for local ecological and physical characteristics. The number of cross-shore profile could be increased for higher resolution (shorter along-shore intervals) at mangrove sites. For example, the more heterogeneous mangrove in MAN was represented with more transects and smaller plot intervals.

4.3.2 Scenarios

A total of four scenarios were used as hydrodynamic settings (Figure 4.14). Overall, the use of both average and extreme hydrodynamic conditions enables the investigation of wave attenuation function provided by mangroves under different natural forcing. The average hydrodynamic conditions provide insights into the wave attenuation function of mangroves during normal tidal and wave conditions. The inclusion of extreme hydrodynamic conditions, the 'worst case scenario' of tropical storm Vamei, could shed light onto the ability of mangroves in coastal protection during storms. The

difference between the low and high water levels within each hydrodynamic condition helps to investigate the extent of wave attenuation.

Figure 4.14 Diagram showing four different hydrodynamic settings for model scenarios.

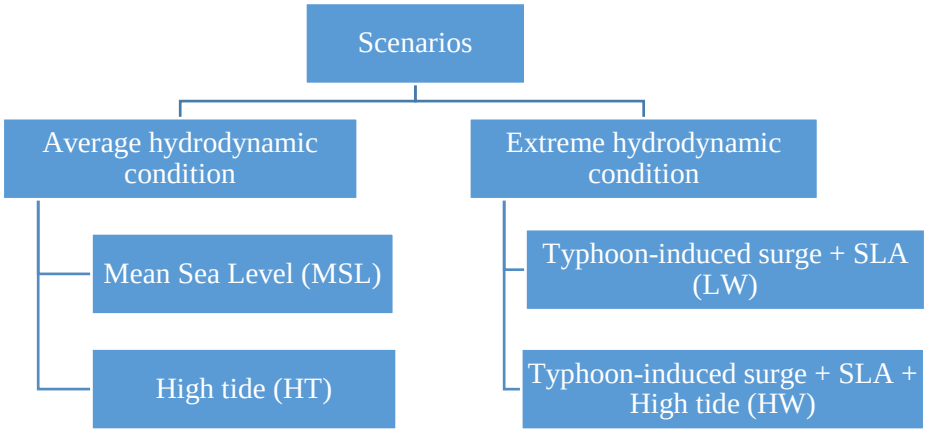

Table 4.5 Summary of model runs with number of vegetation, sediment, and natural forcing settings. Each transect were set up using the dominant vegetation characteristics, three different sets of sediment properties and four hydrodynamic settings.

Site	Number of transects	Vegetation characteristics	Sediment properties	Hydrodynamic settings	Total number of models
BUL	5	1	3	4	60
MAN	5	1	3	4	60
UBI	4	1	3	4	48
TEK	3	1	3	4	36
				Total	204

4.3.3 Data analysis

Outputs from the models were analyzed using R programme (RStudio Team, 2015). The wave attenuation rate in this study was calculated using the mathematical equation by Mazda et al. (2006). The wave attenuation was expressed in terms of wave height reduction per unit distance, r.

$$r = -\frac{\Delta H}{H}\left(\frac{1}{\Delta x}\right)$$

where ΔH is the reduction in wave height over a certain distance, Δx in relation to initial wave height, and H along the direction of the wave propagation.

Under MSL scenario, waves did not propagate into the mangrove forest. Therefore, no wave attenuation result was generated. Data analysis for the average hydrodynamic condition was conducted using the model result from HT scenario. Shapiro-Wilk normality tests were conducted to test the normality of data. Non-parametric tests were used to compare the extent of wave attenuation between sites if the data were not normally distributed. The type I error, α, was set at 0.05. Correlations between wave attenuation and various hydrodynamic, vegetation, and physical factors was examined individually using Spearman's rank correlation coefficient.

5 Vegetation, physical and hydrodynamic characteristics of the study sites

Site-specific vegetation, physical, and hydrodynamic characteristics were required in order to produce realistic estimation of the wave attenuation by local mangroves. In this study, extensive desktop study and field survey were conducted (Table 4.1). The vegetation and physical characteristics of each transect were used as model setup for application of hydrodynamic forcing (Appendix B).

5.1 Vegetation characteristics

5.1.1 Mangrove density

Overall, mangrove density ranged from 0 to 0.35 trees m^{-2}. Within-transect density variation is relatively larger in UBI2/3, ranging from 0.06 to 0.35 trees m^{-2}, compared to UBI4/5. Similarly in MAN, the range of density across transect showed variations. MAN3 was found to be relatively larger (0.05 – 0.24 trees m^{-2}) compared to MAN2 (0.1 – 0.14 trees m^{-2}). Comparing across sites, UBI has a higher density compared to BUL and MAN. There were significant differences between UBI and MAN (Tukey HSD test, p-value < 0.001) and between UBI and BUL (Tukey HSD test, p-value < 0.001). No significant difference in density between BUL and MAN were found (Tukey HSD test, p-value > 0.05) (Appendix C: Table C1, C2).

Table 5.1 Vegetation density of each transect. *SD = standard deviation.*

Transect	Mean ± SD (trees m^{-2})	Range (trees m^{-2})
BUL3	0.09 ± 0.01	0.08 – 0.10
BUL4	0.05 ± 0.03	0.03 – 0.07
BUL5	0.04 ± 0.04	0 – 0.07
BUL6	0.06 ± 0.07	0.01 – 0.14
BUL7	0.08 ± 0.04	0.04 – 0.12
BUL average	0.07 ± 0.04	0 – 0.14

MAN1	0.15 ± 0.06	0.09 – 0.23
MAN2	0.13 ± 0.02	0.10 – 0.14
MAN3	0.12 ± 0.10	0.05 – 0.24
MAN4	0.06 ± 0.04	0.02 – 0.10
MAN5	0.05 ± 0.04	0 – 0.08
MAN average	0.1 ± 0.07	0 – 0.24
UBI2	0.17 ± 0.11	0.06 – 0.35
UBI3	0.19 ± 0.08	0.10 – 0.33
UBI4	0.29 ± 0.04	0.27 – 0.35
UBI5	0.26 ± 0.05	0.21 – 0.32
UBI average	0.22 ± 0.09	0.06 – 0.35
Overall	0.13 ± 0.09	0 – 0.35

5.1.2 Mangrove extent

Mangrove extent varied across and within study sites (Figure 5.1). The width of mangrove forest at UBI was the highest (916 – 1149 m), almost five times wider than transects in MAN and BUL. At TEK, TEK2 has a relatively long cross-shore mangrove extent (858 m), compared to the other two transects (< 200 m). At MAN, mangrove width in MAN1 was the widest (≈ 250 m), while other transects ranged between 100 – 200 m. The mangrove forest at BUL was of a similar extent (90 m to 252 m). Mangroves in BUL3/4/5 were intersected by an embankment, so the mangrove responsible for most of the wave attenuation are the small patches of mangroves growing seawards of the embankment, with a cross-shore distance of less than 50 m.

5.1.3 Mangrove diversity

Overall, a total of 11 genera were identified and recorded. Out of the 1291 individual trees measured (trees in KHA were excluded as they were not measured using transects/plots), the genus *Rhizophora* represents the biggest percentage (33.69%) among the genera recorded, followed by *Bruguiera* (22.85%). *Avicennia* and

Sonneratia accounted for 21.61% and 6.51% respectively. The four dominant genera comprise a total of 84.66% of the trees measured. Each of the remaining six genera recorded represents only 5% or less (Figure 5.2).

Figure 5.1 Cross-shore mangrove extent at each transect surveyed.

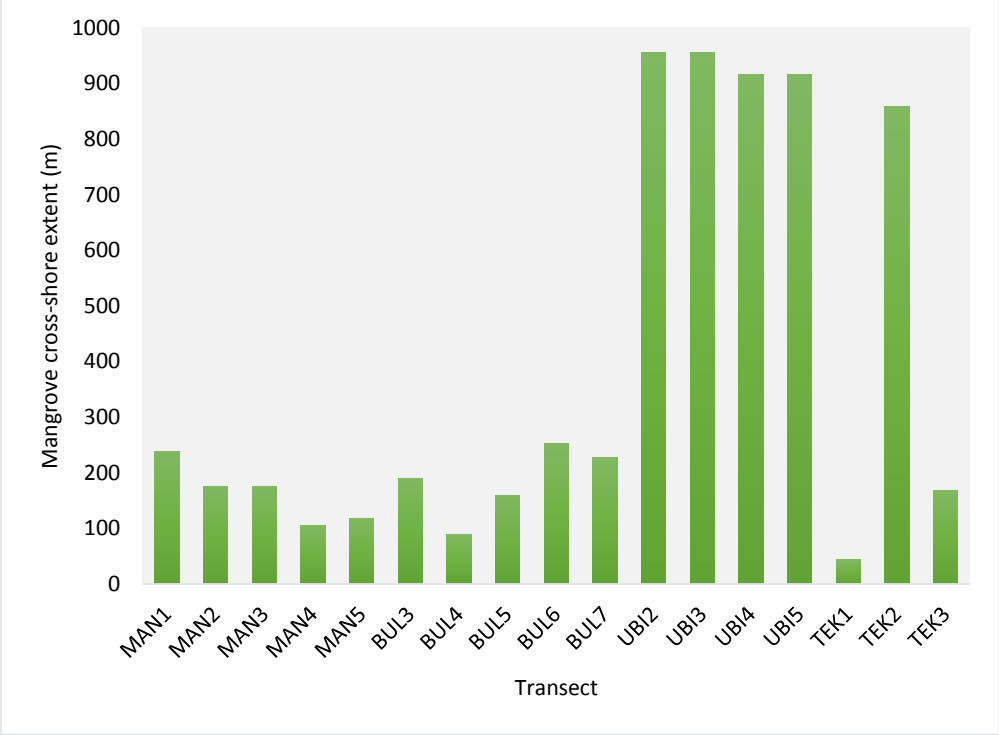

Figure 5.2 Percentage representation of each genus from all individual trees recorded.

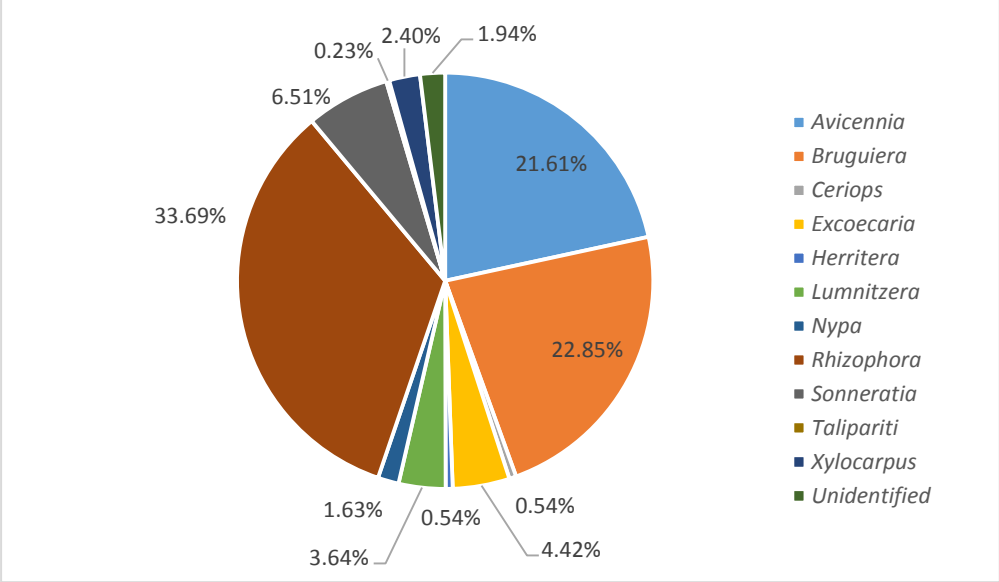

When mangrove diversity was analysed by sites, *Avicennia* was the dominant genus in BUL (29.03%) and MAN (25.58%), followed by *Bruguiera* in BUL (28.39%) and MAN (25.19%). The third and fourth most dominant genus in both sites, however, are different. *Rhizophora* (18.71%) and *Sonneratia* (6.45%) represent the third and fourth most dominant genus in BUL; while in MAN, it was *Excoecaria* (16.28%) and *Lumnitzera* (18.22%). *Excoecaria* and *Lumnitzera* were usually found at the back of mangrove where elevation is higher and being inundated less frequently. The higher percentage of genus representation of these two genera suggests the overall surface elevation is higher at MAN. At the eastern Johor Straits, *Rhizophora* represents the biggest percentage of the population in UBI (> 50%). Second and third most common genera were *Avicennia* (20.42%) and *Bruguiera* (16.21%). There is a lack of back mangrove genus at UBI. *Lumnitzera*, *Herritera* and *Taliparitis* was not found in all the plots measured. Similar to UBI and MAN, *Bruguiera*, *Rhizophora*, *Avicennia*, and *Sonneratia* were found to be the four most populous genus in RIS with 32.95%, 31.80%, 16.09% and 11.11% respectively.

Table 5.2 shows the number of trees measured and the dominant genus in each transect. *Rhizophora* genus is the dominant genus in most plots, including all plots in UBI. Within these plots, the dominance of *Rhizophora* ranged from 33.53% to 65.19%. *Bruguiera* and *Avicennia* both have dominance ranged from 27.12% to 56.82% and 22.92% to 61.90% respectively. The low representation of dominant genus in some plots indicates the heterogeneous nature of the mangrove forest composition in these sites (Figure 5.3).

Table 5.2 Number of individual trees measured within each transect and the respective dominant genus and percentage representation.

Transect	Number of tree measured (n)	Dominant genus	Percentage representation of dominant genus (%)
BUL3	44	*Bruguiera*	56.82
BUL4	16	*Rhizophora*	50.00
BUL5	20	*Avicennia*	40.00
BUL6	27	*Rhizophora*	44.44
BUL7	48	*Avicennia*	22.92
MAN1	91	*Bruguiera*	31.87
MAN2	59	*Bruguiera*	27.12
MAN3	57	*Avicennia*	35.09
MAN4	30	*Avicennia*	36.67
MAN5	21	*Avicennia*	61.90
RIS1	100	*Bruguiera*	34.00
RIS2	82	*Rhizophora*	37.80
RIS3	79	*Bruguiera*	32.91
UBI2	130	*Rhizophora*	40.77
UBI3	150	*Rhizophora*	43.33
UBI4	180	*Rhizophora*	51.67
UBI5	158	*Rhizophora*	65.19
Overall	1291	*Rhizophora*	33.69

Figure 5.3 Genus representation within each site.

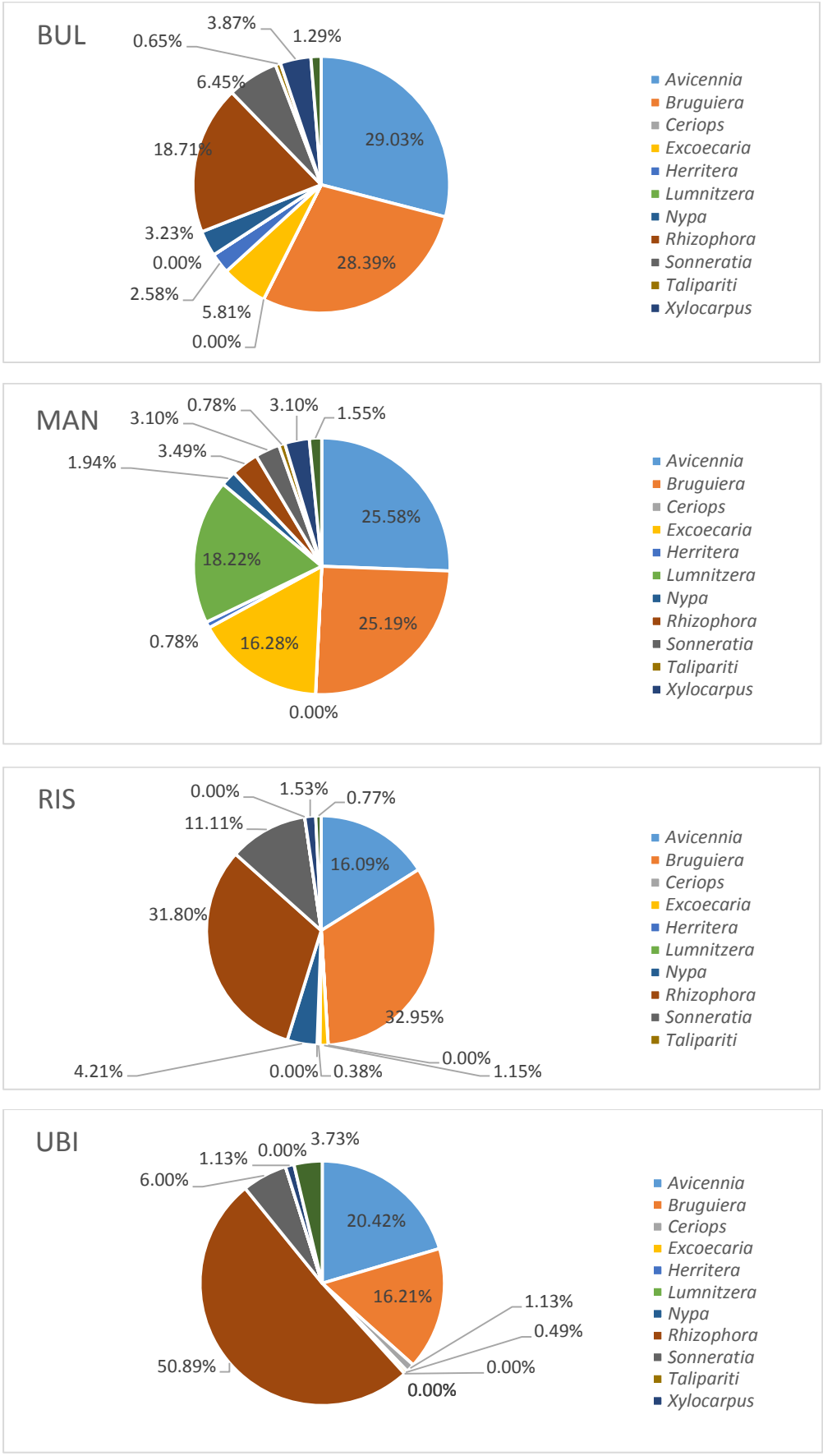

5.1.4 Mangrove tree structure

Out of the 11 genera identified in the field survey, mangrove structures of the four dominant genera, namely *Avicennia*, *Bruguiera*, *Rhizophora,* and *Sonneratia* were surveyed. Mangrove structures (root, trunk, and canopy) were assumed to be similar, with no significant structural difference between species of the same genus.

Roots

The roots for each of the four dominant genera were structurally different. The average root diameter showed some variations across genera. *Bruguiera*, *Rhizophora, and Sonneratia* showed similar root diameters of 0.032 ± 0.005 m, 0.039 m and 0.03 m respectively. As only one subplot measured was dominated by *Sonneratia*, no standard deviation was calculated. *Avicennia* has the smallest average root diameter compared to the other three genera (0.0068 ± 0.0016 m) and was significantly smaller than those of *Bruguiera* (Mann-Whitney test, p-value < 0.05)

On average, the root heights of *Avicennia*, *Bruguiera*, and *Sonneratia* were similar, with an average root height of 0.075 ± 0.034 m, 0.051 ± 0.017 m, and 0.063 ± 0.035 m respectively. The range of the root height was 0.01 – 0.18 m. *Bruguiera* showed a slightly smaller range than *Sonneratia*, followed by *Avicennia*. Statistical analysis, however, showed no significant difference on the average root height between *Avicennia*, *Bruguiera* and *Sonneratia* (Kruskal-Wallis test, p-value > 0.05). Due to the geometry of *Rhizophora* roots, the root height was considerably higher than other genera at 1.4 m above ground level.

Avicennia has the densest pneumatophores with an average of 182.33 ± 126.67 roots m^{-2}, up to 468 roots m^{-2} in the densest subplot. *Sonneratia* pneumatophores were found to have a lower root density of 126.67 ± 88.45 roots m^{-2}. However, no significant difference was found between *Avicennia* and *Sonneratia* root density due to the large

standard deviations (Mann-Whitney test, p-value > 0.05). *Bruguiera* has a significantly lower root density of 70.86 ± 46.29 roots m^{-2} compared to *Avicennia* (Mann-Whitney test, p-value < 0.01), but no significant difference in root density with *Sonneratia* (Mann-Whitney test, p-value > 0.05) (Appendix C: Table C3). The root density of *Rhizophora* calculated was relatively lower than the other three genera.

Table 5.3 Root characteristics of the four dominant genera. SD = standard deviation

Genus (Root types)	**Parameter**	**Unit**	**n**	**Mean ± SD**	**Range**
*Avicenni*a	Height	m	24	0.075 ± 0.034	0.014 – 0.182
(Pencil-shaped)	Diameter	m	5	0.0068 ± 0.0016	0.005 – 0.009
	Density	$1/m^2$	24	182.33 ± 126.67	32 – 468
Bruguiera	Height	m	7	0.051 ± 0.017	0.019 – 0.13
(Knee-shaped)	Diameter	m	6	0.032 ± 0.0051	0.028 – 0.04
	Density	$1/m^2$	7	70.86 ± 46.29	16 – 144
Rhizophora	Height	m	-	1.4*	-
(Prop roots)	Diameter	m	-	0.039*	-
	Density	$1/m^2$	-	4.25*	-
Sonneratia	Height	m	12	0.063 ± 0.035	0.018 – 0.15
(Cone-shaped)	Diameter	m	1	0.030	-
	Density	$1/m^2$	12	126.67 ± 88.45	36 – 312

* Refer to Zhang *et al*. (2015b)

Trunks

Among the four dominant genera, *Sonneratia* has the highest average DBH (0.18 ± 0.08 m), followed by *Avicennia* (0.15 ± 0.1 m). The DBH of *Bruguiera* is the smallest, with an average of 0.08 ± 0.04 m. Statistical analysis found a significant difference between the trunk diameters (Kruskal-Wallis test, p-value < 0.001). *Avicennia* has the largest range of DBH (0.05 – 0.53 m), suggesting a larger age range was measured.

For trunk heights, *Bruguiera* has a significantly lower average trunk height (3.74 ± 1.99 m), compared to *Sonneratia* and *Rhizophora* (Mann-Whitney test, p-value < 0.001), but not *Avicennia* (Mann-Whitney test, p-value > 0.05). Both *Rhizophora* and *Sonneratia* were found to have significantly higher average trunk height compared to other genera (Mann-Whitney test, p-value < 0.001) (Appendix C: Table C4).

Table 5.4 Trunk characteristics of the four dominant genera. *SD = standard deviation.*

Genus	Parameter	Unit	n	Mean ± SD	Range
Avicennia	Height	m	290	4.28 ± 2.71	1.42 – 15.11
	Diameter	m	290	0.15 ± 0.1	0.05 – 0.53
Bruguiera	Height	m	302	3.74 ± 1.99	1.47 – 12.40
	Diameter	m	302	0.08 ± 0.04	0.05 – 0.23
Rhizophora	Height	m	457	4.92 ± 2.03	0.75 – 17.16
	Diameter	m	457	0.10 ± 0.04	0.05 – 0.35
Sonneratia	Height	m	103	9.06 ± 3.65	2.23 – 16.94
	Diameter	m	103	0.18 ± 0.08	0.05 – 0.36

Canopy

The maximum canopy diameter of the main genera was approximately 13 – 14 m, except for *Avicennia* which has a wider canopy (17.37 ± 3.11 m). Similar to trunk diameter, the canopy diameter of *Bruguiera* was significantly smaller compared to *Avicennia* (Mann-Whitney test, p-value < 0.05) and *Sonneratia* (Mann-Whitney test, p-value < 0.05). There was no significant difference between the canopy diameter of *Rhizophora* and *Bruguiera* (Mann-Whitney test, p-value > 0.05) (Appendix C: Table C5). Average canopy heights of the four main genera were similar, ranging from 5 m to 7.5 m, although *Avicennia* showed a significantly lower mean canopy height (Mann-Whitney test, p-value < 0.001), with a large variation observed. The range and maximum of canopy height between genera differs. *Bruguiera* had the highest

maximum canopy height of 24.61 m, which was approximately 6 m higher than that of *Sonneratia* (16.8 m).

Table 5.5 Canopy characteristics of the four dominant genera. *SD = standard deviation*.

Genus	Parameter	Unit	n	Mean ± SD	Range
Avicennia	Height	m	290	5.05 ± 3.24	1.69 – 17.90
	Diameter	m	290	4.67 ± 3.11	1.56 – 17.37
Bruguiera	Height	m	302	7.49 ± 3.25	1.78 – 24.61
	Diameter	m	302	4.42 ± 1.78	2.01 – 13.66
Rhizophora	Height	m	457	5.60 ± 2.40	2.68 – 18.68
	Diameter	m	457	4.32 ± 1.84	2.07 – 14.38
Sonneratia	Height	m	103	6.43 ± 2.84	1.78 – 16.80
	Diameter	m	103	4.87 ± 2.18	1.34 – 13.35

5.2 Coastal physical characteristics

5.2.1 Cross-shore profile

The shape of cross-shore profile across most transects showed some complex microtopography (eg. transects in UBI and MAN). These small, localised variations in elevation were generally due to small depressions along the transect profile (e.g., Figure 5.5, profile 1). Sandy deposits found in the front of mangrove forests (e.g., at MAN) with some deposits being approximately 1.4 m above MSL also contributed to the microtopography. The sand deposit at MAN was heterogeneous across the sites, being higher at MAN2/3 but lower in height and slope at MAN5. At UBI, a stretch of sandy beach (≈1.6 – 1.8 m above MSL) is present in front of UBI2/3, acting as a barrier preventing wave propagation into the mangrove forest.

Artificial embankments were present at some transects at BUL (BUL3/4/5), often protecting abandoned shrimp ponds (Figure 5.4). The embankments were located at 16 – 49 m into the mangrove, approximately 3 – 3.5 m above MSL. Due to the presence

of such a high embankment, only at extreme conditions when the high tide coincides with storm surges and SLA will the water level be high enough to permit direct wave propagation into mangrove forest at the behind the embankments.

The cross-shore profile below MSL also showed variations across sites. Within all the transects at MAN, there were approximately 300 m of gentle sloping mudflat fronting the mangroves before the elevation dropped to 11.8 m below MSL. This geomorphological feature was not found in other sites. Initial simulations at MAN showed negligible wave shoaling as the waves propagated across the mudflat towards the mangroves. In any case, the shoaling effect in front of the mangrove does not affect the wave attenuation analysis since only the wave height reduction within the mangrove forest was analysed.

Figure 5.4 Embankments at BUL3/4/5

Figure 5.5 Cross-shore profiles of all transects at MAN. The cross-shore distance was referenced to the back of mangroves forest within each transects; the vertical elevation is referenced to the mean sea level (MSL). Offshore = the part of cross-shore profile below MSL.

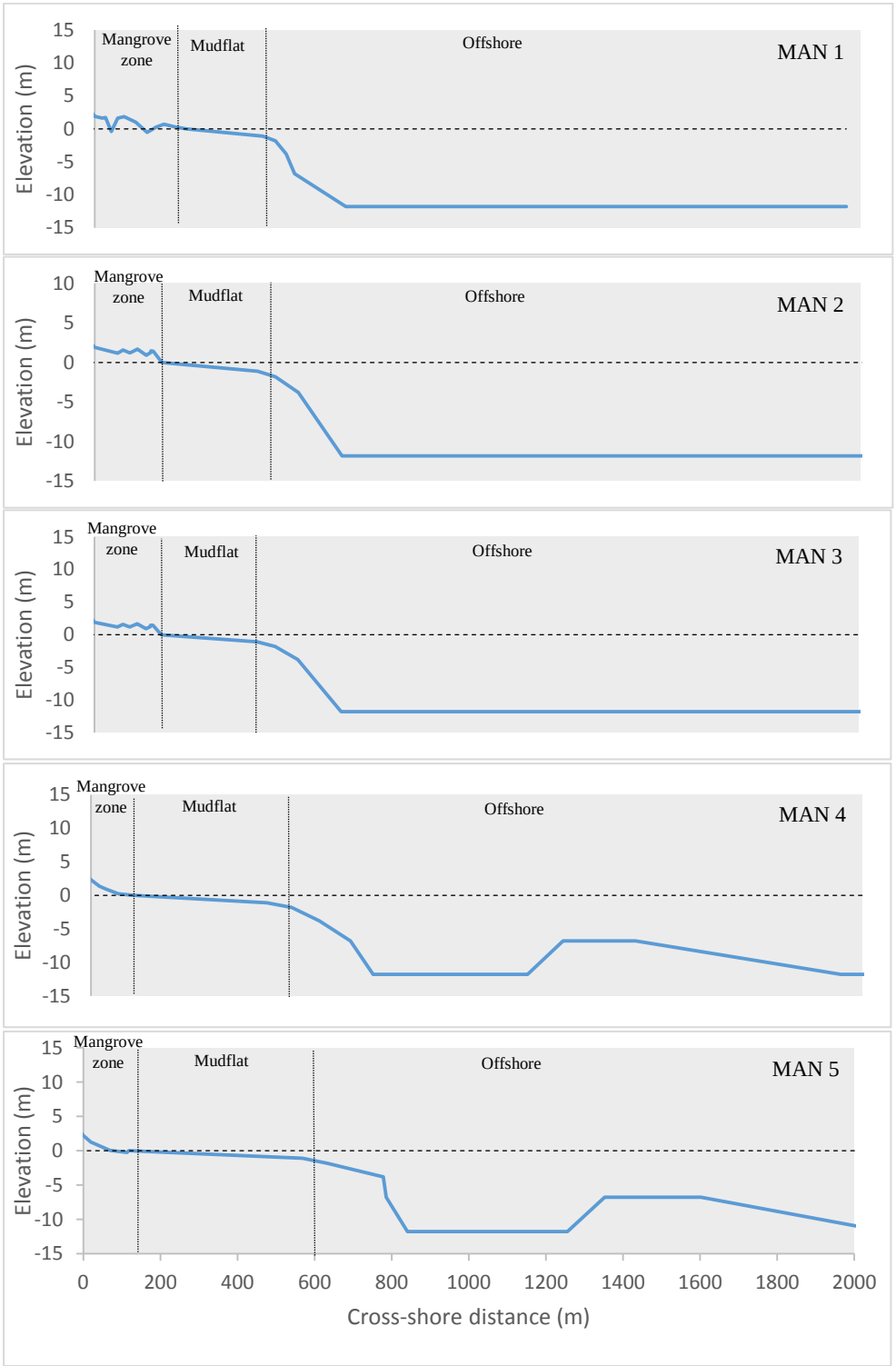

Figure 5.6 Cross-shore profiles of all transects at BUL. The cross-shore distance is referenced to the back of mangroves forest within each transects; the vertical elevation is referenced to the mean sea level (MSL). Offshore = the part of cross-shore profile below MSL.

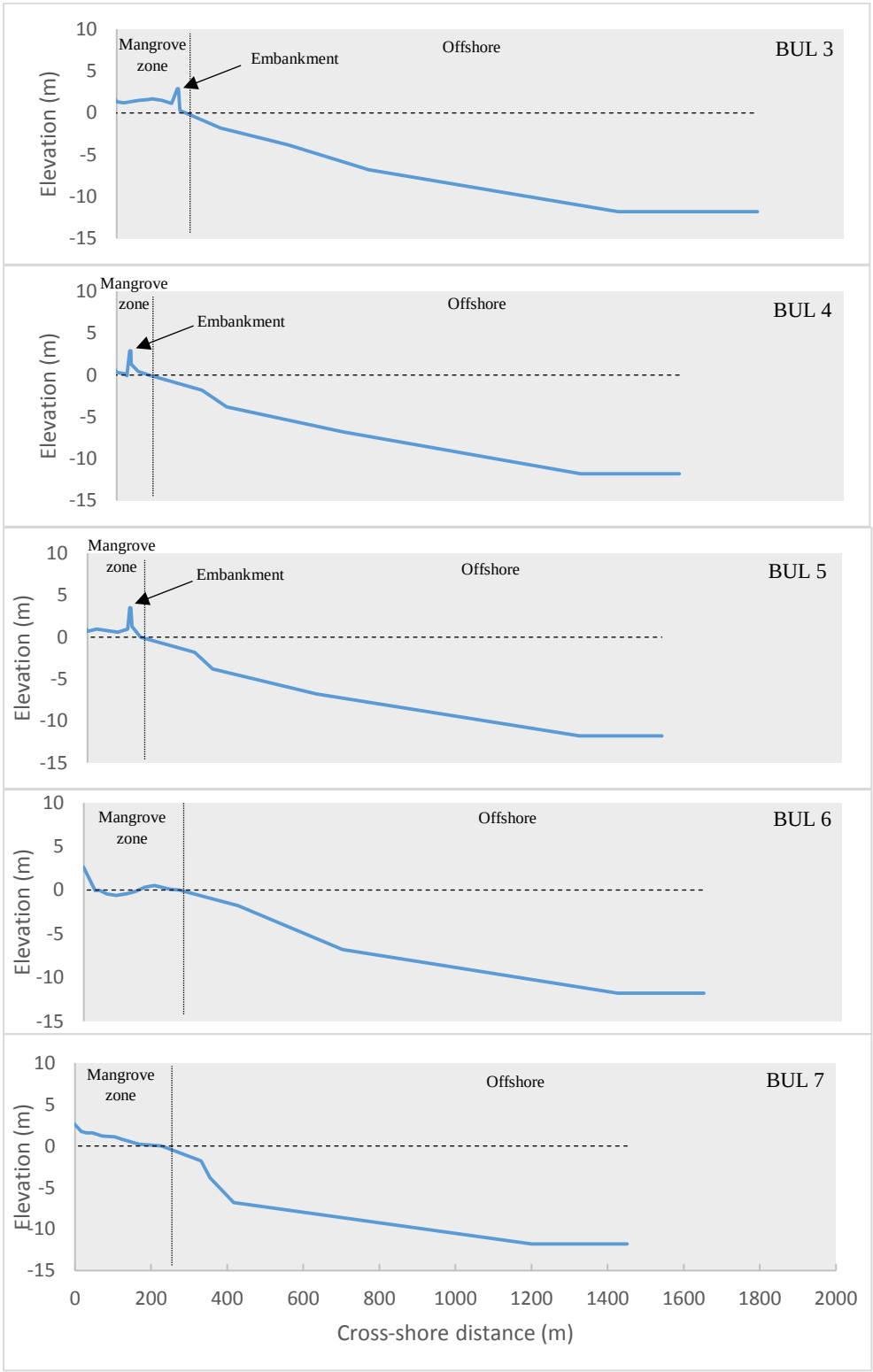

Figure 5.7 Cross-shore profiles of all transects at UBI. The cross-shore distance is referenced to the back of mangroves forest within each transects; the vertical elevation is referenced to the mean sea level (MSL). Offshore = the part of cross-shore profile below MSL.

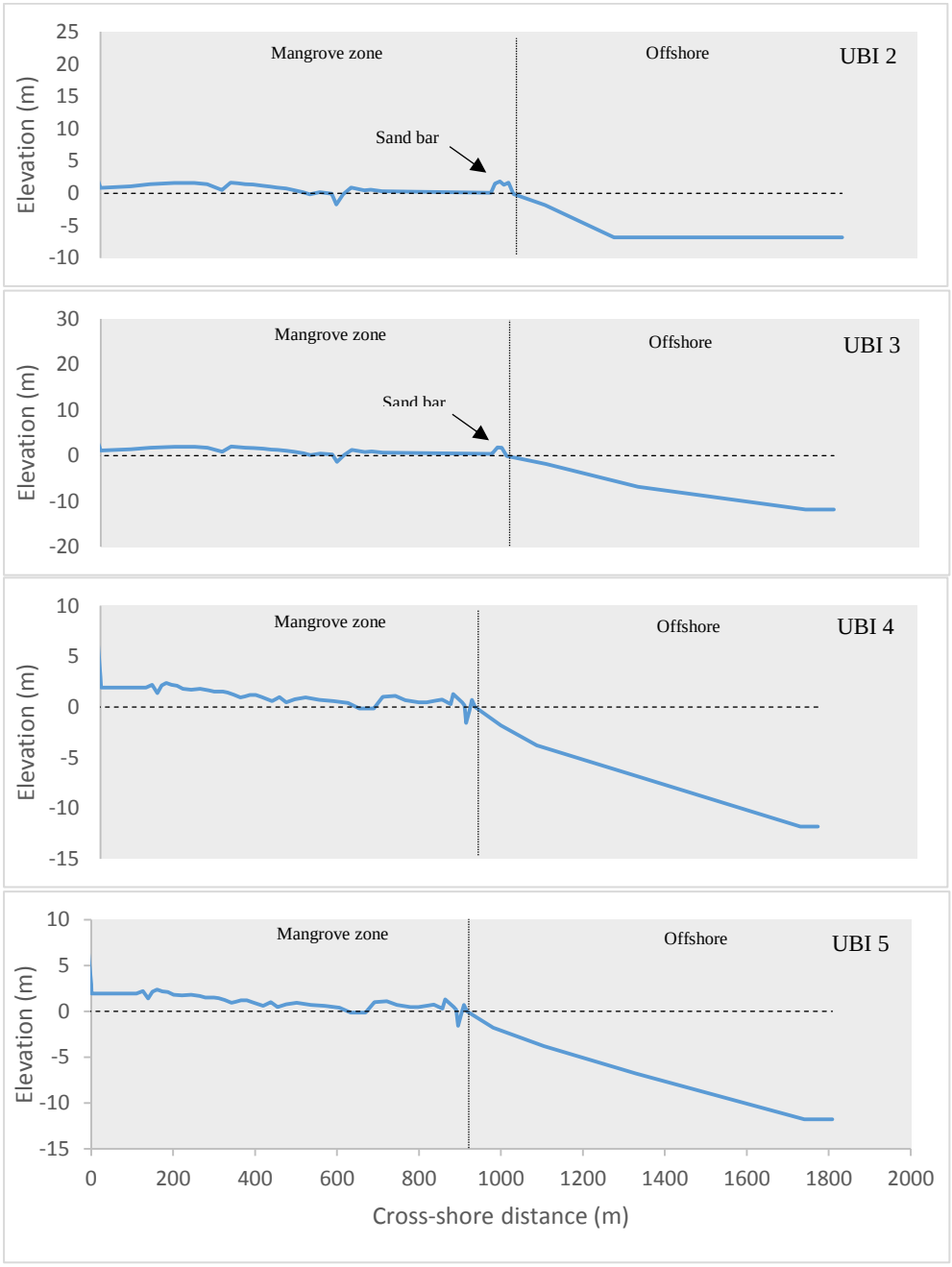

Figure 5.8 Cross-shore profiles of all transects at TEK. The cross-shore distance is referenced to the back of mangroves forest within each transects; the vertical elevation is referenced to the mean sea level (MSL). Offshore = the part of cross-shore profile below MSL.

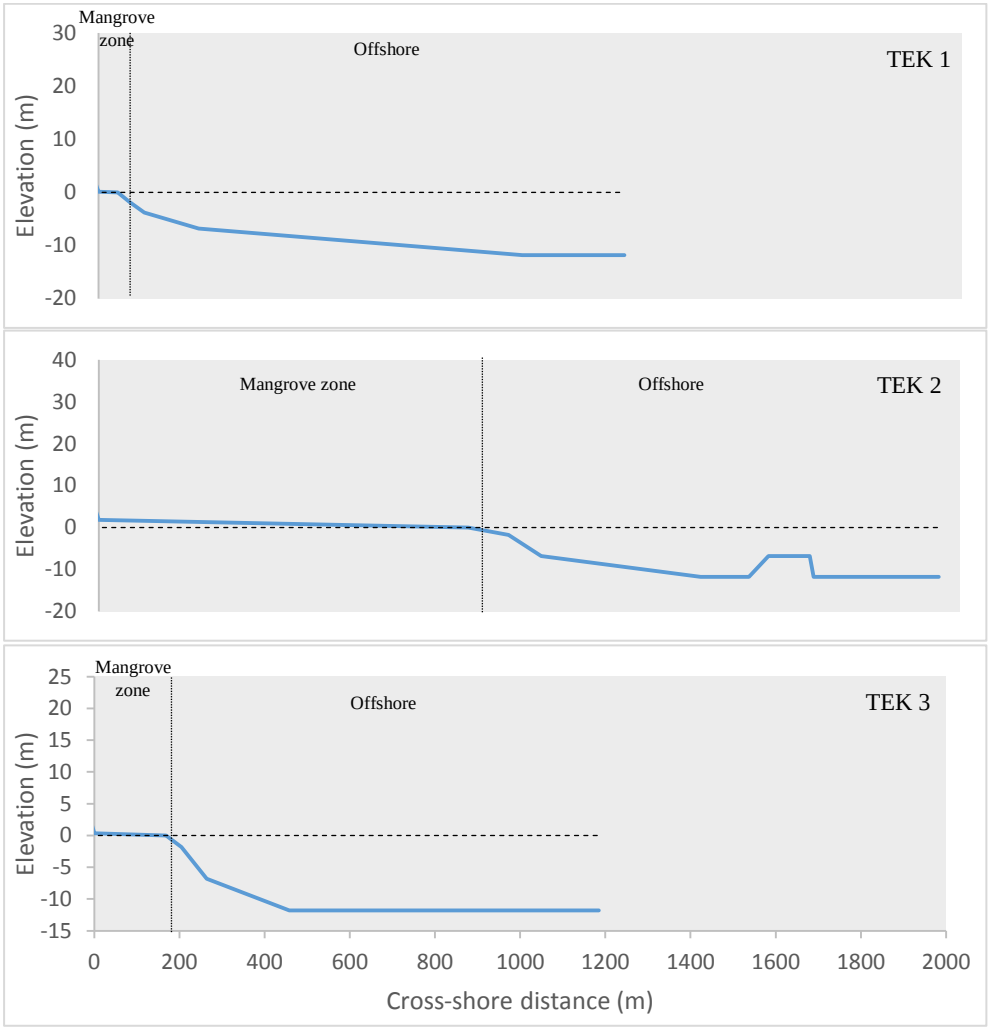

5.2.2 Sediment properties

Overall, the sediment size in MAN was larger. The median, D10 and D90 in MAN are significantly larger than BUL and UBI (Mann-Whitney test, p-value < 0.05) (Appendix C: Table C6). D10 in MAN is an order of magnitude larger than the other two sites, while D90 at MAN is almost twice the size of D90 at BUL. The larger sediment size in MAN was the result of some sand deposits near the mangrove front. The presence of sand deposits was also the reason for a significantly higher median and D90 at BUL than at UBI (Mann-Whitney test, p-value < 0.01). UBI soil is comprises mainly clay and silt. Comparatively, UBI has more homogenous sediment size, with only about 50

μm difference between D10 and D90. Similar to sediment size, bulk density at UBI (334.7 ± 78.6 kg m^{-3}) was significantly smaller than MAN and BUL (Mann-Whitney test, p-value < 0.001) and was also more homogenous. BUL has the significantly highest maximum (1612 kg m^{-3}), average (955.4 kg m^{-3}) and minimum (354 kg m^{-3}) bulk density compared to other sites (Mann-Whitney test, p-value < 0.05). The relatively larger range of bulk density measurements in MAN and BUL corresponds to the relatively larger sediment size range.

Figure 5.9 Sediment size distribution (μm) and bulk density (kg m^{-3}) for each site. D10 is defined as the grain diameter at which 10% is finer than; D25 is associated with 25% finer than; D50 is associated with 50% finer than; D75 is associated with 75% finer than; D90 is associated with 90% is finer than; the bulk density shows the average, minimum and maximum bulk density

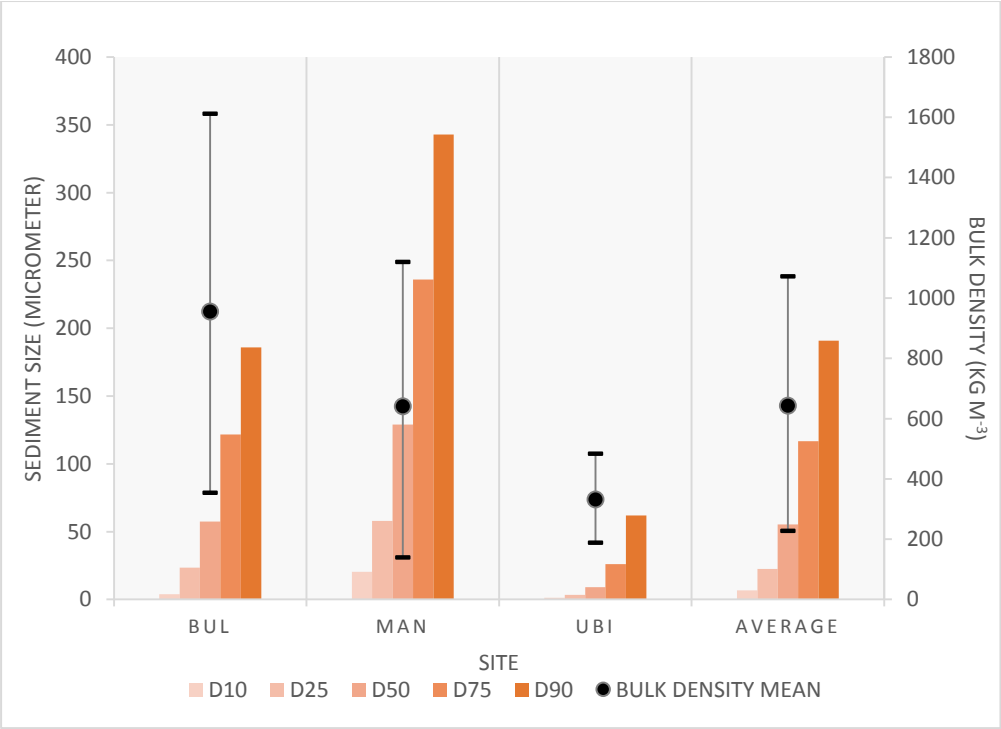

5.3 Hydrodynamic characteristics

5.3.1 Water and tidal level

There is a slight tidal level difference between Tuas and Tanjong Changi tidal stations. The MLWS at Tuas tidal station is 0.5 m with reference to Chart Datum (CD), while the MLWS for Tanjong Changi tidal station is 0.7 m. The tidal range between MLWS

and MHWS for Tuas and Tanjong Changi tidal stations are 2.5 m and 2.2 m respectively. The calculated MHW is 2.6 m for both Tuas and Tanjong Changi tidal stations.

Figure 5.10 Tidal levels at Tuas and Tanjong Changi tidal stations with reference to Chart Datum and MLLW in the bracket. * denotes the calculated MHW based on MHWS and MHWN.

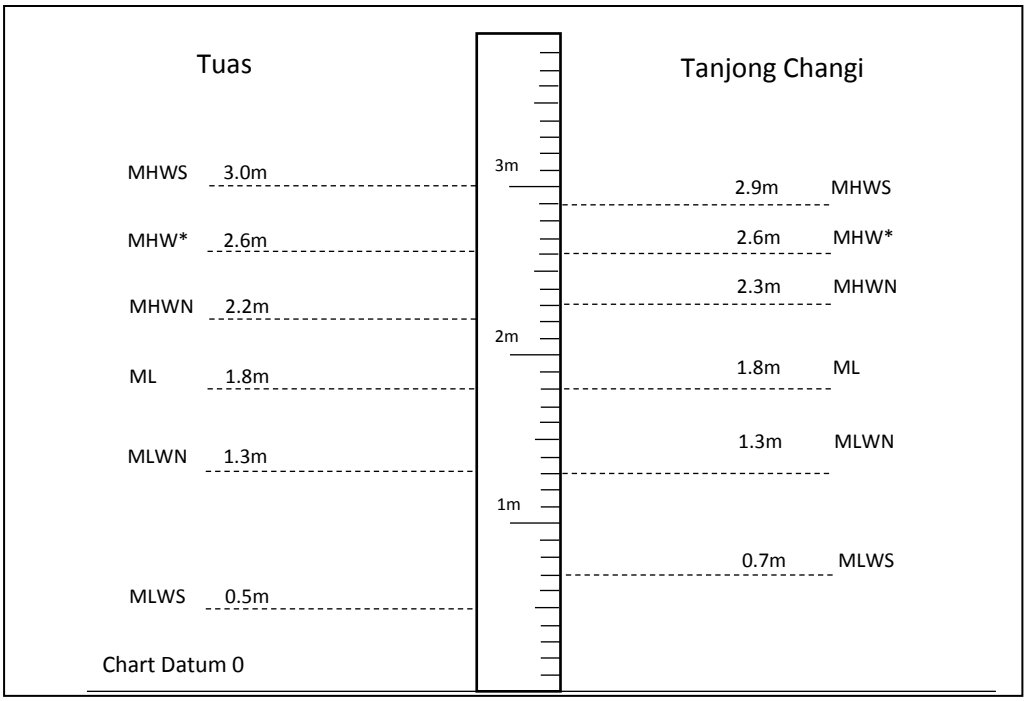

5.3.2 Average hydrodynamic conditions

Under average hydrodynamic conditions, the average significant wave height across the year was less than 10 cm, though showed some differences between the western and eastern Johor Straits. Both UBI and TEK (east Johor Straits) of 0.06 m and 0.047 m respectively, while MAN and BUL showed a significant wave height of 0.027 m. Similarly, peak wave period varied between sites, ranging from 1.13 – 1.3 s. The offshore peak wave period was slightly higher at UBI and TEK compared to MAN and BUL.

5.3.3 Extreme hydrodynamic conditions

Extreme hydrodynamic conditions were simulated based on tropical storm Vamei (Refer to section 4.2.3.2). Under the extreme conditions, offshore significant wave heights reached 1.2 – 1.4 m across all sites with a slightly higher significant wave heights at offshore TEK and UBI (Figure 5.11). The wave heights within the Johor Straits mainly comprise swells generated from nearby deeper water and transformed by shallower bathymetry as it propagates into the Johor Straits. The wave period within the Johor Straits was approximately 3 s during extreme hydrodynamic conditions. The water level during extreme event was also simulated. The high water level was a combination of SLA and typhoon-induced surge, ranging 1.2 – 1.4 m above MSL within the Johor Straits.

Figure 5.11 Significant wave height (m) at study sites during average and extreme condition

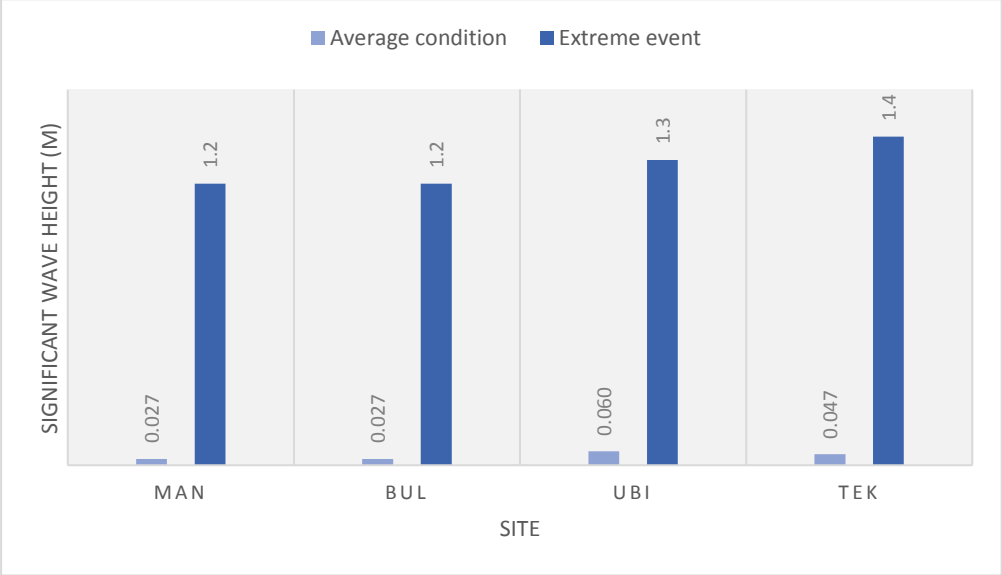

Figure 5.12 Peak wave period (s) at study sites during average and extreme hydrodynamic condition.

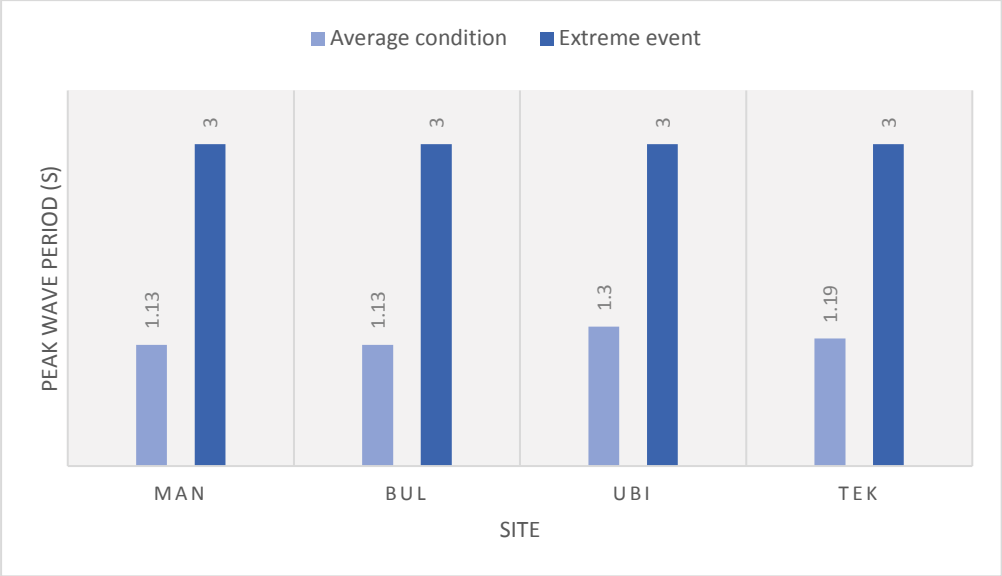

5.4 Vegetation, physical and hydrodynamic characteristics discussion

5.4.1 Mangrove structure and density

Relatively taller and larger *Avicennia* individuals measured in this study suggests that *Avicennia* individuals were more mature than *Bruguiera* recorded. The shorter *Bruguiera* trunk, however, could be the result of measurement method. As the top of a trunk was defined as height of lowest branch, the large canopy height of *Bruguiera* (columnar shape canopy) which spread lower along the trunk has shortened the measured trunk height. The same columnar shape canopy could also be the explanation for the relatively larger canopy height of *Bruguiera*. *Avicennia* also has relatively higher root spatial density (2.5 times more than *Bruguiera*). However, the much smaller *Avicennia*'s root diameters (an order of magnitude lower than other genera) resulted in the area covered by *Avicennia* pneumatophores to be lower than other genera. The canopy, trunk, and pneumatophores of *Sonneratia* individuals measured were bigger and taller compared to other genera, suggesting the *Sonneratia* in the study sites are more mature. Nevertheless, the low number of *Sonneratia* individuals at the sites means *Sonneratia* was not represented as a dominant genus in any transect.

Root characteristics

Based on previous field measurements in Singapore, Australia and New Zealand, *Avicennia* pneumatophores were found to have a density of 24 – 381 roots m^{-2} (Andrea, 2006; Burchett et al., 1998; Harty & Cheng, 2003; Krauss et al., 2003; Young & Harvey, 1996; Zhang et al., 2012). Out of these, the measurements in Singapore (Pasir Ris Park) showed a spatial density of 98 roots m^{-2}. Root density of *Avicennia* pneumatophores recorded in this study fall in between the range measured in previous studies (182.33 ± 126.67 roots m^{-2}) (Table 5.6). However, when compared to local measurement, the mean spatial density was approximately twice higher. The relatively larger range of roots density could be the result of large range of tree sizes measured (and potentially trees wider age range). The association between variation of spatial density and tree size was also mentioned in a study on *Sonneratia*, the trees with 20 – 30% larger trunk diameter, and possibly more mature individuals, was found to have significantly larger spatial density of roots (Zhang et al., 2015a). In addition, there is a difference in the *Avicennia* pneumatophores height (Pasir Ris Park = 23.9 ± 4.1 cm; this study = 7.5 ± 3.4 cm). This could be the result of difference elevation where the pneumatophores were measured as suggested by Zhang et al. (2015a). *Sonneratia* pneumatophores of average height 9 – 14 cm was found to be taller (> 30 cm) along the creek edge where there is higher inundation frequency.

The number of *Rhizophora* roots per trunk was low when compared to other studies. The number of props roots based on study carried out by Zhang et al. (2015b) in Singapore showed an average of 25 roots $trunk^{-1}$. This was lower than an average of 152 prop roots $trunk^{-1}$ counted in Coral Creek, Australia (Mazda et al., 1997b) and was more than an order of magnitude lower compared to measurements in Trang, Thailand (up to 460 roots $trunk^{-1}$) (Horstman et al., 2014). The number of prop roots per trunk was directly related to root density in the *Rhizophora*-dominated forest (Horstman et al., 2014; Mazda et al., 1997b).The higher number of prop roots per trunk, however,

could not be explained by the age inferred from trunk sizes. The trees measured in Trang, Thailand, are within the same range as found in Singapore. The *Rhizophora* trunk diameters at 2 m above ground were found to be 8.2 – 13.5 cm, with largest diameter measured at 39.2 cm, compared to mean DBH of 10 cm and a range of 5 – 35 cm in Singapore. Similar size was recorded for *Rhizophora stylosa* measured in Nakma-Gawa, Japan (5.7 cm) and Coral Creek, Australia (8.6 cm) (Mazda et al., 1997b).

Table 5.6 Comparison of *Avicennia*'s pneumatophore density with existing studies.

Location	**Pneumatophores density (m^{-2})**	**References**
Singapore	32 – 468	This study
Singapore	98	Zhang et al. (2012)
New Zealand	80 – 200	Andrea (2006)
Australia	24 – 347	Harty & Cheng (2003)
Micronesia	45 – 51	Krauss et al., 2003)
Australia	50 – 381	Burchett et al. (1998)
New Zealand	40 – 250	Young & Harvey (1996)

Vegetation density

Vegetation density in Kantang, Thailand ranged from 0.32 – 0.48 trunk m^{-2} in the *Avicennia*/*Sonneratia* dominated fringe mangrove and was as low as 0.01 trunk m^{-2} in Palian, Thailand. The spatial density in the *Rhizophora*-dominated mangrove forest ranged from 0.06 – 0.26 trunk m^{-2} in Kantang, Thailand. They are within the same range as found in this study (0.01 – 0.35 trunk m^{-2}) (Table 5.7). Comparatively, the trunk density of *Rhizophora* in both Iriomote Island, Japan and Coral Creek, Australia are both higher than in Singapore (1.0 trunk m^{-2} at Iriomote Island and 0.8 trunks m^{-2} at Coral Creek). Although the trunk density of *Rhizophora* in Singapore and Thailand were within the same range, the difference in number of prop roots per tree yield a difference in much denser overall vegetation density in the Thailand mangrove forest,

which was expressed as vegetation cover rates at certain height above the stratum (Horstman et al., 2014). The plots dominated by *Rhizophora* also showed a higher trunk density compared to plots in BUL. The site difference in trunk density could affect the wave attenuation ability. The higher the density, more obstruction to water flow and high energy dissipation may occur.

Table 5.7 Comparison of vegetation density with existing studies

Location	**Dominant genus**	**Vegetation density (m^{-2})**	**References**
Singapore	Mix of *Avicennia, Bruguiera* and *Rhizophora*	0.01 – 0.35	This study
Thailand	*Avicennia*/ *Sonneratia*	0.01 – 0.48	Horstman et al. (2014)
Thailand	*Rhizophora*	0.06 – 0.26	Horstman et al. (2014)
Japan	*Rhizophora*	1	Mazda et al. (1997b)
Australia	*Rhizophora*	0.8	Mazda et al. (1997b)

Vegetation extent

Singapore's mangroves are of medium to small size and have a history of encroachment and coastal disturbance (Lai et al., 2015; Yang et al., 2011; Yee et al., 2010). The average width of mangroves in Singapore is similar to the width of mangroves experiencing coastal squeeze in Mekong Delta, Vietnam. The estimated mangrove width in Singapore was as short as 30 m and as wide as 790 m. The main factors of destruction were the timber overexploitation for construction, charcoal and aquaculture (Phan et al., 2014). The fragmented and disturbed mangroves are common in coastal area with urban development (Nguyen et al., 2015; Phan et al., 2014). The fragmentation decreases the stability of mangroves and could lead to the loss of various ecosystem services (Everard et al., 2014; Nguyen et al., 2015; Phan et al., 2014).

5.4.2 Vegetation and geomorphological heterogeneity of Singapore mangroves

Mangroves in Singapore comprise a mix of species. Although the dominant genera were identified in all sites, the percentage representation of the dominant genus was low. In most transects such as in BUL and MAN, the dominant genus only comprised one third of all trees measured; while the second most recorded genus was approximately 20%. Comparatively, in Trang, Thailand, more than 95% of the back mangroves are *Rhizophora* (Horstman et al., 2014), while the predominant *K. candel* made up approximately 88.9% of the species composition in Red River delta, Vietnam (Quartel et al., 2007). The evenness in the genus distribution increases the complexity of the forest through their inherent biotic architectural difference. As a result, the physical processes such as water flow and wave propagation across the vegetation field become more complex.

Geomorphological variations were also observed at study sites. Natural geomorphological features such as basins, sand bars, sand deposits observed within the mangroves changed the topographical profiles and affect wave propagation pattern into mangrove forests. For example, the sand bar located in front of mangroves at UBI2/3 was sufficiently high to prevent direct wave propagation into the mangrove forest under normal hydrodynamic conditions. The presence of artificial embankment also introduces complexity to the mangrove area. Due to the past aquaculture activities, artificial embankments were observed at UBI and BUL. Similar to sand bars, some these artificial embankments are sufficiently high to prevent inundation from the front of the mangrove forest such as the ones observed at BUL. Other old embankments at UBI were eroded and reduced in height and present as microtopographical feature within mangroves.

Heterogeneity of geomorphology and vegetation at each site are possibly related. The local geomorphology, natural or artificial could affect the establishment of mangroves

seedling (Balke et al., 2013; Friess et al., 2012a). Local geomorphology affects the water flow and sediment dynamics over various spatial and temporal scales. In combination with a seedling's ability to establish itself at a specific elevation range, the resulting self-organized biogeomorphic landscape contributes to the heterogeneity of vegetation composition (Balke et al., 2013). In addition, the artificial embankment, usually made of boulders, could not accommodate all species as it is different from muddy sediment where mangrove usually grows.

The complexity within the mangroves was also observed in the sediment properties. As opposed to the homogeneous sediment properties at UBI, the wide range of bulk densities and sediment sizes in MAN and BUL reflected the heterogeneous bed composition. The relatively large sediment size range at MAN and BUL was also a result of the presence of localized sandy patches and muddy substrates within the mangrove forest. As bottom friction arises from the different sediment interacting with the water flow near the bottom, the spatial extent and distribution of these wide variety of sediment type could increase the complexity quantifying the contribution of bottom sediment on wave attenuation.

5.4.3 Implications of vegetation, physical and hydrodynamic characteristics for the model

The complexity of the vegetation and geomorphology of the mangroves in the study sites was difficult to be represented in the model. As transects were represented by only the dominant genus (as required by the model), the mixed genus and the large percentage of the second most dominant genus were not represented. Similarly, the localized sand deposits within some plots and the spatial distribution of sandy and muddy substrates in the more heterogeneous mangroves (vegetation and sediment properties), such as MAN, were difficult to represent in the model. The inability to incorporate the heterogeneity of the mangroves leads to negligence of the mixed effects

of biotic structures on wave attenuation. Nevertheless, in order to minimize the effect of vegetation and geomorphological heterogeneity on the model, a large number of models (and transects) were simulated for each site to obtain a range of wave attenuation outcome.

The effects of the extensive shallow mudflat in the foreshore at MAN were not fully captured in the model, especially during high waves when wave break in the foreshore. The process of wave breaks at the foreshore before entering the mangrove forest causes energy dissipation (a process captured by the model). Secondary turbulence effect generated during wave breaking process, on the other hand, could increase the wave dissipation within the mangrove (Strusińska-Correia et al., 2013). Such secondary wave dissipation processes, however, were not captured in the model. Nevertheless, this effect should not be significant at other study sites given the absence of extensive shallow mudflat foreshore.

Despite the complexity in representing heterogeneous physical and vegetation characteristics, the use of site-specific vegetation and physical characteristics obtained from the extensive site survey provided a more realistic model result. The inclusion of vegetation structural information of the different genus according to the composition at the study sites should improve the reliability of model outcome. On the other hand, the site-specific data input prevented the generalization of mangrove wave attenuation rate to other mangrove sites in Singapore or other countries, since the vegetation composition, topography variation and even hydrodynamic characteristics vary. For example, given the canopy of mangrove vegetation in this study was high and did not intercept the incoming waves, the effect of branches and leaves was not accounted for in the wave attenuation model. However, the canopy effect could be significant at sites where canopy are lower or storm waves are sufficiently high to interact with the branches and leaves.

6 Modelling of wave attenuation of Singapore's mangroves

Using the vegetation, physical, and hydrodynamic characteristics data collected from the extensive field and desktop study, wave attenuation in mangrove forests was simulated using the nearshore wave evolution model in InVEST. Both average and extreme conditions were used as hydrodynamic scenarios. In this chapter, the extent of wave height reduction in the mangroves is shown, alongside the factors contributing to attenuation.

6.1 Extent of wave height reduction

6.1.1 Average conditions

Figure 6.1 shows the percentage of wave height reduction during the average hydrodynamic condition at the four study sites, namely MAN, BUL, UBI, and TEK. Overall, the percentage of wave height reduction ranged from -0.5 to 50.7%. The negative wave height reduction (increase in wave height) was found in BUL5, MAN2, and MAN3 due to wave shoaling. Among the study sites, TEK showed the highest median wave height reduction (22%), while the other three sites showed similar median wave height reduction rate of 1 – 5%, though there was no significant difference between all sites (Kruskal-Wallis test, p-value > 0.05), probably due to the small sample size.

In the western Johor Straits, MAN and BUL showed a median wave height reduction of 2.1% and 4.8% respectively. The slightly higher median in BUL was probably caused by the wave propagation across longer distance within the mangrove at BUL6/7. The same transects also raised the maximum percentage of wave height reduction at BUL. At transects where artificial embankments were present. BUL3/4/5 showed relatively lower percentage of wave height reduction compared to transects without the embankments (10.7% vs 2.0%).

Up to 50.7% of wave height was reduced in TEK. On the contrary, UBI which is located adjacent to TEK, showed a maximum of only 1.14% wave height reduction, and is even lower than the maximum wave height reduction at BUL (12.95%) and MAN (2.89%). Even under the HT scenario, two of the four transects (UBI2/3) at UBI did not experience incoming waves due to a high sand bar in front of the mangrove zone that prevented wave propagation. Similar sand deposits were found in MAN and BUL, affecting the extent of wave height reduction at BUL5, MAN2, and MAN3.

Figure 6.1 Percentage of wave height reduction at each site under average conditions. BUL = Sungei Buloh Wetland Reserve; MAN= Mandai mangroves; TEK = Pulau Tekong; UBI = Pulau Ubin

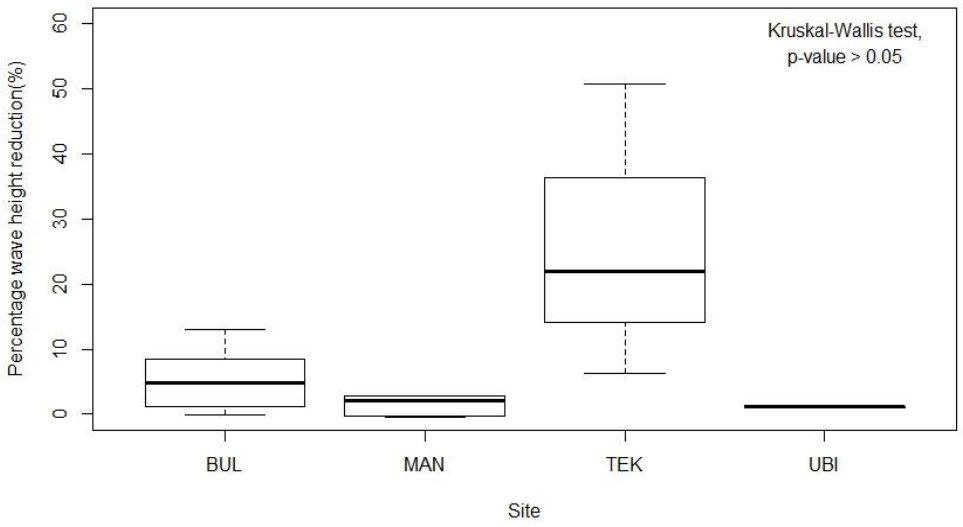

Wave height reduction rate indicated the effectiveness of the mangrove area at each site by taking into account the distance waves travelled within the mangrove forest. Overall, the wave height reduction rate ranged from -2.5×10^{-4} m^{-1} to 1.4×10^{-3} m^{-1} (Figure 6.2). TEK still showed the highest median of 1.3×10^{-3} m^{-1} wave height reduction rate, despite a smaller range compared to percentage of wave height reduction. Statistical analysis showed no difference between wave reduction rate at

TEK, BUL, and UBI (Mann-Whitney test, p-value > 0.05). A slight significant difference was found between TEK and MAN (Mann-Whitney test, p-value < 0.05) (Appendix C: Table C7).

Figure 6.2 Wave height reduction rate at each site under average conditions. Only MAN – TEK shows significant difference in Mann-Whitney test. BUL = Sungei Buloh Wetland Reserve; MAN= Mandai mangroves; TEK = Pulau Tekong; UBI = Pulau Ubin. * indicates p-value < 0.05; ** indicates p-value < 0.01; *** indicates p-value < 0.001.

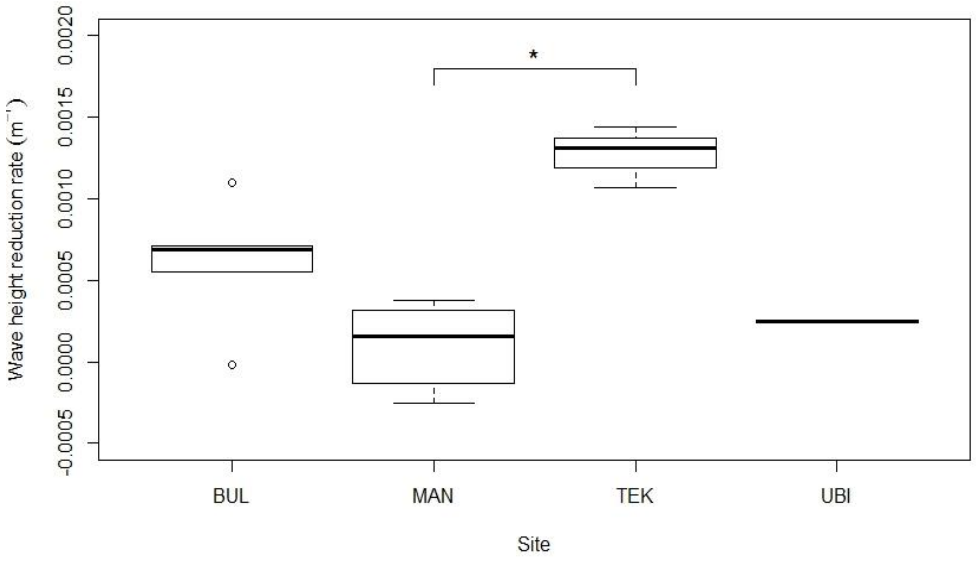

6.1.2 Extreme hydrodynamic conditions

Under extreme hydrodynamic conditions, the median percentage of wave height reduction was approximately 60% for MAN, BUL, and TEK. While UBI showed a higher percentage of wave height reduction (83.4%), there was no significant difference across all sites (Kruskal-Wallis test, p-value > 0.05). The higher median percentage wave height reduction at UBI was due to the longer mangrove cross-shore extent. In the LW scenario, water level was not high enough for the waves to propagate into the mangrove in BUL2/3. Therefore, percentage wave height reduction was only calculated for UBI4/5 (≈ 82.1%). In the HT scenario when the water level was

sufficiently high to reach the mangrove forest, the average percentage of wave height reduction at all transects in UBI was approximately 84.4%.

Although the median percentage of wave height reduction at BUL, MAN, and TEK was relatively lower than UBI, the maximum percentage of wave height reduction is similar to that of UBI (≈ 90%). The large percentage of wave height reduction was probably caused by the steeper slope and an increase in wave breaking. In addition, these maxima were found at LW scenario and were comparatively higher than the correspondent transects at HW scenario, indicating the water level as one of the influencing factors. The range of wave height reduction also varied across sites. The large range at BUL (2.8 – 89.6%) was the result of the difference in mangrove width. Within BUL, relatively lower wave height reduction percentage was found in HW scenario at BUL3/4/5 with artificial embankments. On the contrary, relatively smaller wave height reduction range in UBI was probably the result of similar mangrove width at all transects.

Figure 6.3 Percentage wave height reduction at each site under extreme conditions. BUL = Sungei Buloh Wetland Reserve; MAN= Mandai mangroves; TEK = Pulau Tekong; UBI = Pulau Ubin

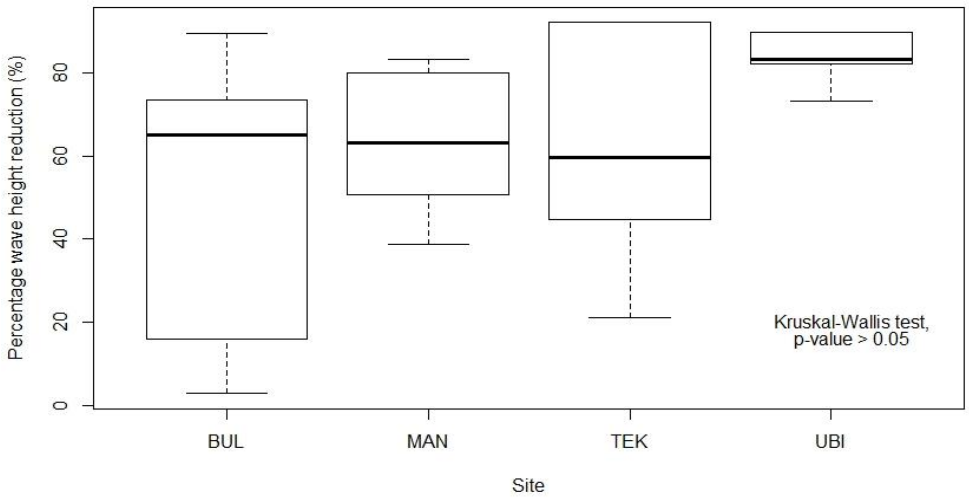

The wave reduction rate across all sites ranged from 7.67 x 10^{-4} m^{-1} at UBI to 2.5 x 10^{-2} m^{-1} at MAN. Except for a few outliers at MAN and BUL, the wave height reduction rate were all less than 1.6 x 10^{-2} m^{-1} with no statistical difference across sites (Kruskal-Wallis test, p-value > 0.05). There is a relatively large difference between median and maximum wave height reduction rates at UBI. This is the result of the high wave height reduction rate at UBI3/4 in LW scenario compared to other transects (1.7 x 10^{-2} m^{-1} vs 7.67 x 10^{-4} – 1.23 x 10^{-3} m^{-1}). As compared to the total percentage of wave height reduction, the wave height reduction rate has a relatively narrower range across all sites.

Figure 6.4 Wave height reduction rate at each site under extreme hydrodynamic conditions. BUL = Sungei Buloh Wetland Reserve; MAN= Mandai mangroves; TEK = Pulau Tekong; UBI = Pulau Ubin

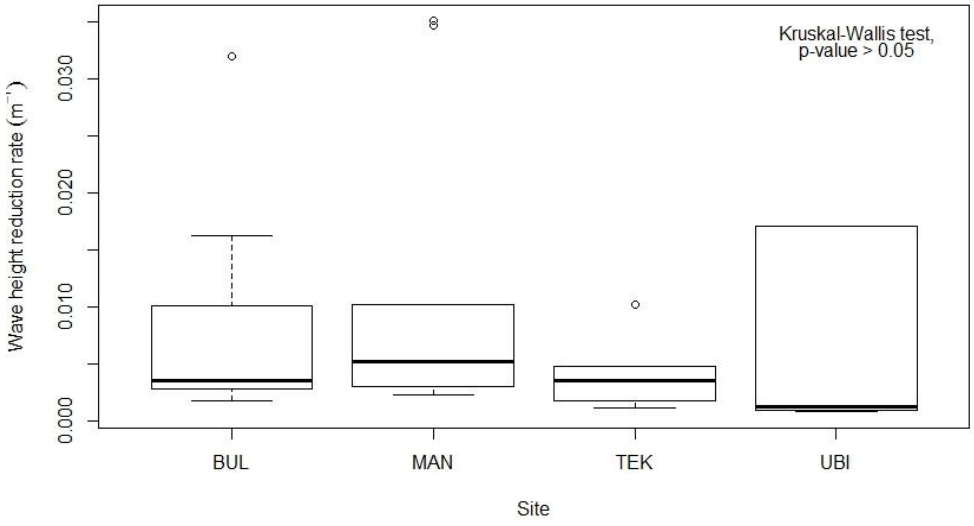

6.1.3 Comparison of wave height reduction during average and extreme hydrodynamic conditions

The total percentage of wave height reduction in general was lower during the average hydrodynamic conditions (Mann-Whitney test, p-value < 0.05). At the maximum, close to 90% wave height reduction was found during extreme hydrodynamic conditions;

while only half of the incoming wave height was reduced during average hydrodynamic conditions. Wave height increased in some transects (BUL5, MAN2 and MAN3) during average conditions. At the same transects where wave height increases, the percentage of wave height reduction reaches 79.6% during the extreme hydrodynamic condition, when the water level and wave height is higher.

The variation of wave height reduction rate across sites was different between average and extreme hydrodynamic conditions. The median wave height reduction rate under average hydrodynamic conditions was lower and ranged from 2.45×10^{-4} m^{-1} to 1.3×10^{-3} m^{-1}; while the median wave height reduction rate during extreme hydrodynamic condition showed a more similar median of $1.2 \times 10^{-3} – 5.2 \times 10^{-3}$ m^{-1}.

6.2 Contribution of wave dissipation factors

6.2.1 Average hydrodynamic conditions

Vegetation was the major contributor to the wave attenuation at BUL, MAN, and TEK (Figure 6.5), contributing 90 – 100% of the total drag force, with the remaining contributed by bottom friction. There was no statistical difference across transects (Kruskal-Wallis test, p-value > 0.05). Nevertheless, some within-site difference was observed at UBI. Although vegetation was still the major contributor to the total drag force, the portion dropped to approximately 60% at UBI4/5. Wave breaking and bottom friction contributes to approximately 34% and 6% respectively of the remaining drag force. No distribution was calculated at UBI2/3 as the waves did not propagate into the mangroves.

Figure 6.5 Average percentage contribution of wave dissipation by vegetation, wave breaking, and bottom friction for respective transect, under average hydrodynamic conditions. N.A. = Not Available.

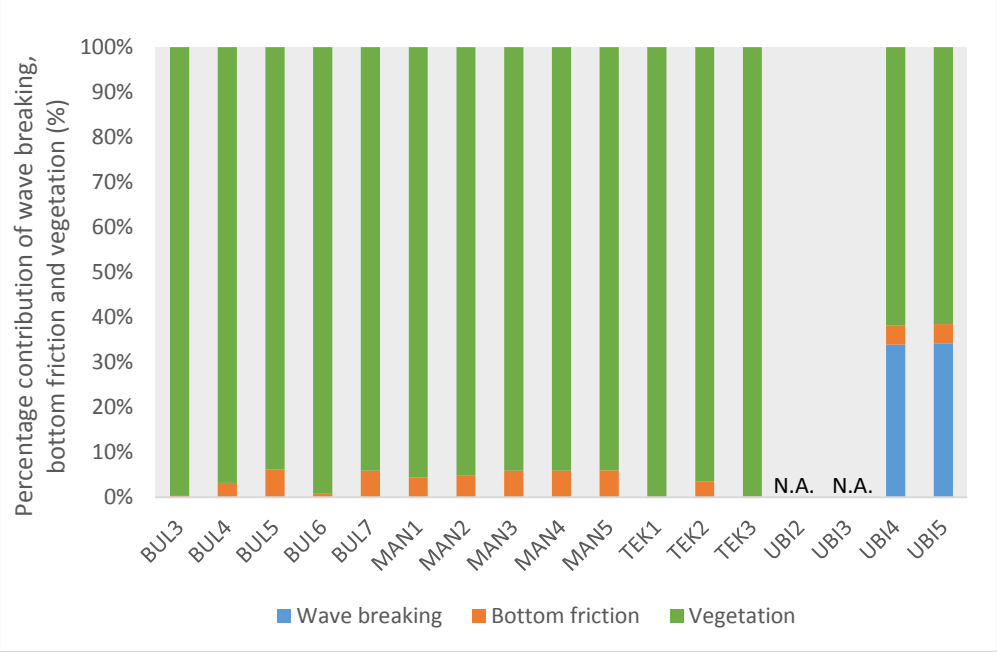

6.2.2 Extreme hydrodynamic conditions

Under extreme hydrodynamic conditions, vegetation and wave breaking are the two main wave dissipation factors (Figure 6.6). In general, vegetation contributed 20 – 83% of total drag force, except for UBI2/3 where vegetation provided up to 97% of total drag force. Dissipation by bottom friction was consistent across all transects (1.3 – 3.2%). The contribution of vegetation was mainly driven by the mangrove extent, with longer cross-shore mangrove extent leading to higher accumulated vegetation drag, resulting in a higher wave energy dissipation. For example, TEK2 had the longest cross-shore extent (858 m), followed by TEK3 (168 m), and TEK1 (44 m); the percentage of vegetation drag force followed the same order. Similar pattern was also found in MAN. In BUL, however, the presence of embankments at BUL3/4/5 disrupted this pattern. Despite the variations observed, statistical analysis showed no significant difference across all site for all drag forces (Kruskal-Wallis test, p-value > 0.05).

Figure 6.6 Average percentage contribution of wave dissipation by vegetation, wave breaking and bottom friction for respective transect, under extreme hydrodynamic condition.

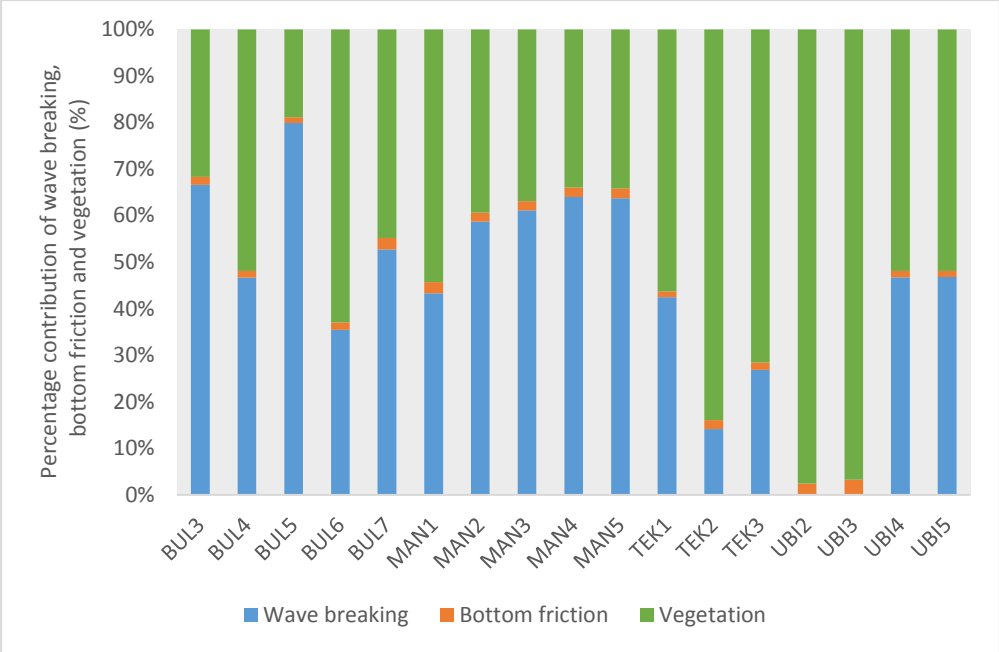

6.2.3 Comparison of dissipation factors during average and extreme hydrodynamic conditions

The main difference between average and extreme hydrodynamic condition was the percentage of wave breaking in total drag force. While less than 1% wave breaking force was found under average hydrodynamic conditions, up to 79% of total drag force was contributed by wave breaking under extreme hydrodynamic conditions (Mann-Whitney test, p-value < 0.001). There is, however, an exception. At UBI, wave breaking at UBI4/5 were similar, approximately 34% in average hydrodynamic conditions and 50% in extreme hydrodynamic conditions. The bottom friction, on the other hand, was relatively consistent (< 10%) even between average and extreme hydrodynamic conditions. Nonetheless, there was a slight statistically difference between the average and extreme conditions (Mann-Whitney test, p-value < 0.05).

6.3 Vegetation, physical and hydrodynamic factors influencing the extent of wave attenuation

6.3.1 Mangrove density

The percentage of wave height reduction for transects were plotted against the mangrove density at corresponding transects (Figure 6.7). Percentage wave height reduction during average hydrodynamic conditions was lower than that under extreme hydrodynamic conditions in general. There was no statistically significant relationship found under average hydrodynamic conditions (Pearson's correlation coefficient = -0.06, p-value > 0.05). Mangrove density was positively correlated with percentage of wave height reduction under extreme conditions with a Pearson's correlation coefficient of 0.40 (p-value < 0.05). During extreme hydrodynamic conditions, the denser the mangrove forest, wave energy dissipation due to vegetation drag force is higher in denser mangrove forests. Despite the correlation, some transects with low mangrove density (< 0.1 trees m^{-2}) has demonstrated similar wave height reduction of denser mangrove (0.28 trees m^{-2}).

Figure 6.7 Scatterplot of percentage of wave height reduction and correspondent mangrove density at each transect. No Line was shown for the statistically non-significant correlation under average hydrodynamic conditions.

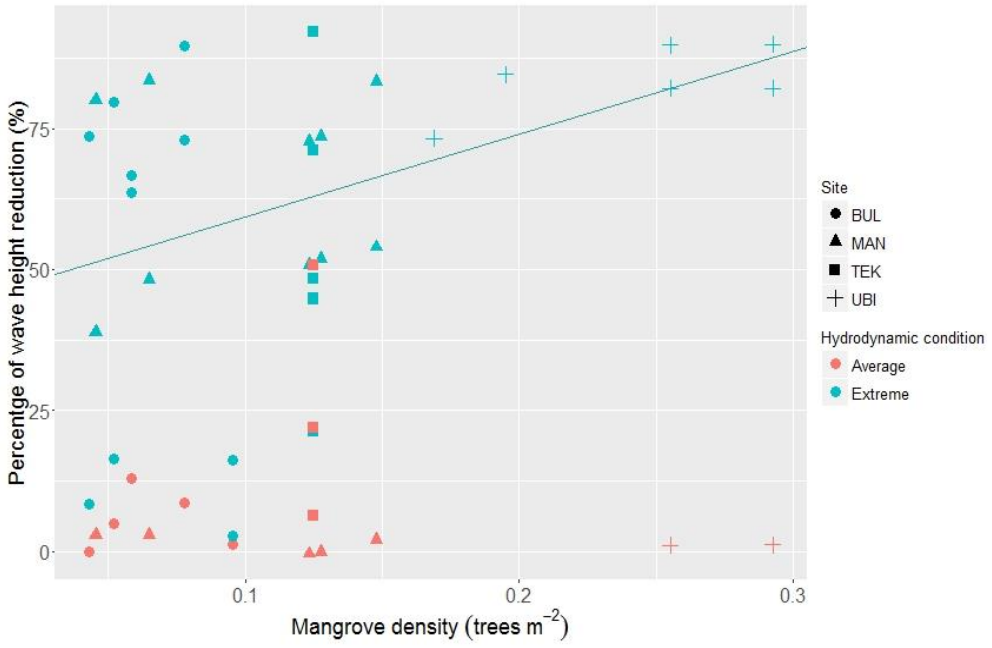

6.3.2 Mangrove extent

Figure 6.8 illustrates the percentage wave height reduction at transects with the correspondent mangrove extent under average and extreme hydrodynamic conditions. For larger mangrove extents, the percentage wave height reduction is more than 50%, except for two cases (UBI4/5) under the average hydrodynamic conditions. Notably, some cases with lower mangrove extent also showed a high wave height reduction. Similar to relationships between mangrove density and percentage of wave height reduction, no statistically significant correlation between mangrove extent and percentage of wave height reduction was found under average hydrodynamic condition (Pearson's correlation coefficient = 0.38, p-value > 0.05); while a statistically significant correlation was found under extreme hydrodynamic condition (Pearson's correlation coefficient = 0.61, p-value < 0.001).

Figure 6.8 Scatterplot of percentage of wave height reduction at each transect and the correspondent mangrove extent. No Line was shown for the statistically non-significant correlation under average hydrodynamic conditions.

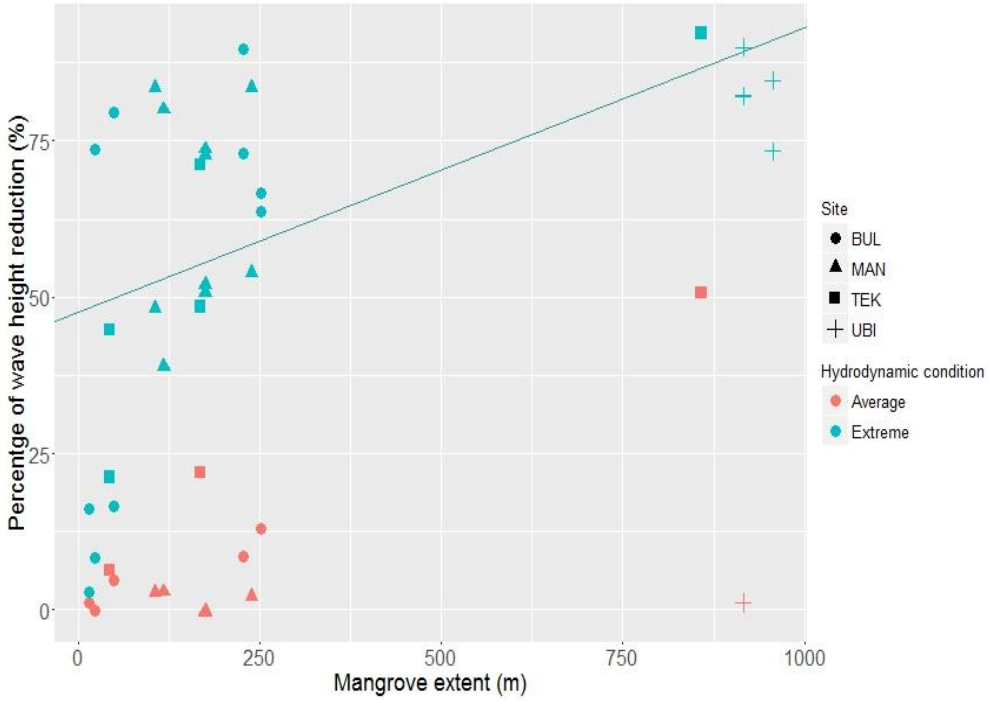

Mangrove density vs mangrove extent

Site grouping was observed in both correlation analyses of mangrove density and mangrove extent with percentage of wave height reduction. The correlation found between mangrove density and percentage of wave height reduction could be influenced by the mangrove extent and *vice versa*. At UBI, where mangrove density was higher (0.16 – 0.29 trees m^{-2}), the cross-shore mangrove extent was also longer (> 800 m). On the contrary, at MAN and BUL, where the cross-shore mangrove extent was shorter (< 250 m), the mangrove density was lower (0.04 – 0.14 trees m^{-2}). The correlation analysis showed a statistically significant positive correlation between mangrove density and mangrove extent ($r = 0.78$, p-value < 0.001).

Figure 6.9 Scatterplot of transect mangrove extent and the correspondent mangrove density.

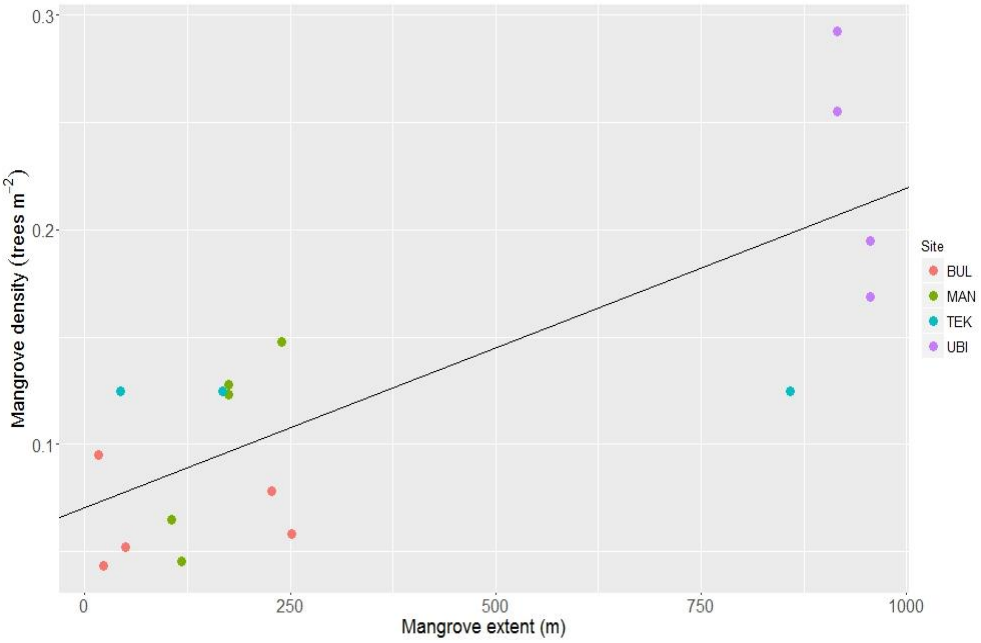

6.3.3 Vegetation type

Under average hydrodynamic conditions, transects dominated by *Rhizophora* showed a relatively higher median wave reduction rate of 1.0 x 10^{-3} m^{-1} compared to 3.14 x 10^{-4} m^{-1} and 1.35 x 10^{-4} m^{-1} for *Avicennia* and *Bruguiera* respectively. There was also a large range of wave reduction rates at transects dominated by *Rhizophora* compared to

transects dominated by other genera. The median wave reduction rate under extreme hydrodynamic conditions was relatively similar ($2.85 \times 10^{-3} – 5.04 \times 10^{-3}$ m^{-1}) and the ranges were relatively smaller, albeit with a few outliers. Despite differences in wave height reduction rates observed, there was no significant difference in wave reduction rate across genera under both average and extreme hydrodynamic conditions (Kruskal-Wallis test, p-value > 0.05). The differences in wave height reduction rate observed between genera could be the result of other wave dissipating factors. For example, the coastal geomorphology effect was more apparent at transects in MAN and BUL where the slope is steeper and could induce a higher wave energy dissipation from wave breaking.

Figure 6.10 Wave height reduction rate of dominant genus under average and extreme hydrodynamic condition.

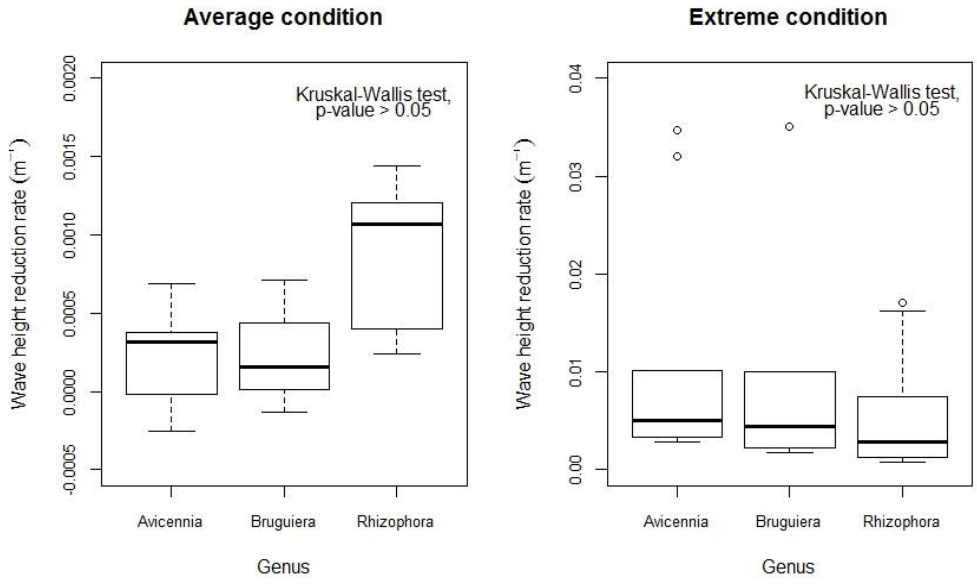

6.3.4 Mangrove structures

Figure 6.11 shows the relative contribution of roots, trunk, and canopy under average hydrodynamic conditions. Mangrove root was found to be the main contributor to the wave dissipation among the three main mangrove structures (root, trunk and canopy). Across all sites except one transect, mangrove roots contributed to 85 – 100% of wave

dissipating drag force; while mangrove trunks made up the rest. The canopy did not provide any drag as the water level was not sufficiently high to submerge the canopy.

At TEK, mangrove root was the sole contributor to the vegetation drag force. All transects at TEK were dominated by *Rhizophora* and have a gentle slope. The combination of gentle slope and *Rhizophora* root height (1.4 m) ensures the surface waves only reach the roots structure. Similar vegetation-slope combinations were also present, affecting the biotic structure inundated at the other three sites, with some within-site variation found at MAN and BUL transects. Shorter pneumatophores (< 10 cm) of *Avicennia* and *Bruguiera* at MAN and BUL were fully submerged during the high tide and trunk would start to exert drag force on the water column. There is one outlier at BUL (6% dissipation by root and 94% dissipation by trunk). This outlier is the result of combined short mangrove extent, slope and short pneumatophores height (*Bruguiera*).

Figure 6.11 Percentage of wave reduction contributed by roots, trunk and canopy at study sites under average hydrodynamic condition.

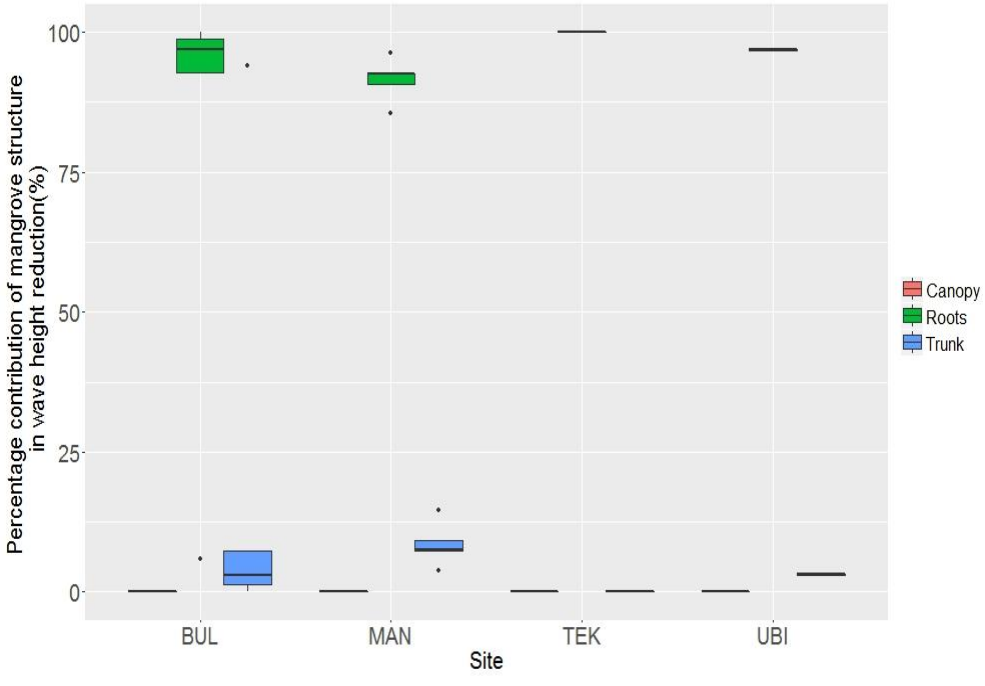

Similarly, under extreme hydrodynamic conditions, mangrove root was the major wave dissipating structure. Overall, mangroves roots contributed between 65% and close to 100% across all sites. The remaining vegetation drag force was provided by mangrove trunk (0 – 35%). The mangrove canopy did not contribute to any drag force as the high water level, even during extreme events when water level was raised by typhoon-induced surge and SLA, did not reach the canopy.

BUL and MAN showed a relatively large range of roots and trunks contribution under extreme hydrodynamic conditions. Such a range was caused by the difference in water level during LW and HW scenarios in association with the topography at respective site. An increase in water level increases the proportion of vegetation structure submerged and affect the amount of drag force exerted. Relatively less variation was found at BUL and TEK where *Rhizophora* was the dominant genus. The tall root structure of *Rhizophora* was able to continue dissipating wave energy when the water level rises (LW and HW scenario) under extreme hydrodynamic conditions.

Figure 6.12 Percentage of wave reduction contributed by roots, trunk and canopy at study sites under extreme hydrodynamic condition.

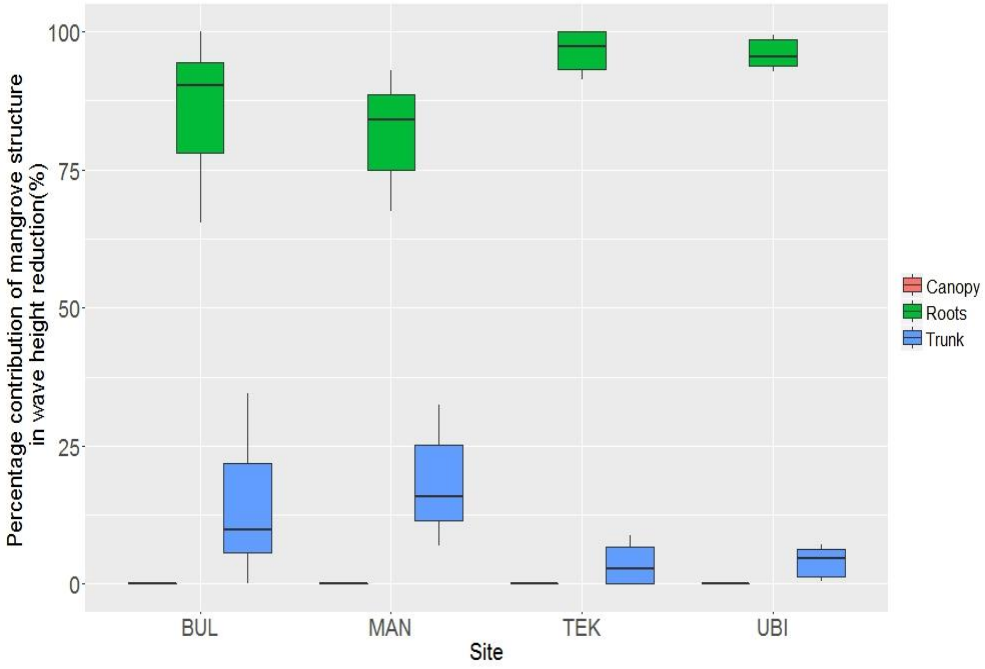

6.3.5 Water level

The water level at which the surface waves propagate directly affects the amount of vegetation, wave breaking, and bottom friction force generated. Figure 6.13 showed the wave height reduction rate at LW and HW scenarios under extreme hydrodynamic conditions. Results showed that the median wave height reduction rate was lower at HW (0.003 m^{-1}) than LW (0.01 m^{-1}). The difference in wave height reduction rate for the two water levels was statistically significant (Mann-Whitney test, p-value < 0.001). Other than the median, HW showed a comparatively smaller range of wave height reduction rate (0.001 – 0.005 m^{-1}), compared to LW scenario (0.002 – 0.025 m^{-1}). The small range of wave height reduction rate under HW scenario was caused by the indifference to the wave dissipation by bottom friction and close-to-the-ground dense pneumatophores system that varied across transects. Under average hydrodynamic conditions, as only the high water level (HW) scenario showed some form of wave height reduction, there was no comparison between the effect of low and high water level on wave attenuation.

Figure 6.13 Wave height reduction rate for low (LW) and high (HW) water level scenario under extreme hydrodynamic conditions. LW = Low Water scenario; HW = High Water scenario.

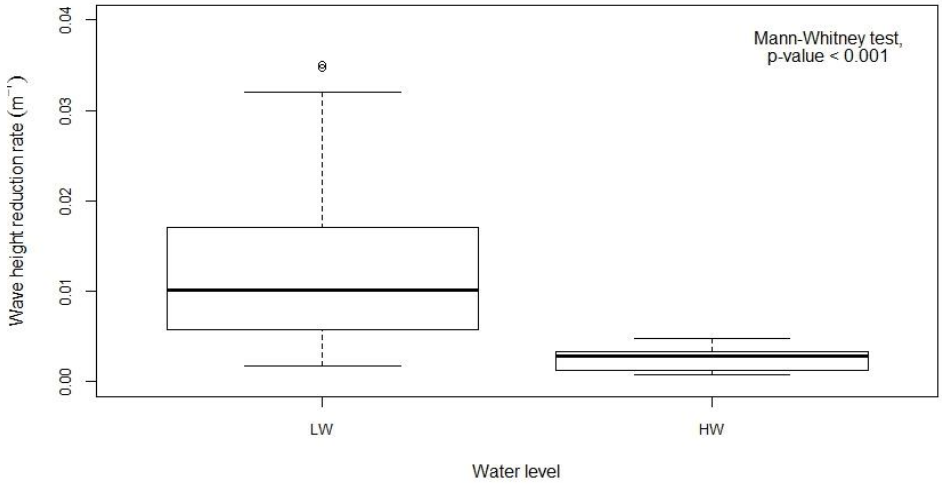

6.3.6 Incident wave height

Under average hydrodynamic conditions, the incident wave heights across all sites can be categorized into three wave height groups – 0.03 m, 0.05 m, and 0.06 m, which were similar to the offshore wave height at the corresponding sites. As opposed to extreme hydrodynamic conditions, the wave heights during average hydrodynamic conditions were low. The waves did not experience much energy dissipation from either wave breaking or bottom friction as it propagates from offshore towards the mangrove forest. The incident wave height during extreme condition ranged from 0.5 m to 0.9 m. The two relatively lower incident wave heights (approximately 0.2 m) occurred at UBI2/3, where the presence of sand bars have reduced the wave height before the wave reached the mangrove forest. No statistically significant relationship was found between incident wave height and wave height reduction rate under both average and extreme hydrodynamic conditions (Pearson's correlation test, p-value > 0.05).

Figure 6.14 Relationship between wave height reduction rate and incident wave height under average condition (top) and extreme condition (bottom). Note the differing scale on the y-axis between both plots.

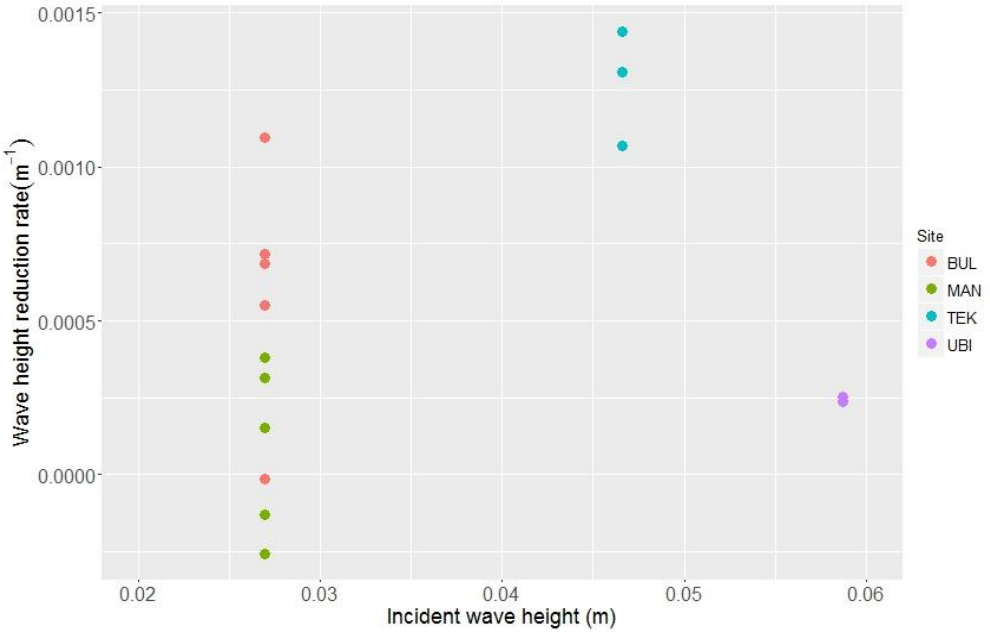

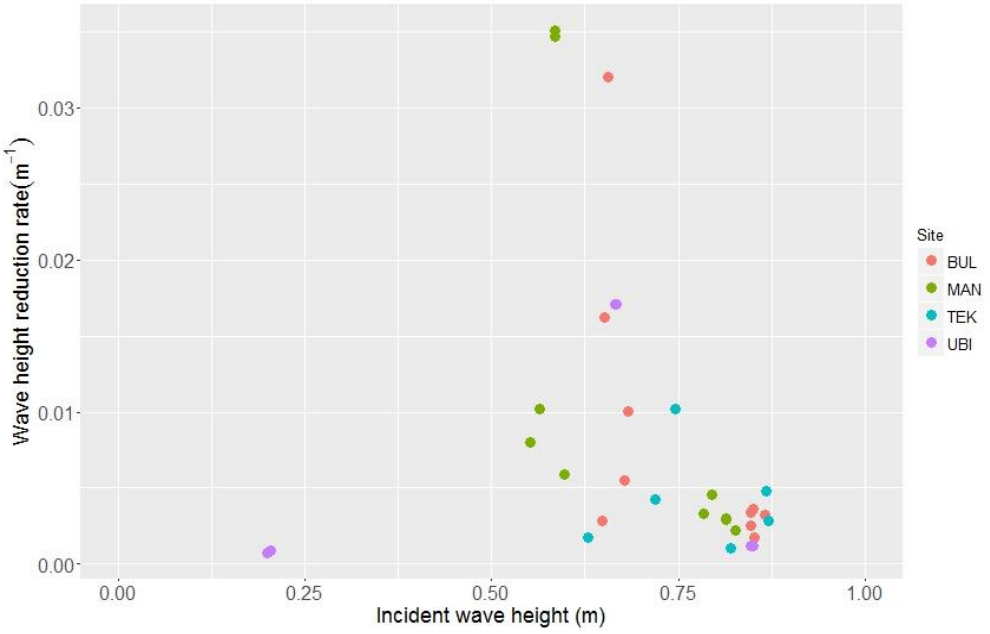

6.4 Discussion

6.4.1 Quantifying wave attenuation by mangroves along the north coast of Singapore

The percentage of wave attenuation during average hydrodynamic conditions was lower than in extreme hydrodynamic conditions. The mean percentage of wave attenuation during average and extreme hydrodynamic conditions was 7.71% and 62.47% respectively. The main reason for such a difference was the combination of the low incident wave height and steep slope within the mangrove forest. The low incident wave height prevented the occurrence of wave breaking, which is one of the main wave energy dissipation factor (Cuc et al., 2015; Strusińska-Correia et al., 2013; Vo-Luong & Massel, 2008). On the contrary, during the extreme events, the high wave induces wave breaking and generates drag force as it passes through the mangrove forest. The wave breaking process was both observed in the field (Horstman et al., 2014) and laboratory studies (Husrin et al., 2012; Strusińska-Correia et al., 2013). In this study, the percentage contribution of drag force from waves breaking increased from an average of < 1% (4.55% if the two outliers in UBI4/5 were included) during average hydrodynamic conditions to an average of 47.19% during extreme hydrodynamic

conditions. The relatively higher wave breaking in UBI4/5 during average condition was due to the steep slope in the first 15 m of mangrove forest, in combination with the relatively higher wave height compared to BUL and MAN.

When compared to field studies, the wave height reduction rate during the average hydrodynamic conditions was low. The range of wave height reduction rate in the mangroves found in this study was comparable to non-vegetated mud bed or beach plain (Mazda et al., 2006; Quartel et al., 2007) and mangrove forest with sparse *K. candel* seedlings of 1 – 2 years old (Mazda et al., 1997a). The wave height reduction rate during the extreme event was more similar to findings in the field studies in the non-storm period (incident wave height < 0.2 m) (Horstman et al., 2014; Mazda et al., 1997a; Quartel et al., 2007). The higher wave attenuation rates found in some field studies was the result of wave dissipation contributed by canopy. The short tree height (0.85 m) in Vinh Quang, Vietnam and the replanted young *K. candel* forest allowed the branches and leaves to dissipate wave energy. The increased area of obstruction due to canopy increases the drag force and wave energy dissipation. Furthermore, compared to the field studies, the seedlings and saplings were not included when calculating wave attenuation, due to the model limitation. Furthermore, it is likely that the model result underestimated the wave attenuation extent. There are other wave dissipation mechanisms that were not included in the near-shore wave evolution model, especially during the wave propagation across vegetation field. These effects include the turbulence that was generated as water flows around the base of a vegetation structure and after wave broke in the foreshore (Leonard & Luther, 1995; Strusińska-Correia et al., 2013; Suzuki et al., 2012; Vo-Luong & Massel, 2008; Zhang et al., 2015b).

The statistically positive relationship between mangrove density and mangrove extent suggests the potential confounder in the form of site grouping. Mangrove extent and mangrove density were found be positively correlated. For example, the site with a

higher cross-shore mangrove extent, such as UBI, also has a higher vegetation density. In this study, the percentage of wave height reduction showed large variation between BUL, MAN, and TEK. Moreover, there is a lack of data in mangroves with cross-shore distance above 250 m and mangrove density above 0.15 m^{-2}. The effect of mangrove density and mangrove extent respectively on wave height reduction should be investigated further with more data from similar mangrove forests and environmental settings.

Some transects (BUL5, MAN2 and MAN3) showed an increase of wave height due to wave shoaling. Wave shoaling occurs when the waves move into shallow water. As the wave speed and wavelength decrease, the wave height increases due to conservation of wave energy per unit area. Wave shoaling effect was observed in both field and laboratory studies (Horstman et al., 2014; Strusińska-Correia et al., 2013). Horstman et al. (2014) suggested 20 – 30% shoaling effect compared to wave reduction. Other than wave shoaling, wave reflection in front of the mangrove forest could also cause an increase in wave height (Harada et al., 2002; Horstman et al., 2014; Strusińska-Correia et al., 2013). However, this physical process was not included in the nearshore wave evolution model used in this study. Nevertheless, the wave reflection effect is thought to be insignificant in the Singapore context, since the mangroves here are less dense compared to other mangroves, such as those in Thailand (Horstman et al., 2014).

6.4.2 Factors contributing to wave attenuation

Vegetation factors

Wave dissipation by drag force generated by mangrove vegetation is one of the main factors influencing the magnitude of wave height reduction. Differences in the drag force exerted by mangroves roots, trunks and canopies of various species are related to the changes in water level. As water level increases, less drag force was generated by the interaction with roots for particular species (e.g. *Avicennia* and *Sonneratia*). Such

a reduction is associated with the structure of mangrove roots, in particular the height. The denser pneumatophores near the ground level occupied a relatively lower portion of the water column, thus less drag force exerted. As opposed to the average hydrodynamic conditions, under the extreme conditions, the lower water level (LW scenario) showed a relatively higher wave height reduction rate (Figure 6.13). During average hydrodynamic conditions, the vegetation drag force exerted by the dense pneumatophores were restricted to the < 10 cm bottom layer; while the emergent *Rhizophora* prop roots (1.4 m), albeit less dense, were able to exert drag force throughout the water column. The effect of vegetation, even during average hydrodynamic conditions was observed in the relatively higher percentage of wave height reduction at *Rhizophora*-dominated transects. Such a difference in submergence with respect to water depth strongly influences the vertical velocity profile and wave attenuation (Leonard & Luther, 1995; Nepf, 2004; Zhang et al., 2015b). The emergent vegetation was found to show higher wave attenuation compared to submerged vegetation, as emergent vegetation occupies the whole water column including the near water surface where orbital velocities were the highest (Augustin et al., 2009). The structural effect of vegetation and the interaction of water level was also studied in other coastal habitats such as saltmarshes (Leonard & Luther, 1995; Leonard & Reed, 2002; Möller, 2006). In a saltmarsh field study, the flow velocity was found to decrease the most at the level where the vertical distribution of plant material was the highest. As the water increases above the vegetation, the water above the canopies was regarded as unobstructed flow except at bottom boundary near the top of the submerged canopy (Leonard & Luther, 1995).

The effects of vegetation were found to be less pronounced during extreme events. Under the average hydrodynamic conditions, *Rhizophora* was found to have a higher median wave height reduction rate compared to *Avicennia* and *Bruguiera*. Such differences between genera were smaller under the extreme hydrodynamic conditions.

During the extreme hydrodynamic conditions, increased wave breaking due to high waves contributed to the large percentage of wave height reduction. The relatively steeper slope at MAN and BUL, where *Avicennia* and *Bruguiera* are the dominant genera, also induces to the wave breaking process. The wave energy dissipation by wave breaking could have masked the genus effect on wave height reduction.

The findings in this study imply wave attenuation potential by vegetation type in urban disturbed mangroves. A higher percentage of wave height reduction (approximately 80% within 50 m) was found in UBI transects with a high vegetation density at the front of mangroves, compared to other transects. Other less dense mangrove transects exhibited similarly high wave height reduction (approximately 70 – 92%) but over longer distance. Nevertheless, the wave height reduction at some transects is comparable to the high wave reduction rate (50 – 70% over 20 m of mangroves) found in natural mangroves such as Can Gio mangrove forest (Vo-Luong & Massel, 2006). Despite large variability across sites, this result suggests the potential of wave attenuation ability of the urban disturbed mangroves in Singapore.

Physical factors

Physical factors often interact with both vegetation factors and hydrodynamic factors to yield the wave attenuation. The elevation within the mangrove zone in combination with water levels, dictate the portion and structure of mangrove vegetation submerged and, therefore, the wave attenuation rate. In the long term, the topography within the mangroves shape the establishment and spatial distribution of mangrove types (Balke et al., 2013; Friess et al., 2012a).

Elevation changes affect the wave attenuation rate through the reduction of incident wave height prior to reaching the mangrove forest, though to a lesser degree than the role of vegetation. The dissipation of waves prior to reaching the mangrove forest is

dependent on coastal geomorphology, such as the presence of mudflat and slope as well as wave height/water depth ratio (Strusińska-Correia et al., 2013). The effects of non-vegetated areas, such as mudflats and beaches, have been demonstrated in previous studies (Horstman et al., 2014; Mazda et al., 2006; Quartel et al., 2007). The muddy or sandy bottom generates turbulent bottom layer and induces wave breaking. The bottom friction generated, however, was found to be small compared to other wave dissipation mechanisms (Guannel et al., 2015; Mazda et al., 1997a; Vo-Luong & Massel, 2008). The average reduction rate of offshore wave height prior to reaching the mangrove forest ranged from 36.9 – 44.6% during extreme hydrodynamic conditions and less than 1% (except for two cases of 2%) during average hydrodynamic conditions. As the incoming waves showed correlation with wave height attenuation rate, the elevation changes at the foreshore could indirectly influence the extent of wave attenuation of mangroves.

Besides natural topography, the presence of artificial coastal structures, such as embankments at BUL and MAN, affect the wave attenuation observed. At BUL, BUL3/4/5 have shorter cross-shore mangrove extents compared to BUL6/7 due to the presence of embankments. Short cross-shore distances and a low elevation profile reduced the effect of bottom friction and more importantly, the effect of dense mangrove root networks. When the waves are able to propagate sufficiently deep into mangroves and to the higher elevation within the mangrove forest, the friction caused by mangroves roots increases the energy dissipation. This happened in BUL6/7 but not BUL3/4/5.

Hydrodynamic factors

The statistically non-significant correlation between incident wave height and wave height reduction rate could suggest that there are other influencing factors at work. Water depth could be one of the factors. As water becomes shallow, the turbulent

bottom boundary layer exert more influence on the water column and slows the flow velocity. The slowing of flow velocity could induce wave breaking which is a dominant wave energy dissipation process. A laboratory study carried out using a non-vegetated sand bottom model suggested that wave breaking occurred when wave heights exceeded 60 – 83% of the water depth (Battjes & Stive, 1985). A more realistic wave breaking ratio by a field study in mangroves showed a threshold of approximately 40% wave height to water depth ratio induces wave breaking (Horstman et al., 2014). The influence of water depth on wave attenuation could even be considered as the primary factor causing an increase of wave breaking, suggested by the difference in wave height reduction rate between low and high water during extreme hydrodynamic conditions.

Water levels influence the cross-shore distances of wave propagation and, in turn, the wave attenuation rates. Compared to other sites, the higher median wave height reduction at TEK was the result of incoming waves propagating deeper into the mangrove forests. Due to the relatively gentler slopes within the TEK mangrove zone, inundation and waves could reach further into the mangrove. Such a setting allowed waves to travel a larger distance and experience a higher drag force, resulting in larger energy dissipation and wave height reduction.

7 General Discussion and Conclusions

7.1 Examination of wave attenuation ability of Singapore's mangrove

The wave attenuation ability of mangrove was found to differ between average and extreme hydrodynamic conditions and was determined by various physical and vegetation characteristics. The hydrodynamic condition in Singapore is generally calm due to its relatively sheltered geographical location. The low significant wave heights (mean significant wave height < 0.1 m) within the Johor Straits did not pose any risk to the coastal area. At MSL, the low waves did not reach the mangrove forests, albeit the mangroves were found to show slight wave attenuation during high tides. In a natural setting, however, the water level changes during tidal fluctuation is more gradual and exhibits spatial and temporal variations. Ship wakes could be a potential risk to the coastlines during normal days. Singapore, as one of the busiest ports in the world, harbours more than 10,000 vessels annually, ranging from tankers to small passenger vessels (MPA, 2016). Ferries, passenger ships, and larger containerships can generate wave height of 0.04 – 0.62 m (Gharbi et al., 2010; Hofmann et al., 2011) and cause erosion to beaches and back-barrier habitats (Hofmann et al., 2011; Zhang et al., 2004). The wave attenuation function of mangroves could potentially be useful in providing coastal protection by attenuating the ship wakes propagating towards the shore.

The wave attenuation ability of mangroves was more apparent under extreme events. The coastal protection during extreme events was highlighted given the potential risks towards the coastal community. In Singapore, despite its relatively sheltered geographical location, there exist some risks of extreme events such as tropical storms (Chang, 2003). In order to provide an indication of current wave attenuation extent in protecting the coastal zone, the mangrove width required for a 100% reduction in wave height during extreme hydrodynamic conditions was estimated (Figure 7.1). BUL,

MAN, and TEK showed a slightly lower than average required mangrove extent while current mangrove extent in UBI was found to provide sufficient protection. Similar mangrove widths required for wave attenuation (> 99% of wave attenuation within 100 m) were found in mangrove forests with a history of degradation and anthropogenic influence in the Mekong Delta (Phan et al., 2014), suggesting the potential of wave attenuation function by disturbed mangrove forests. Current extreme events were modelled based on the worst case scenario of a tropical storm event, additional studies should investigate wave attenuation extent for different storm magnitudes (incident wave heights) and water levels. As the return period of storms varies with magnitude, an illustration of mangrove width required for various storm classes could improve the understanding of the incremental wave attenuation ability of mangroves and facilitate coastal management planning. An example would be the classification of different wave heights based on local historical storm events and estimation of mangrove width required to provide coastal protection in studies in Vietnam (Bao, 2011; Nguyen, 2013).

Figure 7.1 Range of mangrove extent required for 100% wave height reduction under extreme hydrodynamic conditions in comparison with current mangrove extent.

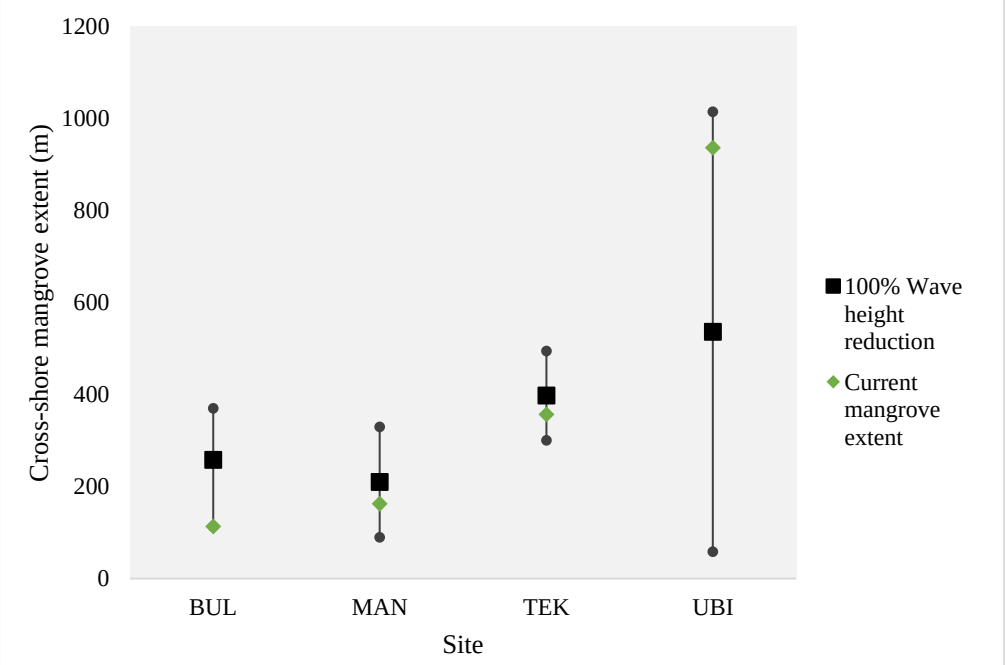

The mangrove extent estimation was made based on current density at each site. As found in section 6.3.1 and previous studies (Horstman et al., 2014; Mazda et al., 1997a; Nguyen, 2013), vegetation density influences the extent of wave attenuation of mangroves. An increase in density could reduce the mangrove width required for the same extent of wave attenuation (Bao, 2011; Nguyen, 2013). Detailed quantification of wave attenuation extent variation with vegetation density, however, was not conducted in this study.

The wave attenuation patterns as a wave propagates through a mangrove forest are not linear (Koch et al., 2009; Narayan, 2009). The patterns of wave height reduction are dependent on the water level and the biotic structures submerged at any given point of time. A non-linear decrease in wave height/ wave energy was demonstrated in previous studies on wave attenuation of coastal habitats (Augustin et al., 2009; Koch et al., 2009; Leonard & Luther, 1995; Möller, 2006; Narayan, 2009). The mangrove width required for effective wave attenuation during extreme events could, therefore, be shorter than as that illustrated in Figure 7.1. An example of the non-linear wave height reduction profile simulated in this study is illustrated in Figure 7.2. Half of the incident wave height was reduced within 82 m of the mangroves while an additional 40% of wave height reduction would requires another 400 m into the mangroves.

While this study has focused on wave attenuation provided by mangroves, the coastal ecosystems does not exist in isolation in Singapore's coastal landscape. The interconnectivity between mangroves and other natural habitats such as coral reefs and seagrasses could improve coastal protection by providing additional wave attenuation. Corals and seagrass beds were found to be able to contribute to wave attenuation through similar biophysical interactions as has been demonstrated in mangrove forests (Costa et al., 2016; Ferrario et al., 2014; Fonseca & Cahalan, 1992; John et al., 2016), with wave breaking and bottom friction caused by both submerged and emergent

structures. Foreshore habitats and their linkages could also amplify the overall wave attenuation function (Alongi, 2008; Barbier, 2011, 2016; Sanchirico & Springborn, 2011). This study did not include the systemic consideration of wave attenuation by the entire seascape and the interconnectivity between coastal habitats due to data and modelling constraints. Nevertheless, the effects of corals could be very small due to the absence of coral reefs in the Johore Straits. Seagrass patches, however, have been observed within mangroves and in the foreshore (Yaakub et al., 2013). The effects of seagrass on wave attenuation at the foreshore should, therefore, be studied together with mangroves.

Figure 7.2 Example of simulated wave height profile across the mangrove forest at TEK2 during extreme hydrodynamic conditions. Dashlines indicate 50% and 90% of incident wave height.

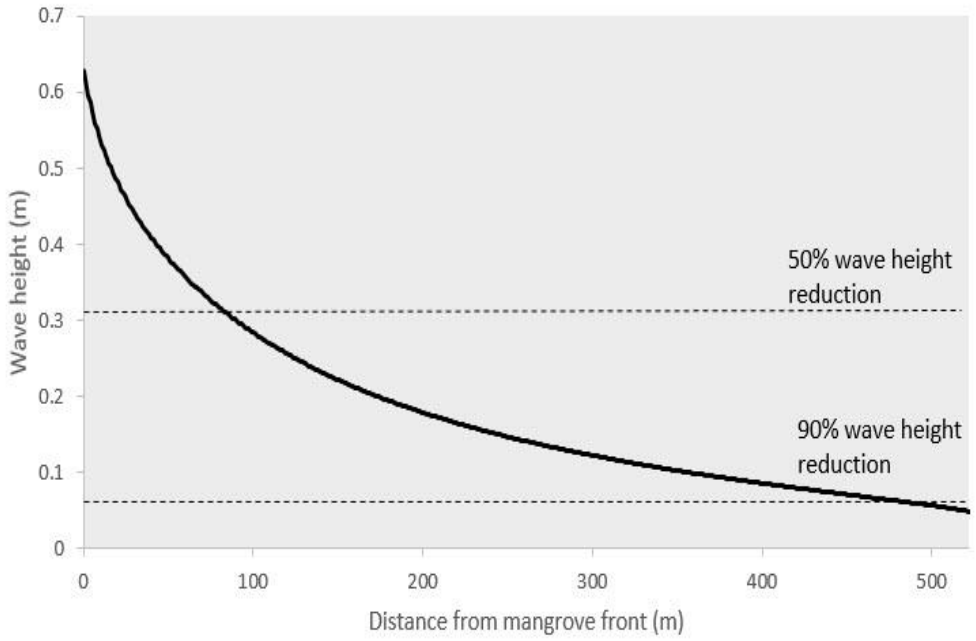

7.2 Implications of this study for coastal management in Singapore

The wave attenuation ability of existing mangrove patches along in the urban landscape of Singapore has been illustrated in this study, along with the factors influencing the extent of wave attenuation. The wave attenuation ability of mangroves was found to be more apparent during extreme hydrodynamic conditions. More importantly, this study

has provided insights into the extent of coastal protection contributed by current mangrove forests in the case of extreme event. Given the exposure of populated urban coastal areas, these findings have important implications for Singapore's coastal management planning. This section describes the key considerations for the coastal management planning in Singapore from this study.

7.2.1 Preventing coastal squeeze

As described in section 7.1, the mangroves along the northern coast of Singapore were within the lower range of mangrove extent required for protection against extreme events. In order for mangroves to offer sufficient protection against extreme events, further narrowing of mangroves should be prevented. Coastal squeeze, as defined by Pontee (2013) as '*where intertidal habitat is lost due to the high water mark being fixed by a defence or structure (i.e. the high water mark residing against a hard structure such as a sea wall) and the low water mark migrating landwards in response to SLR (Sea Level Rise)*', could be a threat to the mangroves in the urban environment of Singapore.

In Singapore, the sea level rises at a rate of approximately 1.2 – 1.7 mm year^{-1} (National Climate Change Secretariat, 2016). As sea level rises, mangroves that survive only within a certain tidal frame needs to migrate landwards (Schleupner, 2008). The urbanized coastlines of Singapore, however, are lined with embankments and have limited the landwards migration of mangroves. As a result, the rising sea level will increase the inundation duration and induce mangrove loss through ecological drowning (Friess et al., 2012a; Krauss et al., 2003; Schleupner, 2008). In addition, lack of sediment supply was found to prevent mangroves in Singapore from accreting at the same pace as the rising sea level (Willemsen et al., 2016).

Both anthropogenic influence and SLR vary across spatial and temporal scales, thus, increasing uncertainty and complexity in coastal management planning (Friess et al., 2015). Short- and mid-term management strategies such as the removal of embankments/causeway could be used to increase the sediment supply. The increase in sediment supply could improve sediment accretion rates, allowing mangroves to keep pace with SLR (Willemsen et al., 2016). Coastal management planning for large scale climate change effects, such as SLR, remains a challenge since it is beyond the control of any management action (Friess et al., 2015). In order to prevent long term coastal squeeze, the synergistic effects and biophysical feedback mechanisms in association with SLR and other stressors such as reduced sediment supply should be better understood. Long term strategies for mitigation of large-scale external stressors could then be developed and implemented.

7.2.2 Ecological engineering

Most of the coastlines of Singapore have already been demarcated as either reclamation zones (reserve sites), industrial areas, residential areas, or open spaces (the definition of open space was not clear) (Urban Redevelopment Authority, 2016). In the Master Plan 2014, MAN, UBI, and TEK were classified as reserve sites or open space with specific usage remains to be determined. Only BUL was categorized as a nature reserve with some form of legal protection. Nevertheless, no buffer or extra space was gazetted for potential expansion for alleviating the potential coastal squeeze in the long term. Economically, such expansion of mangrove forests through landward retreat is not practical due to the high demand for land in the land-scarce Singapore.

Given the continuing coastal development, an ecological engineering approach which combines both soft and hard engineering could provide an alternative solution to manage coastal vulnerability. As found in this study, wave breaking is one of the main mechanisms in wave attenuation during an extreme event. A coastal engineering

approach to recreate an appropriate slope to induce wave breaking could be combined with mangrove vegetation management.

In fact, the ecological engineering approach has been tested in Singapore. In the face of rapid coastal erosion in the northern coast of Pulau Tekong which threatened a mature mangrove forest, National Parks Board (NParks) commissioned an Environmental Monitoring and Management Programme (EMMP) to protect the coastlines through a combination of mangrove replantation and shoreline strengthening (DHI, 2013). The development of ecological engineering solutions requires sound understanding of local hydrodynamic and physical processes along the shores. In addition, the variability of geomorphology and the availability of elevation 'niches' required for mangroves to survive have to be studied in details for each site in order to create a successful replantation program (Friess et al., 2012a; Lewis, 2005). The current study helps to bridge the gap through understanding physical processes and wave attenuation extent in a disturbed mangrove in the urban coastline of Singapore.

7.3 Limitations of this study

7.3.1 Limitation of approach

This study employs the vertical schematization of structures approach to simulate wave attenuation, taking into account of mangrove structures (Cuc et al., 2015; Narayan, 2009; Strusińska-Correia et al., 2013; Suzuki et al., 2012). However, the cylindrical representation of vegetation structure in the model could not take into account of finer details such as the shape of *Rhizophora* prop roots and *Sonneratia* conical roots (Horstman et al., 2014; Mazda et al., 2006). As water level increases, the cross-sectional area varies and changes the extent of obstruction to water flow, hence the energy dissipation extent varies. A laboratory experiment found that the flow velocity varied vertically along the props roots of *Rhizophora* due to the geometry of the prop

roots system (Zhang et al., 2015b). Such changes were also found in emergent and submerged vegetation structures such as saltmarshes (Augustin et al., 2009; Leonard & Luther, 1995; Möller, 2006).

Non-linearity

The wave attenuation varies spatially and temporally (Barbier et al., 2008; Koch et al., 2009). In a meta-analysis, it was suggested that the shoreline protection function of coastal wetland within a smaller wetland could be as effective wetland of a larger spatial scale. However, large-scale physical processes such as tsunamis and large-scale erosion could undermine this function (Gedan et al., 2011; Narayan, 2009; Yanagisawa et al., 2009). Such an effect arises when the strength of large-scale events, such as tsunamis, was too strong for the mangroves to cope. The destruction of mangrove vegetation could result in the loss of all wave attenuation function (Yanagisawa et al., 2009). Variations in temporal scales involve the tidal fluctuation and seasonal effects which affect the density of mangrove vegetation submerged and, thus, the level of obstruction to the water flow. The drag force caused by the mangrove structure at any time depends on the water level and the correspondent proportion of mangrove roots, trunk and canopy submerged. Some small-scale non-linearity was not captured properly, such as the variations of pneumatophores' structure with depth and the shape of props roots (Horstman et al., 2014; Massel et al., 1999; Mazda et al., 2006; Mazda et al., 1997a). In some numerical and field studies, the non-linearity in vegetation structures was captured by calculating the cross-section vegetation cover rate along the vertical profile of vegetation (Horstman et al., 2014; Leonard & Luther, 1995; Mazda et al., 1997b).

7.3.2 Limitation of the model

Vegetation parameters input

The vegetation parameter inputs were limited to one set of vegetation characteristics per model. Such a model set up is better suited to less diverse mangroves such as those in Florida, USA (Doughty, 2015). Singapore's species-rich mangroves were not properly represented in the model. In this study, the incorporation of more cross-shore models in a heterogeneous mangrove forest, compared to a relatively homogenous mangrove forest, can minimize this model limitations. The effects of mangrove seedlings and saplings were not captured in the model. The seedlings and saplings could potentially increase the wave attenuation rate, as their canopy is lower. However, the inclusion of seedlings and saplings in the calculation of vegetation parameters in each model set up might provide an inaccurate vegetation representation, since the presence of high number of saplings and seedlings (field observation) will skew the vegetation parameters. An alternative could be the inclusion of weightage calculation for different size classes.

Spatial distribution of topography and vegetation

The spatial distribution of natural and artificial geomorphological features and microtopography, as well as vegetation, could affect the wave attenuation due to reflection, diffraction, turbulence, etc. The use of one-dimensional cross-shore profile in the model could not take into account the spatial variations of both physical and vegetation factors within mangrove forest. The exclusion of spatial simulation capability also means the loss of spatial-related processes such as horizontal flow and wave refraction (Guannel et al., 2015; Suzuki et al., 2012). The use of 2D or 3D models could alleviate some of these limitations. The flow could be better represented by taking into account the creeks, slopes or artificial embankments. One such model is the Simulating Waves Nearshore (SWAN) model (Cuc et al., 2015; Narayan, 2009; Suzuki et al., 2012). Although such a model could consider more physical processes such as wave diffraction caused by vegetation within mangroves, there remains limitations associated with the fundamental understanding and quantification of physical

processes. For example, the bulk drag coefficient used in most study to represent mangrove vegetation were usually obtained from literature simply due to the lack of understanding of physical effects such as vortex around vegetation structure as well as spatially and temporally varying vegetation parameters (Cuc et al., 2015; Guannel et al., 2015).

In order to provide a more accurate simulation of the wave propagation by taking into account the spatial distribution of physical and vegetation features in a mangrove, topography and vegetation data of high quality are required. Uncertainty of simulation outcome remain or could even increase with 2D/3D model when such data were not available. When topography and vegetation data of sufficient quality are available, a 3D model is favored over 2D. The 3D model could better represent the vertical variations of flow within the water column, as opposed to depth-averaged 2D model (Broekema, 2013).

Simplification of complex processes

The complex physical processes, such as wave-trunk interaction and wave reflection, were not captured in the model. The wave reflection from vegetation structures and natural and artificial structures could affect the hydrodynamics around and within the mangrove forest (Harada et al., 2002; Horstman et al., 2014; Strusińska-Correia et al., 2013; Yanagisawa et al., 2009). An increase in wave reflection could potentially cause more damage during tsunami (Yanagisawa et al., 2009). The reflected waves could also retain some wave energy, reducing the wave energy propagating into the mangroves. Without taking into account the reflected energy, wave energy (wave height) transmitted into the mangrove forest could be overestimated. Subsequently, this could lead to an overestimation of mangrove width or density required for same extent of wave attenuation. Field or laboratory validation of computer model outcomes could improve the reliability of results (Harada et al., 2002; Strusińska-Correia et al., 2013).

7.4 Conclusions

Mangroves have been shown to exhibit the potential to protect coastal areas through wave attenuation processes, where in the Singapore context they play the most prominent role during extreme events. The extent of wave attenuation has been investigated in field, laboratories, and modelling studies. Despite evidence on their ability to attenuate waves, most studies have been carried out in a natural mangrove or a mangrove of bigger spatial extent. A disturbed mangrove could be different from a natural mangrove in terms of their ecological and physical characteristics. These differences could, in turn, affect their wave attenuation ability. The investigation of disturbed mangroves can provide a better understanding of the wave attenuation ability of mangroves in such setting. The study was aimed to investigate and understand the wave attenuation function provided by disturbed mangroves in Singapore. This study also aimed to understand the relationship between main wave attenuation factors and their influence on wave attenuation found.

Objective 1: To quantify the extent of wave attenuation of the mangroves along Singapore's northern coast under average and extreme hydrodynamic conditions

The extent of wave attenuation varied across site as well as within transects. The percentage of wave attenuation was -0.46 – 50.71% during average hydrodynamic conditions and 2.79 – 92.21% during extreme hydrodynamic conditions. Some instances of wave height increase were observed in BUL and MAN under average conditions. There are some variations within each site caused by physical features such as artificial embankments and natural sand deposits. When compare between average and extreme hydrodynamic conditions, the wave attenuation rate during extreme hydrodynamic conditions is an order of magnitude higher. The difference was mainly

due to the increase in wave breaking as wave height increases during extreme hydrodynamic condition.

Objective 2: To investigate the factors affecting the wave attenuation within the mangrove area along Singapore's northern coast.

A number of potential factors influencing the wave attenuation extent of mangroves were investigated. The mangrove density (correlation coefficient = 0.40) and mangrove width (0.61) were found to be significantly correlated with the percentage of wave height reduction. However, this relationship only applies to extreme hydrodynamic conditions. Wave height reduction rate between vegetation types were found to have no statistical difference, although the *Rhizophora* showed a slightly higher median wave attenuation rate under average hydrodynamic conditions. Among the vegetation structures, mangroves roots were observed to be the main wave attenuation contributor (65% – 100%), except for a few cases when trunk contributed more to wave attenuation. The canopy, on the other hand, did not affect the wave attenuation at all due to the water level not reaching the canopy. Water level was found to influence the wave height reduction rate under extreme hydrodynamic conditions. The water level also serves as "facilitator" by affecting the portion of mangroves vegetation submerged and, thus, the obstruction to water flow and wave attenuation.

This study has provided a first insight into the broad extent of wave attenuation in urban disturbed mangrove systems, and the factors influencing the spatial variation of wave attenuation. More importantly, the wave attenuation rate showed in this study highlighted the effectiveness of disturbed mangroves compared to less disturbed mangroves that are usually studied. In spite of their fragmented and disturbed nature, the ability of Singapore's mangroves in attenuating waves under extreme hydrodynamic conditions was found to be as effective as other studies conducted in

natural and less disturbed mangroves. This will be increasingly important in the future because of increasing coastal vulnerability within urbanized coastal areas in the face of climate change. Both the natural (climate change) and anthropogenic (urbanization) stressors also continue to threaten the mangroves which are likely to experience coastal squeeze, while increasing urbanization means that Singapore's disturbed coastal urban landscape will increasingly become the norm for many mangrove systems in the tropics.

8 References

Airy, G. B. (1845). Tides and waves. In *Encyclopaedia metropolitana*.

Allen, J. A., Ewel, K. C., & Jack, J. (2001). Patterns of natural and anthropogenic disturbance of the mangroves on the Pacific Island of Kosrae. *Wetlands Ecology and Management*, *9*, 279–289. http://doi.org/10.1023/A:1011125310794

Allen, J. R. L., & Thornley, D. M. (2004). Laser granulometry of Holocene estuarine silts: effects of hydrogen peroxide treatment. *The Holocene*, *14*(2), 290–295. http://doi.org/10.1191/0959683604hl681rr

Alongi, D. M. (2008). Mangrove forests: Resilience, protection from tsunamis, and responses to global climate change. *Estuarine, Coastal and Shelf Science*, *76*(1), 1–13. http://doi.org/10.1016/j.ecss.2007.08.024

Andrea, A. C. (2006). Benthic macro-invertebrate community composition within a mangrove/seagrass estuary in northern New Zealand. *Estuarine, Coastal and Shelf Science*, *66*(1), 97–110.

Arkema, K. K., Guannel, G., Verutes, G., Wood, S. A., Guerry, A., Ruckelshaus, M., Kareiva, P., Lacayo, M., & Silver, J. M. (2013). Coastal habitats shield people and property from sea-level rise and storms. *Nature Climate Change*, *3*(10), 913–918. http://doi.org/10.1038/nclimate1944

Augustin, L. N., Irish, J. L., & Lynett, P. (2009). Laboratory and numerical studies of wave damping by emergent and near-emergent wetland vegetation. *Coastal Engineering*, *56*, 332–340.

Bacchiocchi, F., & Airoldi, L. (2003). Distribution and dynamics of epibiota on hard structures for coastal protection. *Estuarine, Coastal and Shelf Science*, *56*(5–6), 1157–1166. http://doi.org/10.1016/S0272-7714(02)00322-0

Badola, R., & Hussain, S. A. (2005). Valuing ecosystem functions: an empirical study on the storm protection function of Bhitarkanika mangrove ecosystem, India. *Environmental Conservation*. http://doi.org/10.1017/S0376892905001967

Balke, T., Webb, E. L., den Elzen, E., Galli, D., Herman, P. M. J., & Bouma, T. J. (2013). Seedling establishment in a dynamic sedimentary environment: a conceptual framework using mangroves. *Journal of Applied Ecology*, *50*, 740–747.

Bao, T. Q. (2011). Effect of mangrove forest structures on wave attenuation in coastal Vietnam. *Oceanologia*, *53*(3), 807–818. http://doi.org/10.5697/oc.53-3.807

Barbier, E. B., & Cox, M. (2003). Does economic development lead to mangrove loss? A cross-country analysis. *Contemporary Economic Policy*. http://doi.org/10.1093/cep/byg022

Barbier, E. B. (2007). Valuing ecosystems as productive inputs. *Economic Policy*, *22*, 177–229.

Barbier, E. B., Koch, E. W., Silliman, B. R., Hacker, S. D., Wolanski, E., Primavera, J. H., Granek, E. F., Polasky, S., Aswani, S., Cramer, L. A., Stoms, D. M.,

Kennedy, C. J., Bael, D., Kappel, C. V., Perillo, G. M., & Reed, D. J. (2008). Coastal ecosystem-based management with nonlinear ecological functions and values. *Science*, *319*, 321–323. http://doi.org/10.1126/science.1150349

Barbier, E. B. (2011). Progress and Challenges in Valuing Coastal and Marine Ecosystem Services. *Review of Environmental Economics and Policy*, *6*, 1–19. http://doi.org/10.1093/reep/rer017

Barbier, E. B., Hacker, S. D., Kennedy, C., Koch, E. W., Stier, A. C., & Silliman, B. R. (2011). The value of estuarine and coastal ecosystem services. *Ecological Monographs*, *81*(2), 169–193. http://doi.org/10.1890/10-1510.1

Barbier, E. B. (2016). The protective service of mangrove ecosystems: A review of valuation methods. *Marine Pollution Bulletin*, *109*, 676–681. http://doi.org/10.1016/j.marpolbul.2016.01.033

Battjes, J. A., & Stive, M. J. F. (1985). Calibration and verification of a dissipation model for random breaking waves, *90*, 9159–9167.

Benoit, J., & Roberts, S. (2007). The national academies report on mitigating shore erosion along sheltered coasts. In N. C. Kraus & J. D. Rosati (Eds.), *Coastal Sediments '07* (pp. 1601–1608). New Orleans, Louisiana, United States: American Society of Civil Engineers.

Bolund, P., & Hunhammar, S. (1999). Ecosystem services in urban areas. *Ecological Economics*, *29*(2), 293–301. http://doi.org/10.1016/S0921-8009(99)00013-0

Bouma, T. J., Olenin, S., Reise, K., & Ysebaert, T. (2009). Ecosystem engineering and biodiversity in coastal sediments: Posing hypotheses. *Helgoland Marine Research*, *63*(1), 95–106. http://doi.org/10.1007/s10152-009-0146-y

Brander, L. M., Wagtendonk, A. J., Hussain, S. S., McVittie, A., Verburg, P. H., de Groot, R. S., & van der Ploeg, S. (2012). Ecosystem service values for mangroves in Southeast Asia: A meta-analysis and value transfer application. *Ecosystem Services*, *1*(1), 62–69. http://doi.org/10.1016/j.ecoser.2012.06.003

Brinkman, R. M., Massel, S. R., Ridd, P., & Furukawa, K. (1997). Surface wave attenuation in mangrove forests. In *Proceedings of the Combined Australasian Coastal Engineering and Ports Conference, Christchurch* (pp. 941–946).

Brinkman, R. M. (2006). *Wave attenuation in mangrove forests: an investigation through field and theoretical studies*. James Cook University.

Broekema, Y. (2013). *Hydrodynamic modelling of a mangrove system in Singapore*. Delft University of Technology.

Burchett, M. D., Allen, C., Pulkownki, A., & Macfarlane, G. (1998). Rehabilitation of saline wetlands, Olympics 2000 Site, Sydney (Australia). *Marine Pollution Bulletin*, *37*(8), 526–534.

Burger, B. (2005). *Wave Attenuation in Mangrove Forests*. Delft University of Technology.

Chan, E. S., Tkalich, P., Gin, K. Y. H., & Obbard, J. P. (2006). The physical oceanography of Singapore coastal waters and its implications for oil spills. In

The Environment in Asia Pacific Harbours (pp. 393–412). http://doi.org/10.1007/1-4020-3655-8_23

Chang, C. P. (2003). Typhoon Vamei: An equatorial tropical cyclone formation. *Geophysical Research Letters*, *30*(3), 10–13. http://doi.org/10.1029/2002GL016365

Chang, S. E., Adams, B. J., Alder, J., Berke, P. R., Chuenpagdee, R., Ghosh, S., & Wabnitz, C. (2006). Coastal ecosystems and tsunami protection after the December 2004 Indian Ocean tsunami. *Earthquake Spectra*, *22*(SUPPL. 3). http://doi.org/10.1193/1.2201971

Chapman, M. G., & Underwood, A. J. (2011). Evaluation of ecological engineering of "armoured" shorelines to improve their value as habitat. *Journal of Experimental Marine Biology and Ecology*, *400*(1–2), 302–313. http://doi.org/10.1016/j.jembe.2011.02.025

Chen, M., Murali, K., Khoo, B. C., Lou, J., & Kumar, K. (2005). Circulation Modelling in the Strait of Singapore. *Journal of Coastal Research*, *215*, 960–972. http://doi.org/10.2112/04-0412.1

Chia, L. S., Habibullah, K., & Chou, L. M. (1988). *The coastal environment profile of Singapore*. Manila: WorldFish.

Chua, G. (2010, May 12). Saving Tekong's coastal greenery. *The Straits Time*.

Costa, M. B. S. F., Araújo, M., Araújo, T. C. M., & Siegle, E. (2016). Influence of reef geometry on wave attenuation on a Brazilian coral reef. *Geomorphology*, *253*, 318–327. http://doi.org/10.1016/j.geomorph.2015.11.001

Creel, L. (2003). *Ripple effects: population and coastal regions*. Washington, DC: Population Reference Bureau.

Cuc, N. T. K., Suzuki, T., Ruyter van Steveninck, E. D., & Hai, H. (2015). Modelling the impacts of mangrove vegetation structure on wave dissipation in Ben Tre Province, Vietnam, under different climate change scenarios. *Journal of Coastal Research*, *31*(2), 340–347.

Curran, S., Kumar, A., Lutz, W., & Williams, M. (2002). Interactions between coastal and marine ecosystems and human population systems: perspectives on how consumption mediates this interaction. *AMBIO*, *31*(4), 264–268. http://doi.org/10.1579/0044-7447-31.4.264

Dahdouh-Guebas, F., Jayatissa, L. P., Di Nitto, D., Bosire, J. O., Lo Seen, D., & Koedam, N. (2005). How effective were mangoves as a defence against the recent tsunami? *Current Biology*, *15*(12), R443–R447. http://doi.org/10.1016/j.cub.2005.06.008

Dalrymple, R. A., Kirby, J. T., & Hwang, P. A. (1984). Wave diffraction due to areas of energy dissipation. *Journal ofWaterway, Port, Coastal, and Ocean Engineering*, *110*(1), 67–79.

Danielsen, F., Sørensen, M. K., Olwig, M. F., Selvam, V., Parish, F., Burgess, N. D., Hiraishi, T., Karunagaran, V. M., Rasmussen, M. S., Hansen, L. B., Quarto, A., & Suryadiputra, N. (2005). The Asian tsunami: a protective role for coastal

vegetation. *Science*, *310*, 643. http://doi.org/10.1126/science.1118387

Das, S., & Vincent, J. R. (2009). Mangroves protected villages and reduced death toll during Indian super cyclone. *Proceedings of the National Academy of Sciences of the United States of America*, *106*(18), 7357–7360. http://doi.org/10.1073/pnas.0810440106

Davidson-Arnott, R. (2009). *Introduction to coastal processes and geomorphology*. Cambridge University Press.

Department of Statistics Singapore. (2016). Population and Land Area. Retrieved June 20, 2016, from http://www.singstat.gov.sg/statistics/latest-data#16

DHI. (2013). Tekong EMMP – Protecting the mangroves on Singapore's Tekong Island. Retrieved June 20, 2016, from https://www.dhigroup.com/global/news/imported/2013/6/28/tekongemmp

Doughty, C. L. (2015). *Carbon storage and coastal protection: Uncovering the potential impacts of mangrove range expansion*. Villanova University.

Everard, M., Jha, R. R., & Russell, S. (2014). The benefits of fringing mangrove systems to Mumbai. *Aquatic Conservation: Marine and Freshwater Ecosystems*. http://doi.org/10.1002/aqc.2433

Ferrario, F., Beck, M. W., Storlazzi, C. D., Micheli, F., Shepard, C. C., & Airoldi, L. (2014). The effectiveness of coral reefs for coastal hazard risk reduction and adaptation. *Nature Communications*, *5*, 3794. http://doi.org/10.1038/ncomms4794

Fonseca, M. S., & Cahalan, J. A. (1992). A preliminary evaluation of wave attenuation by four species of seagrass. *Estuarine, Coastal and Shelf Science*, *35*(6), 565–576. http://doi.org/10.1016/S0272-7714(05)80039-3

Forbes, K., & Broadhead, J. (2007). *The role of coastal forests in the mitigation of tsunami impacts*. Bangkok, Thailand.

Friess, D. A., Krauss, K. W., Horstman, E. M., Balke, T., Bouma, T. J., Galli, D., & Webb, E. L. (2012a). Are all intertidal wetlands naturally created equal? Bottlenecks, thresholds and knowledge gaps to mangrove and saltmarsh ecosystems. *Biological Reviews*, *87*(2), 346–366. http://doi.org/10.1111/j.1469-185X.2011.00198.x

Friess, D. A., Phelps, J., Leong, R. C., Lee, W. K., Wee, A. K. S., Sivasothi, N., Oh, R. R. Y., & Webb, E. L. (2012b). Mandai mangrove, Singapore: Lessons for the conservation of Southeast Asia's mangroves. *Raffles Bulletin of Zoology*, *Suppl 25*, 55–65.

Friess, D. A., Phelps, J., Garmendia, E., & Gómez-Baggethun, E. (2015). Payment for Ecosystem Services (PES) in the face of external biophysical stressors. *Global Environmental Change*, *30*, 31–42.

Friess, D. A., Richards, D. R., & Phang, V. X. H. (2016). Mangrove forests store high densities of carbon across the tropical urban landscape of Singapore. *Urban Ecosystems*, *19*(2), 795–810. http://doi.org/10.1007/s11252-015-0511-3

Gedan, K. B., Kirwan, M. L., Wolanski, E., Barbier, E. B., & Silliman, B. R. (2011). The present and future role of coastal wetland vegetation in protecting shorelines: Answering recent challenges to the paradigm. *Climatic Change*. http://doi.org/10.1007/s10584-010-0003-7

Gharbi, S., Valkov, G., Hamdi, S., & Nistor, I. (2010). Numerical and field study of ship-induced waves along the St. Lawrence Waterway, Canada. *Natural Hazards*, *54*, 605–621. http://doi.org/10.1007/s11069-009-9489-6

Goodsell, P. J., Chapman, M. G., & Underwood, A. J. (2007). Differences between biota in anthropogenically fragmented habitats and in naturally patchy habitats. *Marine Ecology Progress Series*, *351*, 15–23. http://doi.org/10.3354/meps07144

Granek, E. F., & Ruttenberg, B. I. (2007). Protective capacity of mangroves during tropical storms: A case study from "Wilma" and "Gamma" in Belize. *Marine Ecology Progress Series*, *343*, 101–105. http://doi.org/10.3354/meps07141

Guannel, G., Ruggiero, P., Faries, J., Arkema, K., Pinsky, M., Gelfenbaum, G., Guerry, A., & Kim, C. K. (2015). Integrated modeling framework to quantify the coastal protection services supplied by vegetation. *Journal of Geophysical Research C: Oceans*, *120*(1), 324–345. http://doi.org/10.1002/2014JC009821

Harada, K. (2003). *Hydrological study on the tsunami mitigation effect of coastal forest*. Tohoku University, Japan.

Harada, K., Imamura, F., & Hiraishi, T. (2002). Experimental study on the effect in reducing tsunami by the coastal permeable structures. In *Twelfth International Offshore and Polar Engineering Conference*. Kitakyushu, Japan.

Harty, C., & Cheng, D. (2003). Ecological assessment and strategies for the management of mangroves in Brisbane water—Gosford, New South Wales, Australia. *Landscape and Urban Planning*, *62*(4), 219–240.

Hashim, A. M., Catherine, S. M. P., & Takaijudin, H. (2013). Effectiveness of mangrove forests in surface wave attenuation: A review. *Research Journal of Applied Sciences, Engineering and Technology*.

Hilton, M. J., & Manning, S. S. (1995). Conversion of Coastal Habitats in Singapore: Indications of Unsustainable Development. *Environmental Conservation*, *22*(4), 307–322. http://doi.org/10.1017/S0376892900034883

Hofmann, H., Lorke, A., & Peeters, F. (2011). Wind and ship wave-induced resuspension in the littoral zone of a large lake. *Water Resources Research*, *47*, W09505. http://doi.org/10.1029/2010WR010012

Horstman, E. M., Dohmen-Janssen, C. M., Narra, P. M. F., van den Berg, N. J. F., Siemerink, M., & Hulscher, S. J. M. H. (2014). Wave attenuation in mangroves: A quantitative approach to field observations. *Coastal Engineering*, *94*, 47–62. http://doi.org/10.1016/j.coastaleng.2014.08.005

Husrin, S., Strusińska, A., & Oumeraci, H. (2012). Experimental study on tsunami attenuation by mangrove forest. *Earth, Planets and Space*, *64*(10), 973–989. http://doi.org/10.5047/eps.2011.11.008

Huxham, M., Emerton, L., Kairo, J., Munyi, F., Abdirizak, H., Muriuki, T., Nunan,

F., & Briers, R. A. (2015). Applying climate compatible development and economic valuation to coastal management: a case study of Kenya's mangrove forests. *Journal of Environmental Management*, *157*, 168–181. http://doi.org/10.1016/j.jenvman.2015.04.018

IPCC. (2014). *Climate Change 2014: Synthesis Report.* Geneva, Switzerland.

John, B. M., Shirlal, K. G., Rao, S., & Rajasekaran, C. (2016). Effect of artificial seagrass on wave attenuation and wave run-up. *International Journal of Ocean and Climate Systems*, *7*(1), 14–19. http://doi.org/10.1177/1759313115623163

Joint Typhoon Warning Center. (2001). *Annual Tropical Cyclone Report*. Pearl Harbour, Hawaii. Retrieved from http://www.usno.navy.mil/NOOC/nmfc-ph/RSS/jtwc/atcr/2001atcr.pdf

Kathiresan, K., & Rajendran, N. (2005). Coastal mangrove forests mitigated tsunami. *Estuarine, Coastal and Shelf Science*, *65*(3), 601–606. http://doi.org/10.1016/j.ecss.2005.06.022

Kauffman, J. B., & Donato, D. C. (2012). *Protocols for the measurement, monitoring and reporting of structure, biomass and carbon stocks in mangrove forests*. Bogor, Indonesia.

Kerr, A. M., Baird, A. H., & Campbell, S. J. (2006). Comments on "coastal mangrove forests mitigated tsunami" by k.Kathiresan and n.Rajendran [estuar. Coast. Shelf sci. 65(2005) 601 - 606]". *Estuarine, Coastal and Shelf Science*, *3*(67), 539–541.

Kerr, A. M., & Baird, A. H. (2007). Natural Barriers to Natural Disasters. *BioScience*, *57*(2), 102. http://doi.org/10.1641/B570202

Klein, R. J. T., & Maciver, D. C. (1999). Adaptation to Climate Variability and Change: Methodological Issues. *Mitigation and Adaptation Strategies for Global Change*, *4*, 189–198. Retrieved from http://dx.doi.org/10.1023/A:1009690729283

Kobayashi, N., Raichle, A. W., & Asano, T. (1993). Wave attenuation by vegetation. *Journal of Waterway, Port, Coastal, and Ocean Engineering*, *119*, 30–48.

Koch, E. W., Barbier, E. B., Silliman, B. R., Reed, D. J., Perillo, G. M. E., Hacker, S. D., Granek, E. F., Primavera, J. H., Muthiga, N., Polasky, S., Halpern, B. S., Kennedy, C. J., Kappel, C. V., & Wolanski, E. (2009). Non-linearity in ecosystem services: Temporal and spatial variability in coastal protection. *Frontiers in Ecology and the Environment*, *7*(1), 29–37. http://doi.org/10.1890/080126

Krauss, K. W., Allen, J. A., & Cahoon, D. R. (2003). Differential rates of vertical accretion and elevation change among aerial root types in Micronesian mangrove forests. *Estuarine, Coastal and Shelf Science*, *56*(2), 251–259. http://doi.org/10.1016/S0272-7714(02)00184-1

Kurniawan, A., Ooi, S. K., Hummel, S., & Gerritsen, H. (2011). Sensitivity analysis of the tidal representation in Singapore Regional Waters in a data assimilation environment. *Ocean Dynamics*, *61*(8), 1121–1136.

Lai, S., Loke, L. H. L., Hilton, M. J., Bouma, T. J., & Todd, P. A. (2015). The effects of urbanisation on coastal habitats and the potential for ecological engineering: A Singapore case study. *Ocean and Coastal Management*, *103*, 78–85. http://doi.org/10.1016/j.ocecoaman.2014.11.006

Lee, S. Y., Primavera, J. H., Dahdouh-Guebas, F., McKee, K., Bosire, J. O., Cannicci, S., Diele, K., Fromard, F., Koedam, N., Marchand, C., Mendelssohn, I., Mukherjee, N., & Record, S. (2014). Ecological role and services of tropical mangrove ecosystems: a reassessment. *Global Ecology and Biogeography*, *23*, 726–743.

Leonard, L. A., & Luther, M. E. (1995). Flow hydrodynamics in tidal marsh canopies. *Limnology and Oceanography*, *40*(8), 1474–1484.

Leonard, L. A., & Reed, D. J. (2002). Hydrodynamics and sediment transport through tidal marsh canopies. *Journal of Coastal Research*, *36*(2), 459–469.

Lewis, R. R. (2005). Ecological engineering for successful management and restoration of mangrove forests. *Ecological Engineering*, *24*, 403–418.

Magi, M., Mazda, Y., Ikeda, Y., & Kurokawa, T. (1996). Wave reduction in a mangrove area near the mouth of Shiira River on the Iriomote Island, Japan. *Mangrove Sci*, *1*, 35–42.

Massel, S. R., Furukawa, K., & Brinkman, R. M. (1999). Surface wave propagation in mangrove forests. *Fluid Dynamics Research*, *24*(4), 219–249. http://doi.org/10.1016/S0169-5983(98)00024-0

Mazda, Y., Magi, M., Kogo, M., & Hong, P. N. (1997a). Mangroves as a coastal protection from waves in the Tong King delta, Vietnam. *Mangroves and Salt Marshes*. http://doi.org/10.1023/A:1009928003700

Mazda, Y., Wolanski, E., King, B., Sase, A., Ohtsuka, D., & Magi, M. (1997b). Drag force due to vegetation in mangrove swamps. *Mangroves and Salt Marshes*, *1*, 193–199. http://doi.org/10.1023/A:1009949411068

Mazda, Y., Magi, M., Ikeda, Y., Kurokawa, T., & Asano, T. (2006). Wave reduction in a mangrove forest dominated by Sonneratia sp. *Wetlands Ecology and Management*, *14*(4), 365–378. http://doi.org/10.1007/s11273-005-5388-0

Mazda, Y., Wolanski, E., & Ridd, P. (2007). *The Role of Physical Processes in Mangrove Environments – Manual for the preservation and utilization of mangrove ecosystems*. Tokyo: TERRAPUB.

McIvor, A., Möller, I., Spencer, T., & Spalding, M. (2012). *Reduction of Wind and Swell Waves by Mangroves. Natural Coastal Protection Series*. http://doi.org/ISSN 2050-7941.

Mendez, F. J., & Losada, I. J. (2004). An empirical model to estimate the propagation of random breaking and nonbreaking waves over vegetation fields. *Coastal Engineering*, *51*(2), 103–118. http://doi.org/10.1016/j.coastaleng.2003.11.003

Mohamed, M. O. S., Neukermans, G., Kairo, J. G., Dahdouh-Guebas, F., & Koedam, N. (2009). Mangrove forests in a peri-urban setting: The case of Mombasa (Kenya). *Wetlands Ecology and Management*, *17*(3), 243–255.

http://doi.org/10.1007/s11273-008-9104-8

Möller, I. (2006). Quantifying saltmarsh vegetation and its effect on wave height dissipation: Results from a UK East coast saltmarsh. *Estuarine, Coastal and Shelf Science*, *69*(3–4), 337–351. http://doi.org/10.1016/j.ecss.2006.05.003

Morris, J. T. (2007). Ecological engineering in intertidal saltmarshes. *Hydrobiologia*, *577*(1), 161–168. http://doi.org/10.1007/s10750-006-0425-4

MPA. (2016). Port statistics. Retrieved June 20, 2016, from http://www.mpa.gov.sg/web/portal/home/port-of-singapore/port-statistics

Murray, M. R. (2002). Is laser particle size determination possible for carbonate-rich lake sediments? *Journal of Paleolimnology*, *27*(2), 173–183. http://doi.org/10.1023/A:1014281412035

Narayan, S. (2009). *On the effectiveness of mangroves in attenuating cyclone-induced waves*. Delft University of Technology.

National Climate Change Secretariat. (2016). Impact of climate change on Singapore. Retrieved August 1, 2016, from https://www.nccs.gov.sg/climate-change-and-singapore/national-circumstances/impact-climate-change-singapore

National Environment Agency. (2016). Weather statistics. Retrieved June 20, 2016, from http://www.nea.gov.sg/weather-climate/climate-information/weather-statistics

Natural Capital Project. (2016). Integrated valuation of ecosystem services and tradeoffs. Retrieved June 20, 2016, from http://www.naturalcapitalproject.org/invest/

Nepf, H. M. (2004). Vegetated flow dynamics. In S. Fagherazzi, M. Marani, & L. Blum (Eds.), *Ecogeomorphology of Tidal Marshes, Coastal and Estuarine Studies, Volume 59* (pp. 137–164).

Nguyen, H. H. (2013). *Functional values and management of coastal mangroves: Case study in Kien Gian Coast, Southern Vietmam*. The University of Queensland, Australia.

Nguyen, H. H., McAlpine, C., Pullar, D., Leisz, S. J., & Galina, G. (2015). Drivers of Coastal Shoreline Change: Case Study of Hon Dat Coast, Kien Giang, Vietnam. *Environmental Management*, *55*(5), 1093–1108. http://doi.org/10.1007/s00267-015-0455-7

Nicholls, R. J., Hoozemans, F. M. J., & Marchand, M. (1999). Increasing flood risk and wetland losses due to global sea-level rise: Regional and global analyses. *Global Climate Change*, *9*, S69–S87.

Nicholls, R. J., Wong, P. P., Burkett, V., Woodroffe, C. D., & Hay, J. (2008). Climate change and coastal vulnerability assessment: scenarios for integrated assessment. *Sustainability Science*, *3*(1), 89–102.

Phan, L. K., van Thiel de Vries, J. S., & Stive, M. J. F. (2014). Coastal Mangrove Squeeze in the Mekong Delta. *Journal of Coastal Research*, *31*(2), 233–243. http://doi.org/10.2112/JCOASTRES-D-14-00049.1

Phang, V. X. H., Chou, L. M., & Friess, D. A. (2015). Ecosystem carbon stocks across a tropical intertidal habitat mosaic of mangrove forest, seagrass meadow, mudflat and sandbar. *Earth Surface Processes and Landforms*, *40*(10), 1387–1400. http://doi.org/10.1002/esp.3745

Polidoro, B. A., Carpenter, K. E., Collins, L., Duke, N. C., Ellison, A. M., Ellison, J. C., Farnsworth, E. J., Fernando, E. S., Kathiresan, K., Koedam, N. E., Livingstone, S. R., Miyagi, T., Moore, G. E., Nam, V. N., Ong, J. E., Primavera, J. H., Salmo, S. G., Sanciangco, J. C., Sukardjo, S., Wang, Y., & Yong, J. W. H. (2010). The loss of species: Mangrove extinction risk and geographic areas of global concern. *PLoS ONE*, *5*(4). http://doi.org/10.1371/journal.pone.0010095

Pontee, N. (2013). Defining coastal squeeze: A discussion. *Ocean and Coastal Management*, *84*, 204–207.

Quartel, S., Kroon, A., Augustinus, P. G. E. F., Van Santen, P., & Tri, N. H. (2007). Wave attenuation in coastal mangroves in the Red River Delta, Vietnam. *Journal of Asian Earth Sciences*, *29*(4), 576–584. http://doi.org/10.1016/j.jseaes.2006.05.008

Richards, D. R., & Friess, D. A. (2015). A rapid indicator of cultural ecosystem service usage at a fine spatial scale: Content analysis of social media photographs. *Ecological Indicators*, *53*, 187–195. http://doi.org/10.1016/j.ecolind.2015.01.034

Richards, D. R., & Friess, D. A. (2016). Rates and drivers of mangrove deforestation in Southeast Asia, 2000–2012. *Proceedings of the National Academy of Sciences*, *113*(2), 344–349. http://doi.org/10.1073/pnas.1510272113

RStudio Team. (2015). RStudio: Integrated Development for R. Boston, MA: RStudio, Inc. Retrieved from http://www.rstudio.com/

Sanchirico, J. N., & Springborn, M. (2011). How to get there from there: Ecological and economic dynamics of ecosystem service provision. *Environmental and Resource Economics*, *48*(2), 243–267. http://doi.org/10.1007/s10640-010-9410-5

Sarkar, D., & Haldar, A. (2005). *Physical and chemical methods in soil analysis: fundamental concepts of analytical chemistry and instrumental techniques*. New Delhi: New Age Internatinal (P) Ltd.

Sathirathai, S., & Barbier, E. B. (2001). Valuing mangrove conservation in Southern Thailand. *Contemporary Economic Policy*, *19*(2), 109–122.

Schleupner, C. (2008). Evaluation of coastal squeeze and its consequences for the Caribbean island Martinique. *Ocean and Coastal Management*, *51*, 383–390.

Schumacher, B. A. (2002). *Methods for the determination of total organic carbon (TOC) in soils and sediments*. *Ecological Risk Assessment Support Center*. Retrieved from http://epa.gov/nerlesd1/cmb/research/papers/bs116.pdf

Shepard, C. C., Agostini, V. N., Gilmer, B., Allen, T., Stone, J., Brooks, W., & Beck, M. W. (2012). Assessing future risk: Quantifying the effects of sea level rise on storm surge risk for the southern shores of Long Island, New York. *Natural Hazards*, *60*(2), 727–745. http://doi.org/10.1007/s11069-011-0046-8

Small, C., & Nicholls, R. J. (2003). A global analysis of human settlement in coastal zones. *Journal of Coastal Research*, *19*(3), 584–599. http://doi.org/10.2307/4299200

Spalding, M. D., McIvor, A., Tonneijck, F. H., Tol, S., & van Eijk, P. (2014). *Mangroves for coastal defence. Guidelines for coastal managers & policy makers*. *Wetlands International and The Nature Conservancy*. Retrieved from http://www.nature.org/media/oceansandcoasts/mangroves-for-coastal-defence.pdf

Strusińska-Correia, A., Husrin, S., & Oumeraci, H. (2013). Tsunami damping by mangrove forest: a laboratory sutdy using parameterized trees. *Natural Hazards and Earth System Sciences*, *13*, 483–503.

Struve, J., Falconer, R. A., & Wu, Y. (2003). Influence of model mangrove trees on the hydrodynamics in a flume. *Estuarine, Coastal and Shelf Science*, *58*(1), 163–171. http://doi.org/10.1016/S0272-7714(03)00072-6

Suzuki, T., Zijlema, M., Burger, B., Meijer, M. C., & Narayan, S. (2012). Wave dissipation by vegetation with layer schematization in SWAN. *Coastal Engineering*, *59*(1), 64–71. http://doi.org/10.1016/j.coastaleng.2011.07.006

Tan, X. Y., & Friess, D. A. (2015). *Examining mangrove loss and fragmentation in the southern Johor region: A spatio-temporal study*. Unpublished data.

Tay, S. H. X. (2010). *Typhoon - induced extreme water levels near Singapore*. Delft University of Technology.

Thiagarajah, J., Wong, S. K. M., Richards, D. R., & Friess, D. A. (2015). Historical and contemporary cultural ecosystem service values in the rapidly urbanizing city state of Singapore. *AMBIO*, *44*(7), 666–677. http://doi.org/10.1007/s13280-015-0647-7

Tkalich, P., Vethamony, P., Babu, M. T., & Pokratath, R. (2009). Seasonal Sea Level Variability and Anomalies in the Singapore Strait. In *Proceedings of Intarnational Conference in Ocean Engineering, ICOE 2009* (pp. 874–880). Chennai, India: IIT Madras.

Tkalich, P., Vethamony, P., Babu, M. T., & Malanotte-Rizzoli, P. (2013). Storm surges in the Singapore Strait due to winds in the South China Sea. *Natural Hazards*, *66*(3), 1345–1362. http://doi.org/10.1007/s11069-012-0211-8

Urban Redevelopment Authority. (2016). Master Plan 2014. Retrieved August 1, 2016, from https://www.ura.gov.sg/uol/master-plan.aspx?p1=View-Master-Plan&p2=master-plan-2014

Vaasma, T. (2008). Grain-size analysis of lacustrine sediments: a comparison of pre-treatment methods. *Estonian Journal of Ecology*, *57*(4), 231–243.

Van Rijn, L. C. (1989). *Handbook - Sediment transport by currents and waves*.

Van Rijn, L. C. (2008). *Principles of fluid flow and surface waves in rivers, estuaries, seas and oceans*. The Netherlands: Aqua Publications.

Vo-Luong, P. H., & Massel, S. R. (2006). Experiments on wave motion and

suspended sediment concentration at Nang Hai, Can Gio mangrove forest, Southern Vietnam. *Oceanologia*, *48*(1), 23–40.

Vo-Luong, P. H., & Massel, S. R. (2008). Energy dissipation in non-uniform mangrove forests of arbitrary depth. *Journal of Marine Systems*, *74*(1), 603–622. http://doi.org/10.1016/j.jmarsys.2008.05.004

Wee, Y. C., & Corlett, R. T. (1986). *The city and the forest : plant life in urban Singapore*. Singapore: Singapore University Press.

Willemsen, P. W. J. M., Horstman, E. M., Borsje, B. W., Friess, D. A., & Dohmen-Janssen, C. M. (2016). Sensitivity of sediment trapping capcaity of estuarine mangrove forests. *Geomorphology*, Manuscript submitted for publication.

Yaakub, S. M., Lim, R. L. F., Lim, W. L., & Todd, P. A. (2013). The diversity and distribution of seagrass in Singapore. *Nature in Singapore*, *6*, 105–111.

Yanagisawa, H., Koshimura, S., Goto, K., Miyagi, T., Imamura, F., Ruangrassamee, A., & Tanavud, C. (2009). The reduction effects of mangrove forest on a tsunami based on field surveys at Pakarang Cape, Thailand and numerical analysis. *Estuarine, Coastal and Shelf Science*, *81*(1), 27–37.

Yang, S., Lim, R. L. F., Sheue, C. R., & Yong, J. W. H. (2011). The current status of mangrove forests in Singapore. In *Proceedings of Nature Society, Singapore's Conference on "Nature Conservation for a Sustainable Singapore"* (pp. 99–120).

Yee, A. T. K., Ang, W. F., Teo, S., Liew, S. C., & Tan, H. T. W. (2010). The present extent of mangrove forests in Singapore. *Nature in Singapore*, *3*, 139–145.

Young, B. M., & Harvey, E. L. (1996). A spatial analysis of the relationship between mangrove (Avicennia marinavar. Australasica) physiognomy and sediment accretion in the Hauraki Plains, New Zealand. *Estuarine, Coastal and Shelf Science*, *42*(2), 231–246.

Zhang, K., Douglas, B. C., & Leatherman, S. P. (2004). Global warming and coastal erosion. *Climatic Change*, *64*(1–2), 41–58. http://doi.org/10.1023/B:CLIM.0000024690.32682.48

Zhang, K., Liu, H., Li, Y., Xu, H., Shen, J., Rhome, J., & Simth, T. J. (2012). The role of mangroves in attenuating storm surges. *Estuarine, Coastal and Shelf Science*, *102–103*, 11–23.

Zhang, X., Chua, V. P., & Cheong, H. F. (2015a). Geometrical and material properties of Sonneratia alba mangrove roots. *Trees*, *29*(1), 285–297. http://doi.org/10.1007/s00468-014-1117-8

Zhang, X., Chua, V. P., & Cheong, H. F. (2015b). Hydrodynamics in mangrove prop roots and their physical properties. *Journal of Hydro-Environment Research*, *9*(2), 281–294. http://doi.org/10.1016/j.jher.2014.07.010

Ziegler, A. D., Terry, J. P., Oliver, G. J. H., Friess, D. A., Chuah, C. J., Chow, W. T. L., & Wasson, R. J. (2014). Increasing Singapore's resilience to drought. *Hydrological Processes*, *28*(15), 4543–4548. http://doi.org/10.1002/hyp.10212

9. Appendices

Appendix A. Nearshore wave evolution model

Equation 1 Wave energy equation

$$\frac{1}{8}\rho g\frac{\partial C_g H^2}{\partial x} = -D$$

where ρ is density of seawater (1024 kg m^{-3}); g = 9.81 m s^{-2} is the acceleration of gravity, H is the wave height representation of the random wave field, C_g is the speed at which wave energy travels, and D represents the dissipation of wave energy.

The dissipation of wave energy occurs as wave travels towards the shore over different media. This dissipation is primarily caused by wave breaking D_{Break}, bottom friction D_{Bot}, and submerged vegetation D_{Veg}.

Equation 2 Drag force

$$D = D_{Break} + D_{Bot} + D_{Veg}$$

Dissipation due to breaking is calculated using the formula and parameters presented by Alsina and Baldock (2007). The formula and parameters had been validated with field measurements (Apotsos et al., 2008).

Equation 3 Drag force from wave breaking

$$D_{Break} = A\frac{H^3}{h}\left[\left(\left(\frac{H_b}{H}\right)^3 + \frac{3H_b}{2H}\right)\exp\left(-\left(\frac{H_b}{H}\right)^2\right) + \frac{3\sqrt{\pi}}{4}\left(1 - erf\left(\frac{H_b}{H}\right)\right)\right]$$

where erf is the Gaussian error function, h is the local water depth, A is the sediment scale factor, and H_b is the maximum wave height prior to breaking.

Equation 4 Maximum height before breaking

$$H_b = \frac{0.88}{k}tanh\left(\gamma\frac{kh}{0.88}\right)$$

where κ is the wave number (κ = wavelength/2π) and γ is a calibration parameters called breaking index. The breaking index, γ, used in the model is the value proposed by Battjes and Stive (1985):

Equation 5 Breaking index

$$\gamma = 0.5 + 0.4 \tanh\left(33 \frac{H_o}{L_o}\right)$$

where H_o and L_o are the deep water wave height and wavelength, respectively.

The next dissipation terms is the drag force applied by vegetation on the incident waves. This drag force is a function of the characteristics of the natural habitats that are present along the profile of interest. As waves move into the length of profile where vegetation is located, the dissipation terms were included. Dissipation due to vegetation is expressed by:

Equation 6 Drag force from vegetation

$$D_{Veg} = \frac{1}{2\sqrt{\pi}} \rho N d C_d \left(\frac{kg}{2\sigma}\right)^3 \frac{\sinh^3 k\alpha h + 3\sinh k\alpha h}{3k\cosh^3 kh} H^3$$

where N is the density of vegetation (stems per unit area), d is the frontal width or diameter of vegetation stem, and α represents the fraction of the water depth h occupied by vegetation elements of average stem height h_c *:* $\alpha = h_c / h$. In the case of emergent vegetation (hc > h), a maximum of $\alpha = 1$ was applied. C_d is a taxa-specific drag coefficient. Default values of drag coefficient (Bradley & Houser, 2009; Burger, 2005; Kobayashi et al., 1993) are applied in the model. In this study, the drag coefficient is applied is $C_d = 1$, which is the coefficient for trees.

For mangroves, the contribution of roots, trunk and canopy were assumed to contribute to the dissipation independently. D_{veg} becomes:

Equation 7 Component of vegetation drag force

$$D_{Veg} = D_{Roots} + D_{Trunk} + D_{Canopy}$$

Bottom friction force is another dissipation component in the nearshore wave evolution model. This friction force generally initiated when waves propagate towards the shallower water. The friction force experience in higher in coarser bottom than smoother bottom. The bottom friction force was modelled following Thornton and Guza (1983):

Equation 8 Drag force from bottom friction

$$D_{Bot} = \rho C_f \frac{1}{16\sqrt{\pi}} \left[\frac{\sigma H}{\sinh kh} \right]^3$$

where C_f is the bed friction coefficient for bottom, which is the function of the roughness of the bed. The σ is wave frequency, which is also $2\pi/T$. In this model, the C_f is assumed to be a 0.01.

References

Alsina, J. M., & Baldock, T. E. (2007). Improved representation of breaking wave energy dissipation in parametric wave transformation models. *Coastal Engineering*, *54*(10), 765–769. http://doi.org/10.1016/j.coastaleng.2007.05.005

Apotsos, A., Raubenheimer, B., Elgar, S., & Guza, R. T. (2008). Testing and calibrating parametric wave transformation models on natural beaches. *Coastal Engineering*, *55*(3), 224–235. http://doi.org/10.1016/j.coastaleng.2007.10.002

Battjes, J. A., & Stive, M. J. F. (1985). Calibration and verification of a dissipation model for random breaking waves, *90*, 9159–9167.

Bradley, K., & Houser, C. (2009). Relative velocity of seagrass blades: Implications for wave attenuation in low-energy environments. *Journal of Geophysical Research: Earth Surface*, *114*(F1), 2156–2202. http://doi.org/10.1029/2007JF000951

Burger, B. (2005). *Wave Attenuation in Mangrove Forests*. Delft University of Technology.

Kobayashi, N., Raichle, A. W., & Asano, T. (1993). Wave attenuation by vegetation. *Journal of Waterway, Port, Coastal, and Ocean Engineering*, *119*, 30–48.

Thornton, E. B., & Guza, R. T. (1983). Transformation of wave height distribution. *Journal of Geophysical Research: Oceans*, *88*(C10), 5925–5938. http://doi.org/10.1029/JC088iC10p05925

Appendix B. Vegetation, coastal physical and hydrodynamic characteristics model input

Vegetation characteristics

Table B1. Mangrove extent, dominant genus and vegetation density at each transect.

Site	Transect	Mangrove extent (m)	Dominant genus	Vegetation density (trees m^{-2})
BUL	BUL3	94.8	*Bruguiera*	0.09527
	BUL4	55.9	*Rhizophora*	0.05197
	BUL5	155	*Avicennia*	0.04331
	BUL6	200.5	*Rhizophora*	0.05847
	BUL7	308.9	*Avicennia*	0.07795
MAN	MAN1	296.1	*Bruguiera*	0.14779
	MAN2	236.3	*Bruguiera*	0.12776
	MAN3	182.2	*Avicennia*	0.12343
	MAN4	151.2	*Avicennia*	0.06496
	MAN5	184.7	*Avicennia*	0.04547
UBI	UBI2	986.8	*Rhizophora*	0.1689
	UBI3	954.3	*Rhizophora*	0.19488
	UBI4	770.7	*Rhizophora*	0.29323
	UBI5	862.2	*Rhizophora*	0.25497
TEK	TEK1	44.2	*Rhizophora*	0.12482
	TEK2	858.2	*Rhizophora*	0.12482
	TEK3	167.3	*Rhizophora*	0.12482

Table B2. Genus-specific vegetation characteristics.

Genus	Tree structure	Height (m)	Diameter (m)	Density ($1/m^2$)
Avicennia	Roots	0.0718	0.0068	182.33
	Trunk	4.2825	0.1485	Transect- dependent
	Canopy	5.0507	4.6713	Transect- dependent
Bruguiera	Roots	0.0514	0.032	70.86
	Trunk	3.7438	0.085	Transect- dependent
	Canopy	7.489	4.4162	Transect- dependent
Rhizophora	Roots*	1.4	0.039	4.25
	Trunk	4.9169	0.1043	Transect- dependent
	Canopy	5.6021	4.3167	Transect- dependent
Sonneratia	Roots	0.0585	0.03	126.67
	Trunk	9.0595	0.1844	Transect- dependent
	Canopy	6.432	4.8701	Transect- dependent

*Refer to Zhang *et al*., 2015

Coastal physical characteristics

Table B3. Sediment size and bulk density for each transect. At BUL4, only two sediment properties measurements as there were only two plots within transect.

Transect	Minimum		Median		Maximum	
	D50 (mm)	Bulk density (kg m^{-3})	D50 (mm)	Bulk density (kg m^{-3})	D50 (mm)	Bulk density (kg m^{-3})
BUL3	0.17	764.54	0.20	702.58	0.30	904.01
BUL4	0.01	882.56	-	-	0.06	1316.24
BUL5	0.01	1184.72	0.01	354.08	0.01	471.44
BUL6	0.01	878.12	0.02	1194.48	0.03	785.72
BUL7	0.01	1612.08	0.01	1533.36	0.02	1288.24
MAN1	0.02	534.88	0.25	908.24	0.34	664.00
MAN2	0.04	346.88	0.04	140.00	0.38	1120.16
MAN3	0.03	652.56	0.20	774.24	0.22	609.28
MAN4	0.01	268.64	0.03	911.84	0.12	678.16
MAN5	0.01	398.48	0.12	564.32	0.26	1004.32
UBI2	0.01	426.14	0.01	330.284	0.01	371.09
UBI3	0.01	425.68	0.01	483.64	0.01	235.40
UBI4	0.01	304.00	0.01	260.72	0.01	376.68
UBI5	0.01	263.28	0.01	272.48	0.01	188.72
Overall	0.01	425.68	0.02	321.04	0.38	1120.16

Hydrodynamic characteristics

Table B4. Mean Sea Level (MSL) and Mena High Water (MHW) with reference to Mean Lower Low Water for study sites.

Site	Mean Sea Level (MSL)	Mean High Water (MHW)
BUL	1.3	2.1
MAN	1.3	2.1
UBI	1.1	1.9
TEK	1.1	1.9

Table B5. Wave height, wave period, low and high water levels at each site. MSL = Mean Sea Level scenario; HT = High Tide scenario, LW = Low Water scenario; HW = High water scenario; MSL = mean sea level.

Site	Wave Height (m)	Wave Period (s)	MSL/ LW (m above MSL)	HT/ HW (m above MSL)
Average condition				
BUL	0.02702	1.13	0	1.2
MAN	0.02702	1.13	0	1.2
UBI	0.05997	1.3	0	1.1
TEK	0.04708	1.19	0	1.1
Extreme condition				
BUL	1.2	3	1.4	2.8
MAN	1.2	3	1.4	2.8
UBI	1.3	3	1.2	2.2
TEK	1.4	3	1.2	2.1

Appendix C. Statistical analysis

Table C1. ANOVA test for mangrove density comparison across study sites. *indicates p-value <0.05; ** indicates p-value <0.01; *** indicates p-value <0.001

	df	SS	MS	F value	P value
Site	3	0.2349	0.07830	17.45	<0.001***
Residuals	55	0.2469	0.00449		

Table C2. Tukey HSD test for mangrove density comparison across study sites. * indicates p-value < 0.05; ** indicates p-value < 0.01; *** indicates p-value < 0.001.

	BUL	MAN	UBI
BUL		0.37	<0.001***
MAN			<0.001***
UBI			

Table C3. Non-parametric test (Mann-Whitney) for mangrove root density comparison across genera. * indicates p-value < 0.05; ** indicates p-value < 0.01; *** indicates p-value < 0.001.

	Avicennia	*Bruguiera*	*Sonneratia*
Avicennia		0.003**	0.067
Bruguiera			0.117
Sonneratia			

Table C4. Non-parametric test (Mann-Whitney) for mangrove trunk height comparison across genera. * indicates p-value < 0.05; ** indicates p-value < 0.01; *** indicates p-value < 0.001.

	Avicennia	*Bruguiera*	*Sonneratia*	*Rhizophora*
Avicennia		0.44	<0.001***	<0.001***
Bruguiera			<0.001***	<0.001***
Sonneratia				<0.001***
Rhizophora				

Table C5. Non-parametric test (Mann-Whitney) for mangrove canopy diameter comparison across genera. * indicates p-value < 0.05; ** indicates p-value < 0.01; *** indicates p-value < 0.001.

	Avicennia	*Bruguiera*	*Sonneratia*	*Rhizophora*
Avicennia		0.021*	0.021*	0.094
Bruguiera			0.023*	0.21
Sonneratia				0.009**
Rhizophora				

Table C6. Non-parametric test (Mann-Whitney) for sediment size (D10, D50 and D90) and bulk density comparison across sites. * indicates p-value < 0.05; ** indicates p-value < 0.01; *** indicates p-value < 0.001.

	BUL	MAN	UBI
D10			
BUL		0.004**	0.29
MAN			<0.001***
UBI			
D50			
BUL		0.022*	<0.001***
MAN			<0.001***
UBI			
D90			
BUL		0.014*	0.009**
MAN			<0.001***
UBI			
Bulk density			
BUL		0.022*	<0.001***
MAN			<0.001***
UBI			

Table C7. Non-parametric test (Mann-Whitney) for wave height reduction rate comparison across sites. * indicates p-value < 0.05; ** indicates p-value < 0.01; *** indicates p-value < 0.001.

	BUL	MAN	TEK	UBI
BUL		0.056	0.071	0.381
MAN			0.036*	0.857
TEK				0.2
UBI				